Glutaredoxin 5 as a novel target for β cell survival and regeneration

Inaugural Dissertation

submitted to the

Faculty of Medicine

in partial fulfillment of the requirements

for the PhD-Degree

of the Faculties of Veterinary Medicine and Medicine

of the Justus Liebig University Giessen

by

Mengmeng Zhou

of

Chongqing, China

Giessen 2025

From the

Clinical Research Unit,

Head: Univ.-Prof. Dr. med. Thomas Linn

Affiliated to Medical Clinic and Policlinic 3

Director: Prof. Dr. med. Andreas Schäffler

Universitätsklinikum Gießen und Marburg GmbH, Standort Gießen

Justus Liebig University

First Supervisor and Committee Member: Univ.-Prof. Dr. med. Thomas Linn

Second Supervisor: Prof. Dr. Sybille Mazurek

Chairman of Committee Member: Prof. Dr. Friedemann Weber

Committee Member: Prof. Dr. Klaus-Dieter Schlüter

External Examiner: Prof. Miriam Cnop

Date of Doctoral Defense: 23.10.2025

Ehrenwörtliche Erklärung

„Hiermit erkläre ich, dass ich die vorliegende Arbeit selbständig und ohne unzulässige Hilfe oder Benutzung anderer als der angegebenen Hilfsmittel angefertigt habe. Alle Textstellen, die wörtlich oder sinngemäß aus veröffentlichten oder nichtveröffentlichten Schriften entnommen sind, und alle Angaben, die auf mündlichen Auskünften beruhen, sind als solche kenntlich gemacht. Bei den von mir durchgeführten und in der Dissertation erwähnten Untersuchungen habe ich die Grundsätze guter wissenschaftlicher Praxis, wie sie in der „Satzung der Justus-Liebig-Universität Gießen zur Sicherung guter wissenschaftlicher Praxis“ niedergelegt sind, eingehalten sowie ethische, datenschutzrechtliche und tierschutzrechtliche Grundsätze befolgt. Ich versichere, dass Dritte von mir weder unmittelbar noch mittelbar geldwerte Leistungen für Arbeiten erhalten haben, die im Zusammenhang mit dem Inhalt der vorgelegten Dissertation stehen. Die vorgelegte Arbeit wurde weder im Inland noch im Ausland in gleicher oder ähnlicher Form einer anderen Prüfungsbehörde zum Zweck einer Promotion oder eines anderen Prüfungsverfahrens vorgelegt. Alles aus anderen Quellen und von anderen Personen übernommene Material, das in der Arbeit verwendet wurde oder auf welches direkt Bezug genommen wird, wurde als solches kenntlich gemacht. Insbesondere wurden alle Personen genannt, die direkt und indirekt an der Entstehung der vorliegenden Arbeit beteiligt waren. Mit der Überprüfung meiner Arbeit durch eine Plagiatserkennungssoftware bzw. ein internetbasiertes Softwareprogramm erkläre ich mich einverstanden.“

Mengmeng Zhou

Date: 23.10.2025

Place: Giessen, Germany

Table of Contents

List of Tables

List of Figures

List of Abbreviations

4-HNE	4-hydroxy-2-nonenal
ACC	Acetyl-CoA carboxylase
ADA	American Diabetes Association
ADP	Adenosine diphosphate
AGE	Advanced glycation end product
AGI	α-glucosidase inhibitor
Akt	Protein kinase B
AmmFe	Ammonium iron (II) sulfate hexahydrate
AP-1	Activator protein 1
ASK1	Apoptosis signal-regulating kinase 1
ATF4	Activating transcription factor 4
ATP	Adenosine triphosphate
BH_4	Tetrahydrobiopterin
Bpy	2,2'-Bipyridine
BSA	Bovine serum albumin
Ca^{2+}	Calcium
CCL2	Chemokine (C-C motif) ligand 2
CCO	Cytochrome c oxidase
Cdkal1	Cdk5-regulatory subunit-associated protein 1-like 1
CHOP	C/EBP homologous protein
CoQ10	Coenzyme Q10
COX	Cyclooxygenases
CPT	Carnitine palmitoyltransferase
CRP	c-reactive protein
CVDs	Cardiovascular diseases
CXCL1	Chemokine (C-X-C motif) ligand 1
CYP	Cytochrome P450

Cys	Cysteine
DAG	Diacylglycerol
DFOM	Deferoxamine mesylate (salt)
DHAP	Dihydroxyacetone phosphate
DHODH	Dihydroorotate dehydrogenase
DKA	Diabetic ketoacidosis
DM	Diabetes mellitus
DMEM	Dulbecco’s Modified Eagle Medium
DMSO	Dimethyl sulfoxide
DMT1	Divalent metal transporter 1
DPBS	Dulbecco’s phosphate buffered saline
DPP-4	Dipeptidyl peptidase 4
EDTA	Ethylene diamine tetra acetic acid
ELISA	Enzyme-linked immunosorbent assay
ER	Endoplasmic reticulum
ERK	Extracellular signal-regulated kinase
FBG	Fasting blood glucose
FBS	Fetal bovine serum
FCS	Fetal calf serum
FeO	FerroOrange
Fer-1	Ferrostatin-1
FFA	Free fatty acid
FFAR1	FFA receptor 1
FoxO	Forkhead box
FPN1	Ferroportin 1
Frau-6P	Fructose-6-phosphat
FSP1	FSP1
FTH1	Ferritin heavy chain
FTL	Ferritin light chain

G-6-P	Glucose-6-phosphat
GA-3P	Glyceraldehyde 3-phosphate
GADA	Glutamic acid decarboxylase autoantibodies
GAPDH	Glyceraldehyde 3-phosphate dehydrogenase
GCH1	GTP cyclohydrolase 1
GDM	gestational diabetes mellitus
GIP	Glucose-dependent insulinotropic polypeptide
GK	Glucokinase
GLP-1	Glucagon-like peptide-1
GLP-1RA	GLP-1 receptor agonist
GLUT	Glucose transporters
GO	Glyoxal
Gpx4	Glutathione peroxidase 4
GR	Glutathione reductase
Grx	Glutaredoxin
GSH	Glutathione
GSIS	Glucose-stimulated insulin secretion
GSK-3β	Glycogen synthase kinase 3β
GSSG	Glutathione disulfide
GWAS	Genome-wide association studies
H_2O_2	hydrogen peroxide
HBSS	Hanks' balanced salt solution
HCM	Hypertrophic cardiomyopathy
HD	Homology domain
HFD	High-fat diet
HHS	Hyperosmolar hyperglycemic syndrome
HIF	Hypoxia-inducible factor
HLA	Human leukocyte antigens
HOMA-IR	Homeostatic model assessment for insulin resistance

Hsp	Heat shock protein
hTERT	Human telomerase reverse transcriptase
IA-2A	Tyrosine phosphatase-like protein 2 autoantibodies
IAA	Insulin autoantibody
IAPP	Islet amyloid polypeptide
ICA	Islet cell autoantigen
IDF	International Diabetes Federation
IFN-γ	Interferon-gamma
IGR	Impaired glucose regulation
IL-1RA	IL-1 receptor antagonists
IL-1β	Interleukin 1 beta
IL-6	Interleukin-6
IL-8	Interleukin-8
iNO	Nitric oxide synthase
IP3R	Inositol 1,4,5-trisphosphate receptor
ipGTT	Intraperitoneal glucose tolerance test
iPLA2β	Calcium-independent phospholipase A2β
IR	Insulin resistance
IRE	Iron response elements
IRE1α	Inositol-requiring enzyme 1 α
IRP1	Iron regulatory protein 1
IRP2	Iron regulatory protein 2
ISCU	Iron-sulfur cluster assembly enzyme
ISG	Immature secretory granules
JNK	c-Jun N-terminal kinase
JNKK	Jun kinase kinase
KATP	ATP-dependent K+
IRE	Iron response elements
LC-CoA	Long-chain acyl-CoA

LIP	Labile iron pool
Lip-1	Liproxstatin-1
LOOH	Lipid hydroperoxides
LOX	Lipoxygenases
MCFA	Medium chain FA
MDA	Malondialdehyde
MFG	Mito-FerroGreen
MFRN	Mitoferrin
MG	Methylglyoxal
MIN6	Mouse insulinoma, 6th subclone
MnSOD	Manganese superoxide dismutase
MODY	Maturity onset diabetes of the young
MSG	Mature secretory granules
MTT	3-(4,5-dimethylthiazol-2-yl)-2,5-diphenyltetrazolium bromide
MUFA	Monounsaturated FA
NADH	Nicotinamide adenine dinucleotide
NADPH	Nicotinamide adenine dinucleotide phosphate
NAFLD	Non-alcoholic fatty liver disease
NaOH	Sodium hydroxide solution
NCDs	Non-communicable diseases
NF-κB	Nuclear factor-kappa B
NGT	Normal glucose tolerance
NOX	NADPH oxidase
OA	Oleic acid
O-GlcNAc protein	O-linked N-acetylglucosamine
OMM	Mitochondrial outer membrane
p38 MAPK	P38-mitogen activated protein kinases
PA	Palmitic acid
PBS	Phosphate buffered saline

PC1/3	Prohormone convertases 1/3
PC2	Prohormone convertases 2
PDX1	Pancreatic and duodenal homeobox factor 1
PERK	Protein kinase R-like ER kinase
PI	Pseudoislets
PI	Propidium iodide
PI3K	Phosphatidylinositol 3-kinase
PKC	Protein kinase C
PNDM	Permanent neonatal diabetes mellitus
PUFA	Polyunsaturated FA
PUFA-PL	PUFA-containing phospholipids
RAGE	Receptor for AGE
RER	Rough endoplasmic reticulum
RNS	Reactive nitrogen species
ROS	Reactive oxygen species
RRP	Readily releasable poold
SCD	Stearoyl-CoA-desaturase
SCFA	Short chain FA
SCID	Severe combined immunodeficient
SD	Standard diet
SDS	Sodium dodecyl sulfate
SERCA	Sarco-ER Ca^{2+} ATPase
SFA	Saturated FA
SG	Secretory granules
SGLT2	Sodium-glucose cotransporter 2
SREBP1	Sterol regulatory element-binding protein 1
STZ	Streptozotocin
SV40T	Simian virus 40T
T1DM	Type 1 Diabetes mellitus

T2DM	type 2 Diabetes mellitus
TAM	4-hydroxytamoxifen
t-BHP	tert-butyl hydroperoxide
TCA cycle	Tricarboxylic acid cycle
Tf	Transferrin
TfR1	Transferrin receptor protein 1
TGF-β	Transforming growth factor beta
TLR4	Toll-like receptor 4
TNDM	Transient neonatal diabetes mellitus
TNF-α	Tumor necrosis factor alpha
TRAF2	TNF receptor associated factor 2
Trx	Thioredoxin
TXNRD1	Thioredoxin reductase 1
TZD	Thiazolidinediones
UDP-NAcGlcNH$_2$	UDP-N-acetylglucosamine
UTR	Untranslated region
VDAC1	Voltage-dependent anion channel 1
VDCC	L-type voltage dependent Ca^{2+} channels
VLCFA	Very long chain FA
WHO	World Health Organization
WT	Wild type
xCT	Cystine/glutamate antiporter SLC7A11
ZnT8A	Zinc transporter 8 autoantibodies

1 Introduction

1.1 Pancreatic islets and β cells

1.1.1 Pancreatic islets

The pancreas consists of two tissue parts that are crucial for regulating blood glucose levels as well as splanchnic secretion (endocrine) and producing and secreting digestive enzymes (exocrine). The exocrine portion is mainly composed of acinar cells and ducts. Acinar cells are responsible for secreting digestive enzymes, which are mixed with bicarbonate, sodium, potassium, chloride ions, and water secreted by the ductal epithelial cells, collectively known as pancreatic juice (Pandol, 2010). The endocrine portion is pancreatic islets, also known as islets of Langerhans, which were discovered by Dr. Paul Langerhans in 1869 (Langerhans, 1869). There are glucagon-secreting α cells, insulin-secreting β cells, pancreatic polypeptide-secreting pp cells, somatostatin-secreting δ cells, and gastrin-secreting ε cells in pancreatic islets.

There are about (1-2) x10^6 islets in the human pancreas, which only accounts for about 1-2% of the total mass of the pancreas (Atkinson et al., 2020). Each islet contains about 2000-4000 cells (Kulkarni, 2004). Slightly different proportions of different cell types in islets of humans and mice have been found. β cells account for the largest proportion, about 50-75% of islet cell mass in humans and 60-80% in mice, followed by α cells at 20-35% of islet cell mass in humans and 15-20% in mice. In both mice and humans, δ cells are less than 10% of islet cell mass, and pp cells and ε cells are less than 1% of islet cell mass (Figure 1) (Bonner-Weir et al., 2015; Steiner et al., 2010). However, there are differences in the distribution of cells within human and mouse islets. Human islets exhibit a random distribution of cells, while mouse islets have a core of β cells surrounded by α cells and δ cells located at the periphery (Figure 1) (Steiner et al., 2010; Dolenšek et al., 2015).

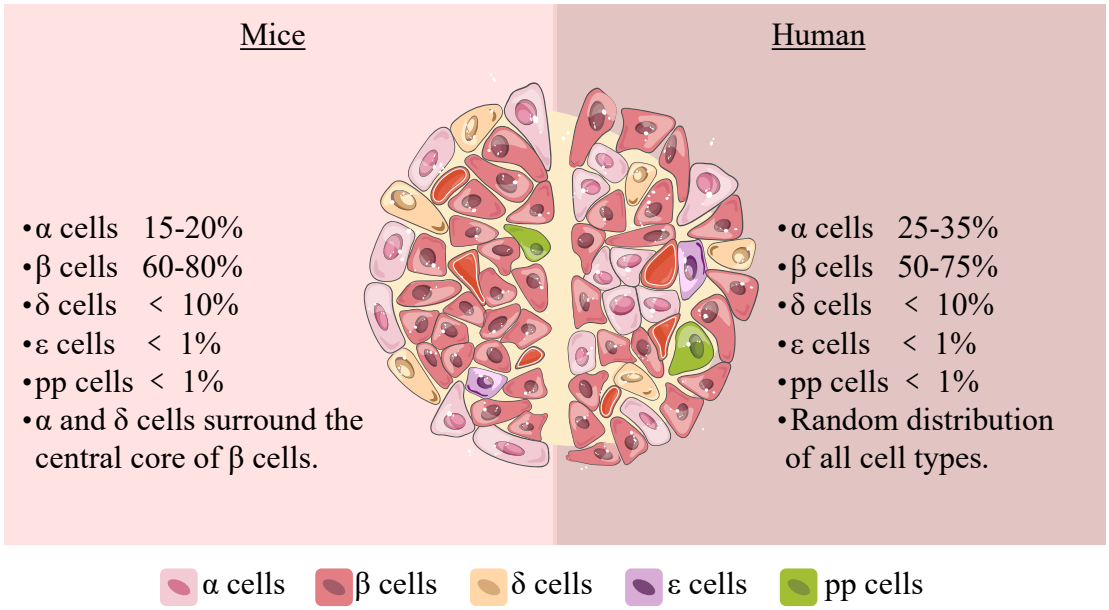

Figure 1 Architecture of human and mice islets. Cell composition and distribution of the islets of Langerhans within the pancreas in mice (left) and humans (right). In mice, α and δ cells are distributed at the periphery of the islets, while β cells are distributed in the islet core; in humans, α and β cells are distributed throughout the islets. The figure was partly generated using Servier Medical Art, provided by Servier.

1.1.2 Pancreatic β cells

1.1.2.1 Biosynthesis of insulin

β cells are responsible for the biosynthesis, storage, and secretion of insulin, which is essential for maintaining blood glucose levels. Insulin biosynthesis begins with the transcription of the insulin gene into mRNA, followed by translation into preproinsulin. Preproinsulin is then processed to proinsulin in the rough endoplasmic reticulum (RER), transported to the Golgi complex, and packaged into immature secretory granules (ISG) (Orci et al., 1984). As the ISG acidifies, the properly folded proinsulin is cleaved into insulin and c-peptide by prohormone convertases 1/3 (PC1/3) and PC2 (Orci et al., 1986; Rhodes and Halban, 1987). Subsequently, during the maturation of secretory granules (SG), insulin monomers are co-crystallized with zinc and calcium to form insulin

hexamers and stored in mature secretory granules (MSG) (Hill et al., 1991). Most insulin SGs are located in the cytoplasm and need transport to the cell membrane before release. A small number of them are pre-docked near the cell membrane, also known as the "readily releasable pool" (RRP), which may explain the "biphasic secretion" pattern of glucose-induced insulin (Rutter, 2001; Straub and Sharp, 2002; Hou et al., 2009) (Figure 2).

1.1.2.2 Mechanisms of insulin secretion

Glucose, the major stimulant, regulates both the biosynthesis of proinsulin and the release of insulin. The biosynthesis of proinsulin is triggered by glucose concentrations ranging from 2 to 4 mM, while the release of insulin is triggered by glucose concentrations ranging from 4 to 6 mM (Ashcroft, 1980). This ensures the storage of insulin and its prompt release when stimulated by glucose. In response to the rise in blood glucose level, glucose enters β cells through glucose transporters (GLUT) (Thorens, 1992). Then the cytosolic glucose is phosphorylated and metabolized through glycolysis, resulting in the formation of pyruvate, nicotinamide adenine dinucleotide (NADH), and adenosine triphosphate (ATP). Pyruvate is incorporated into the Krebs cycle in the mitochondria to generate more ATP, which, together with ATP generated from glycolysis, leads to the increase of the ATP/ADP ratio. This causes the closure of ATP-dependent K+ (KATP) channels, depolarizing the plasma membrane, and the opening of L-type voltage-dependent Ca^{2+} channels (VDCCs), which allow influx of Ca^{2+} ions, triggering exocytosis of insulin granules from the β cell (Henquin, 2000). Subsequently, the second phase of insulin secretion requires the recruitment of insulin SG from the cytoplasm to the plasma membrane (Bratanova-Tochkova et al., 2002; Straub and Sharp, 2002; Hou et al., 2009). In addition to glucose, β cells also respond to other nutrients (amino acids, fatty acids, ketone bodies) and multiple neurohormones, as well as sympathetic and parasympathetic nerves (Fu et al., 2013; Kong et al., 2023) (Figure 2).

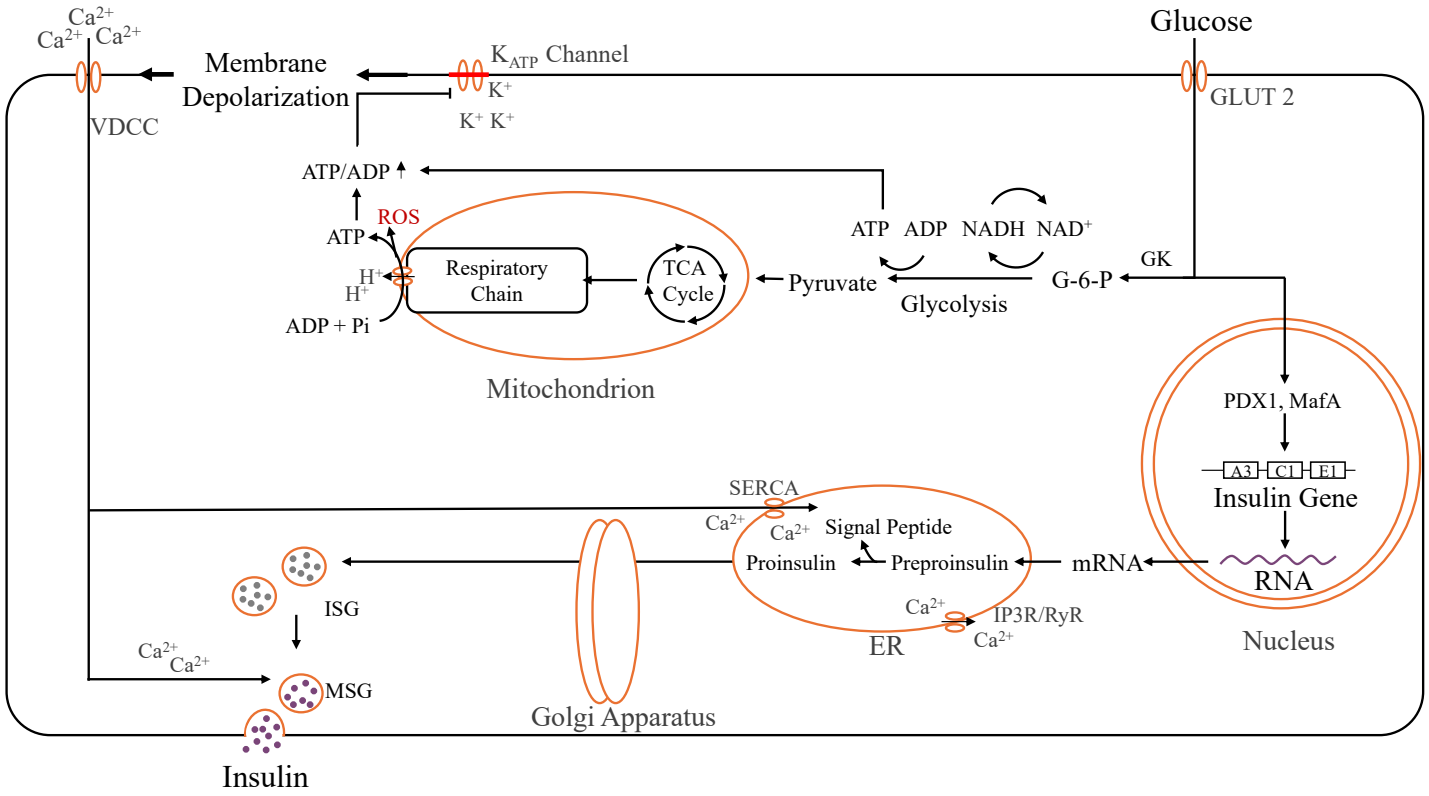

Figure 2 Insulin synthesis and secretion in pancreatic β cells. The biosynthesis of insulin begins with the transcription of the insulin gene in the nucleus and the translation of mRNA into preproinsulin. Followed by translocation into the ER, where preproinsulin removes the signal peptide to produce proinsulin. Subsequently, in the Golgi apparatus, it is packaged into SG. Glucose is transported to β cells via GLUT and then phosphorylated by GK to G-6-P, entering the glycolysis pathway to generate pyruvate, NADH, and ATP. Then pyruvate enters the TCA cycle to produce ATP in the mitochondria, then together with ATP produced by glycolysis, causing an increase of the ATP/ADP ratio, leading to the close of the K_{ATP} channels and depolarization of the membrane, resulting in the open of VDCCs and allowing an influx of Ca^{2+} ions, triggering exocytosis of insulin granules from the β cell.

1.2 Diabetes Mellitus

1.2.1 Definition and complications

Diabetes mellitus (DM) is a group of metabolic disorders caused by a combination of genetic and environmental factors, characterized by chronic hyperglycemia due to defective insulin secretion and/or defective insulin action. It is considered to be one of the most prevalent and severe chronic non-communicable diseases (NCDs). Globally, the prevalence of DM is still rising. As reported by the International Diabetes Federation (IDF), the number of adults living with DM worldwide has increased by nearly 47%, from 366 million in 2011 to 537 million in 2021 (Whiting et al., 2011; Sun et al., 2022). With the aging of the population and the rising of obesity rates, the number of DM patients is expected to climb to 783 million in 2045 (Sun et al., 2022).

Symptoms of DM include polyuria due to osmotic diuresis in response to elevated blood glucose, followed by thirst and polydipsia; weight loss and growth retardation due to impaired glucose utilization by peripheral tissues, increased lipolysis, and a negative balance of protein metabolism, also known as "three more and one less," i.e., polyuria, polydipsia, polyphagia, and weight loss (American Diabetes Association, 2009).

Acute severe metabolic disorders caused by uncontrolled DM include hypoglycemia, diabetic ketoacidosis (DKA), and hyperosmolar hyperglycemic syndrome (HHS) (Fasanmade et al., 2008; Pasquel and Umpierrez, 2014; Umpierrez and Korytkowski, 2016). However, the main cause of DM morbidity and mortality is chronic complications involving micro/macrovascular and nervous systems (American Diabetes Association, 2009; Vijan, 2010). The main manifestations are diabetic nephropathy, diabetic retinopathy or diabetic cardiomyopathy caused by microvascular disease (Bloomgarden, 2005; Cheung et al., 2010; Dillmann, 2019); coronary heart disease and ischemic or hemorrhagic cerebrovascular disease caused by macrovascular disease

(Malmberg et al., 2000; Zhou et al., 2014); cognitive dysfunction caused by central nervous system disease (Zilliox et al., 2016); sensory ataxia and neuropathic arthropathy caused by peripheral neuropathy (Bansod et al., 2023); delayed gastric emptying, diarrhea, constipation, tachycardia, orthostatic hypotension, silent myocardial ischemia, bladder emptying difficulties and sexual dysfunction caused by autonomic neuropathy (Vinik et al., 2003; Nichols et al., 2009; Fox et al., 2004; Lee et al., 2004); Diabetic foot caused by the combination of peripheral neuropathy and peripheral vascular disease (Boulton, 2008; Volmer-Thole and Lobmann, 2016).

Furthermore, macular degeneration, cataracts, glaucoma, periodontal disease, skin lesions, as well as depression and anxiety are also prevalent in individuals with DM (Browning et al., 2018; Mrugacz et al., 2023; Tang et al., 2023; Genco and Borgnakke, 2020; Lima et al., 2017; Meurs et al., 2016). Chronic non-alcoholic fatty liver disease (NAFLD) is also considered to be a neglected complication of DM (Akshintala et al., 2019; Bril and Cusi, 2016; Cusi, 2020a, 2020b). Additionally, studies indicate a higher incidence and mortality of colorectal cancer, liver cancer, pancreatic cancer, and breast cancer among individuals with DM (Song, 2021; Ling et al., 2023). Diabetic foot ulcers are the leading cause of non-traumatic amputations in DM (Singh and Chawla, 2006). Diabetic nephropathy is a common cause of end-stage renal failure and the leading cause of death in type 1 DM (T1DM) (Bjornstad et al., 2014). Cardiovascular diseases (CVDs) have long been considered the leading cause of death in patients with type 2 DM (T2DM), but over the past 30 years, the mortality of cardiovascular disease has declined worldwide due to the combined effects of improved diet and lifestyle, as well as improved survival rates after myocardial infarction (Mensah et al., 2017). More and more studies have shown that cancer has overtaken cardiovascular disease to become the leading cause of death in T2DM (Song, 2021; Ling et al., 2023).

1.2.2 Classification, etiology and diagnosis of DM

DM is categorized based on genetics, metabolomics, pathophysiology, and other characteristics. T1DM, T2DM, gestational diabetes mellitus (GDM), and other uncommon forms of DM are mostly included. The World Health Organization (WHO) updated and added unclassified and hybrid forms of DM in 2019 (World Health Organization, 2019).

T1DM is characterized by the progressive destruction of β cells, resulting in absolute insulin deficiency. Genetic and environmental factors as well as autoimmune are involved in its pathophysiology. In identical twins, the comorbidity rate of T1DM ranges between 30% and 40% (Verge et al., 1995; Redondo et al., 2001; Jerram and Leslie, 2017). The genetic susceptibility of T1DM includes human leukocyte antigens (HLA) genes and non-HLA genes. It is known that the HLA gene located on the short arm of chromosome 6 is the major gene, and the others are minor genes. Specific HLA-DR3-DQ2/DR4-DQ8 are associated with an increased risk of the onset of T1DM (Undlien et al., 2001; Cucca et al., 2001; Pietropaolo et al., 2002). Environmental factors such as viral infection, chemicals, and dietary factors are likely to contribute to the onset of islet autoimmunity (Rewers and Ludvigsson, 2016). Moreover, T1DM is frequently associated with autoimmunity, anti-islet autoantibodies can be detected in 70-90% of patients with newly diagnosed T1DM, including islet cell autoantigen (ICA) (Bottazzo et al., 1974), insulin autoantibody (IAA) (Palmer et al., 1983), glutamic acid decarboxylase autoantibodies (GADA) (Baekkeskov et al., 1990), tyrosine phosphatase-like protein 2 autoantibodies (IA-2A) (Lan et al., 1994), and zinc transporter 8 autoantibodies (ZnT8A) (Wenzlau et al., 2007) and others, which can serve as the marker of T1DM and assist in classification and guiding treatment. Furthermore, abnormal cellular immunity plays a crucial role in the pathogenesis of T1DM, with T lymphocytes considered to be the final executors of β cell destruction (Burrack et al., 2017).

T2DM is a complex polygenic inheritance disorder that also develops from the interaction between genetic and environmental factors, with a heritability of 30-70% (Almgren et al., 2011). It is the most common type of DM, accounting for 90-95% of DM cases

(Sun et al., 2022). However, the exact etiology and pathogenesis of T2DM are not fully understood. Multiple independent genome-wide association studies (GWAS) have shown that more than 500 independent loci are associated with T2DM by the end of 2022 (Kreienkamp et al., 2023). Environmental factors such as lifestyle, aging, stress, and chemical factors work together with genetic factors and are closely related to the onset and development of T2DM. Insulin resistance (IR) and β cell dysfunction are key mechanisms in the development of T2DM. In addition, pancreatic α cell dysfunction and glucagon-like peptide-1 (GLP-1) secretion defects also contribute significantly to the development of T2DM (Moon and Won, 2015).

Hyperglycemia first detected in pregnancy is divided into DM in pregnancy and GDM, and the prognosis of DM in pregnancy is equivalent to T2DM diagnosed before pregnancy. The diagnostic criteria for DM in pregnancy are consistent with those of non-pregnant adult DM, whereas those for GDM are lower (Colagiuri et al., 2014).

New updated hybrid forms of DM include slowly evolving immune-mediated DM of adults (Chiu et al., 2007) and ketosis-prone T2DM (Choukem et al., 2013), and those that cannot be well-defined at the time of diagnosis may be temporarily categorized as unclassified DM (World Health Organization, 2019). The classification of DM encompasses not only the various etiologies of DM but also the clinical stages of disease progression, thus providing guidance for diagnosis and treatment.

The diagnosis of DM is based on abnormally elevated blood glucose. Diagnostic clues include symptoms of DM, complications of DM, history of IGR, overweight or obesity, family history of T2DM, history of GDM, etc. The classification and diagnostic criteria of DM are summarized in Table 1.

Table 1 Classifications and diagnostic criteria of DM

Classifications and Diagnostic Criteria of DM
T1DM Absolute insulin deficiency caused by autoimmune destruction of pancreatic β cells
T2DM Gradual loss of functional pancreatic β cells and IR
Hybrid forms of DM Slowly evolving immune-mediated DM of adults: autoimmune destruction of pancreatic β cells and IR Ketosis prone T2DM: reversible β cell and α cell dysfunction but common prone to ketosis.
Other specific types Monogenic DM Monogenic defects of β cell function: MODY, PNDM, TNDM, and genetic syndromes. Monogenic defects in insulin action: Type A IR, leprechaunism, Rabson-Mendenhall syndrome, Lipoatrophic DM and others Diseases of the exocrine pancreas: Pancreatitis, Trauma/pancreatectomy, Neoplasia, Cystic fibrosis, Hemochromatosis, Fibrocalculous pancreatopathy and others Endocrine disorders: Cushing's syndrome, Acromegaly, Phaeochromocytoma, Glucagonoma, Hyperthyroidism, Somatostatinoma, Aldosteronoma and others Drug- or chemical-induced: Glucocorticoids, Thyroid hormone, Thiazides, Pentamidine, Dilantin, Nicotinic acid, Pyrinuron, Interferon-alpha, α/β-adrenergic agonists and others Infections: Congenital rubella, Cytomegalovirus, Adenovirus, Mumps and others Uncommon specific forms of immune-mediated DM: "stiff-man" syndrome, Anti-insulin receptor antibodies and others Other genetic syndromes sometimes associated with DM: Down's syndrome, Friedreich's ataxia, Huntington's chorea, Klinefelter's syndrome, Bardet-Bieldel syndrome, Myotonic dystrophy, Porphyria, Prader-Willi syndrome, Turner's syndrome and others
Unclassified DM Temporary classification until a definite diagnosis
Hyperglycemia first detected during pregnancy DM in pregnancy: defined by the same criteria as in non-pregnant persons GDM: defined by lower glucose cut-off points than those for DM
Diagnostic Criteria
Diagnostic criteria for DM: fasting plasma glucose ≥ 7.0 mmol/L or 2-hour post-load plasma glucose ≥ 11.1 mmol/L or Hba1c ≥ 48 mmol/mol Diagnostic criteria for GDM: fasting plasma glucose 5.1–6.9 mmol/L or 1-hour post-load plasma glucose ≥ 10.0 mmol/L or 2-hour post-load plasma glucose 8.5–11.0 mmol/L

MODY: maturity onset diabetes of the Young; PNDM: Permanent neonatal DM; TNDM: Transient neonatal DM.

In general, the natural history of DM includes the progression from normal glucose tolerance (NGT) to impaired glucose regulation (IGR), and then to the stage of DM, with the phases progressing from not requiring insulin treatment to requiring insulin to control blood glucose, and finally to requiring insulin to survive (Alberti and Zimmet, 1998). T1DM and DM caused by drugs like pyrinuron (Vacor) that permanently destroy pancreatic β cells will inevitably develop to the stage where insulin is required to survive (Alberti and Zimmet, 1998). Patients with T2DM and other types of DM may develop from one stage to another, but not everyone will go through all stages (Ramlo-Halsted and Edelman, 1999; Alejandro et al., 2015).

1.2.3 Pathophysiology of T2DM

IR and β cell dysfunction interact with each other and play an important role in the pathogenesis of T2DM. β cell dysfunction impairs insulin secretion, while IR leads to reduced glucose uptake, further stimulating insulin secretion. Subsequently, this dysfunctional feedback loop between insulin action and insulin secretion leads to hyperglycemia (Stumvoll et al., 2005). β cell dysfunction is considered to be the essential determinant of T2DM (Ashcroft and Rorsman, 2012). Oxidative damage, endoplasmic reticulum (ER) stress, and inflammation are the initiators of β cell dysfunction and also lead to further deterioration. The mechanism of IR is still unclear, excess lipid availability and inflammation are the two main hypotheses. Many theories, including ectopic lipid accumulation, the glucose-fatty acid cycle, the hexosamine biosynthesis pathway, diacylglycerol (DAG)-protein kinase C (PKC) pathway, and the ceramide hypothesis, have been proposed as the main mechanisms leading to IR caused by lipid excess (Lee et al., 2022). Moreover, ER stress and inflammation intersect and complement lipid overload, leading to the development of IR (Boden, 2009). Although the mechanism of β cell dysfunction and IR has not yet been elucidated, oxidative distress, ER stress, and inflammation are jointly involved in the occurrence and development of β cell

dysfunction and IR, creating a vicious cycle and ultimately leading to further aggravation of T2DM.

1.2.3.1 Oxidative distress

The imbalance between pro-oxidants and antioxidants was initially referred to as oxidative stress (Sies, 1985). However, in order to distinguish between cells changing their behavior in response to stimuli and cells or tissue dysfunctioning in response to stimuli, the concepts of "oxidative eustress" and "oxidative distress" were introduced (Sies, 2015; Sies et al., 2017; Sies and Jones, 2020). Oxidative distress is triggered by the accumulation of reactive oxygen species (ROS) and leads to macromolecular damage and cell death through nonspecific and irreversible protein oxidation.

ROS are physiologically generated during the metabolism of β cells from mitochondria, ER, peroxisomes, and cytoplasm and are essential in the process of signal transduction (Roma and Jonas, 2020; Leloup et al., 2009). However, excessive ROS can trigger β cell dysfunction. In DM, such an excess of ROS can arise through the interaction of glucotoxicity, lipotoxicity, and inflammatory cytokines. Hyperglycemia-induced ROS generation pathways include the polyol pathway, glycolysis pathway, DAG-PKC pathway, hexosamine route, enhanced formation of advanced glycation end products (AGEs), and deactivation of the insulin signaling (Ighodaro, 2018) (Figure 3). The absorption of free fatty acid (FFA) in β cells is mediated by cluster of differentiation 36 (CD36) and G protein-coupled receptors (GPR40, GRP119, GPR120) (Ly et al., 2017; Morgan and Dhayal, 2009). Among them, CD36 (Pepino et al., 2014), GPR40 (Itoh et al., 2003), GPR120 (Hirasawa et al., 2005) are all long-chain fatty acid (LCFA) receptors. The potential mechanism of FFA-induced ROS generation is still unclear. Possible mechanisms include FFA-induced peroxisomal β-oxidation (Elsner et al., 2011), mitochondrial β-oxidation (Koshkin et al., 2003), stimulation of glutathione depletion (Schönfeld and Wojtczak, 2007), and activation of NADPH oxidase (Morgan et al.,

2007; Koulajian et al., 2013) (Figure 4). Among them, peroxisomal β-oxidation is considered to be the major site, while mitochondria are the minor site (Elsner et al., 2011). Inflammatory cytokines are also involved in promoting ROS and reactive nitrogen species (RNS) generation through various mechanisms (Kowluru, 2020; Pugliese et al., 2023).

In addition to disrupting the ER and stimulating proinflammatory cytokines, increased ROS and RNS, on the one hand, directly damage and oxidize DNA, proteins, and lipids, and on the other hand, inhibit the expression and activity of insulin transcription factors including MafA and pancreatic and duodenal homeobox factor 1 (PDX1) and also activate multiple pathways such as nuclear factor-kappa B (NF-κB), c-Jun N-terminal kinase (JNK), and p38-mitogen-activated protein kinases (p38 MAPK), eventually inducing β cell dysfunction and death (Yaribeygi et al., 2020). Furthermore, oxidative distress induces IR by inducing β cell dysfunction, reducing the expression and localization of GLUT-4, and impairing the insulin signaling pathway (Yaribeygi et al., 2020).

1.2.3.2 Endoplasmic reticulum distress

ER stress occurs when protein misfolding in the ER accumulation exceeds the threshold level, which is closely related to oxidative distress. Oxidative distress can induce protein misfolding, which in turn can result in the production of ROS (Cao and Kaufman, 2014). Therefore, hyperglycemia, hyperlipidemia, and cytokines that induce oxidative distress also induce the occurrence of ER stress (Figure 3, Figure 4). In addition, hyperlipidemia also directly causes ER stress through mechanisms that are independent of oxidative distress, including inhibiting sarco-ER Ca^{2+} ATPase (SERCA) responsible for ER Ca^{2+} mobilization; activating inositol 1,4,5-trisphosphate receptors (IP3Rs); and increasing the saturated lipid content of the ER, resulting in damage to the morphology and integrity of the ER, leading to ER stress (Sehgal et al., 2017; Galicia-Garcia et al., 2020) (Figure 4). Moreover, cytokines such as interleukin 1 beta (IL-1β) and interferon-

gamma (IFN-γ) can also induce the occurrence of ER stress in β cells through mechanisms unrelated to oxidative distress, such as consuming ER Ca^{2+} (Cardozo et al., 2005) (Figure 4). And due to the progression of DM, the demand for synthesis and secretion of insulin by the remaining β cells continues to increase, and the pressure of ER biosynthesis increases, which also drives the occurrence of ER stress.

ER stress interferes with β cell processing and storage of insulin by affecting molecular chaperones and disulfide bond formation and also causes β cell apoptosis via mechanisms such as protein kinase R-like ER kinase/activating transcription factor 4 (PERK/ATF4)-mediated C/EBP homologous protein (CHOP) activation and inositol-requiring enzyme 1α/TNF receptor-associated factor 2/apoptosis signal-regulating kinase 1 (IRE1α/TRAF2/ASK1)-mediated JNK activation (Papa, 2012). In addition, the unfolded protein response in β cells also reduces the transcription and translation of insulin (Walter and Ron, 2011).

1.2.3.3 Inflammation

Increased levels of the inflammatory marker c-reactive protein (CRP) are linked to β cell dysfunction and IR as T2DM progresses (PrayGod et al., 2021). Elevated CRP promotes tissue damage and accelerates apoptosis by inducing proinflammatory mechanisms involving Toll-like receptor 4 (TLR4), NF-κB, transforming growth factor beta (TGF-β), and extracellular signal-regulated kinase (ERK) pathways (Sun et al., 2019; Zhang et al., 2019). Additionally, inflammation and oxidative distress are also closely related. Chronic inflammation leads to continuous ROS production, which leads to the occurrence of oxidative distress (Luc et al., 2019; Oguntibeju, 2019). In turn, ROS stimulate the expression of proinflammatory cytokines by stimulating the activation of transcription factors such as NF-κB and activator protein 1 (AP-1) (Padgett et al., 2013). As well, excess glucose and FFA increase the pressure on pancreatic islets and insulin-sensitive tissues, leading to local production and release of cytokines and chemokines,

and a decrease in IL-1 receptor antagonists (IL-1RA) produced by β cells, leading to tissue inflammation (Donath and Shoelson, 2011). And excessive adipose tissue in T2DM also secretes pro-inflammatory cytokines, further promoting chronic inflammation, ER stress, and oxidative distress (Oguntibeju, 2019; Cardozo et al., 2005). In fact, the effects of chronic inflammation and oxidative distress on β cells are difficult to differentiate.

Meanwhile, pancreatic amyloid deposition, mitochondrial dysfunction, and impaired autophagy are also involved in the occurrence of β cell dysfunction and IR.

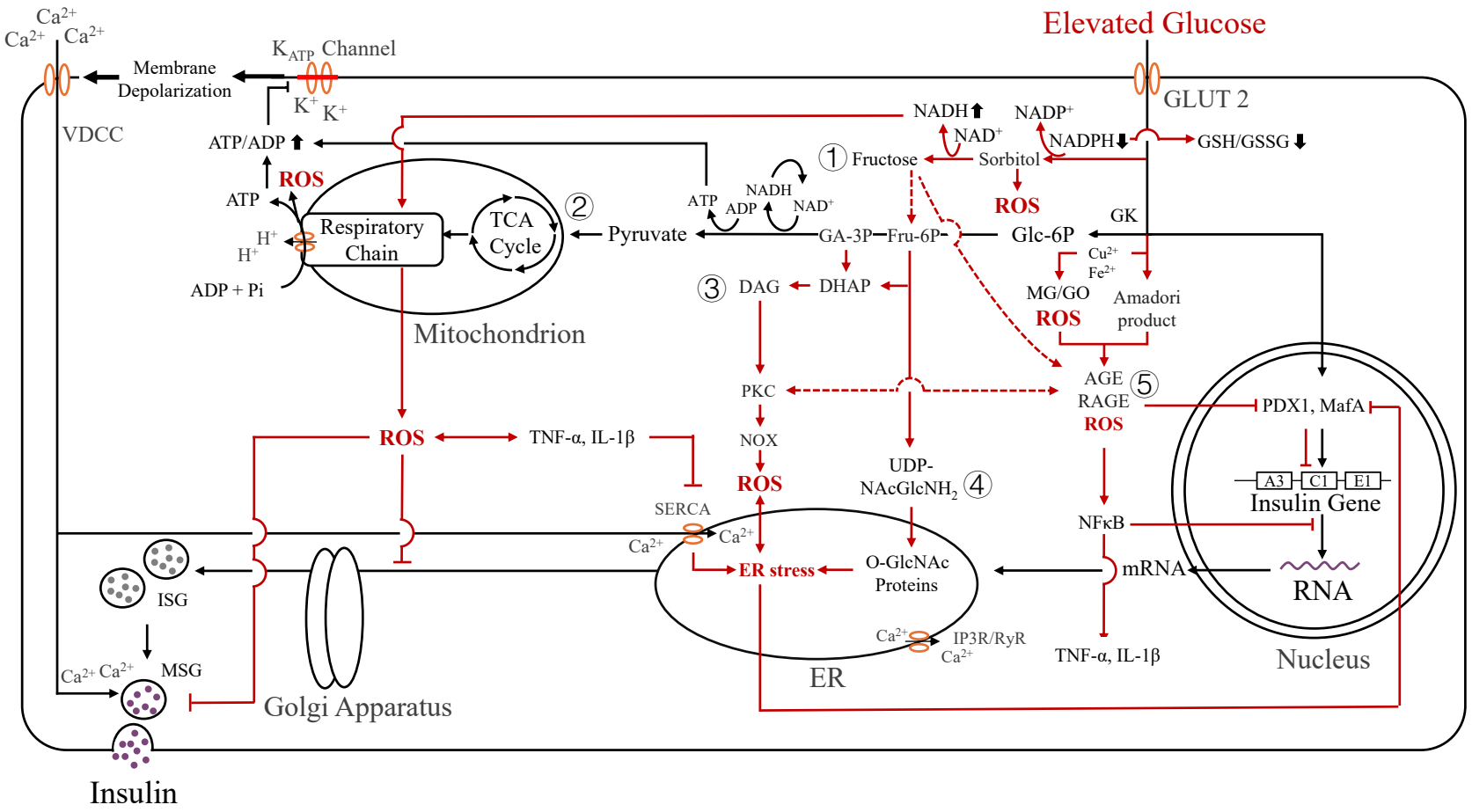

Figure 3 Mechanisms of activation of oxidative distress, ER stress, and inflammation by hyperglycemia in β cells. Glucose metabolism and multiple pathways leading to ROS generation, including 1. polyol pathway; 2. glycolysis pathway; 3. DAG-PKC pathway; 4. hexosamine route; and 5. enhanced formation of AGEs. Excessive ROS generation leads to oxidative distress, ER stress, increases stimulating proinflammatory cytokines, and inhibits the expression and activity of insulin transcription factors, including MafA and PDX1, eventually inducing β cell dysfunction and death.

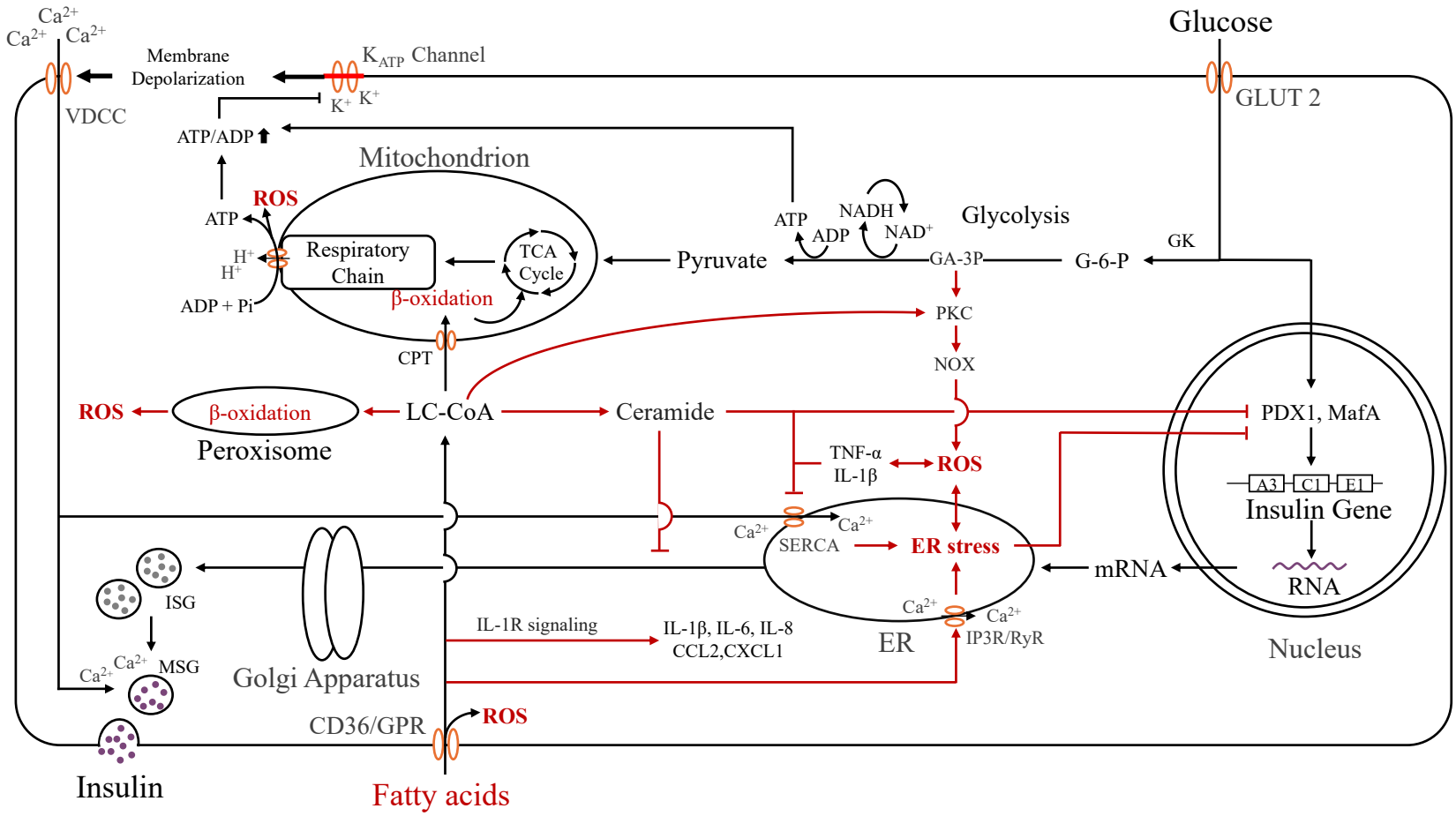

Figure 4 Mechanisms of activation of oxidative distress, ER stress, and inflammation by free fatty acids in β cells. Possible mechanisms of ROS generation induced by FA include peroxisomal β-oxidation, mitochondrial β-oxidation, and activation of NOX. Possible mechanisms of ER stress induced by FA independently of oxidative distress include inhibition of SERCA, activation of IP3R, and induction of ceramide and cytokine production. Cytokines also induce ER stress through mechanisms independent of oxidative distress, such as consumption of ER Ca^{2+}. In addition, FA and cytokines impair insulin gene expression, ultimately leading to β cell dysfunction and death.

1.2.4 Current treatment options and limitations of T1DM and T2DM

Rather than aiming at the underlying cause, current treatment strategies for DM focus on symptom management and prevention of complications. The short-term goal of DM treatment is to control diabetic symptoms and prevent acute severe metabolic disorders by controlling hyperglycemia and related metabolic disorders, while the long-term goal is to prevent and delay the onset and progression of chronic complications. Basic management measures for DM include health education, medical nutrition therapy, exercise therapy, and blood glucose monitoring.

Exogenous insulin supplementation, including subcutaneous injection and insulin pump, remains the most common T1DM treatment strategy (McAdams and Rizvi, 2016; Akil et al., 2021). The common adverse effects of insulin are hypoglycemia and weight gain; thus, for obese T1DM patients who are prone to hypoglycemia and have residual β cell function, combined non-insulin drug therapy may reduce hyperglycemia without increasing the risk of hypoglycemia or other adverse events (Frandsen et al., 2016). Pancreas and islet transplantation can replace exogenous insulin supplementation therapy and normalize metabolic control, but the technology has progressed slowly, and there are still many limitations, which emphasize the need for future research on human islets (Ricordi and Strom, 2004). Pseudoislets aggregated by the EndoC-βH cell line, a human β cell line, provide a good model for future islet transplantation research (Lecomte et al., 2016; Zhou et al., 2024b). In recent years, gene therapy and stem cell therapies have also been found to have potential application value in the treatment of T1DM (Akil et al., 2021).

Drug treatments for T2DM include oral antidiabetics, insulin, incretin mimetics (GLP-1 receptor agonist (GLP-1RA), dipeptidyl peptidase 4 (DPP-4) inhibitors, dual glucose-dependent insulinotropic polypeptide (GIP) and GLP-1RA), and amylin analogs (American Diabetes Association Professional Practice Committee, 2024). Oral

antidiabetics include sulfonylureas and meglitinides, biguanides, thiazolidinediones (TZDs), α-glucosidase inhibitors (AGIs), and sodium-glucose cotransporter 2 (SGLT2) inhibitors (Chaudhury et al., 2017; Padhi et al., 2020). For patients who cannot achieve glycemic control with monotherapy with first-line medication, usually Metformin, combination therapy is recommended; refer to the 2024 American Diabetes Association (ADA) guidelines (American Diabetes Association Professional Practice Committee, 2024). Moreover, drug delivery systems based on nanotechnology have made certain progress in T2DM treatment (Padhi et al., 2020). Other options for T2DM, such as weight loss surgery and pancreas and islet transplantation, are not in routine clinical practice. In addition to drug development, more and more research is focusing on restoring the molecular mechanisms of insulin secretion and action, such as targeting the proliferation, protection, and regeneration of β cells (Basile et al., 2022; Jain et al., 2022; Wagner, 2022), inhibiting inflammatory cytokines (Wagner, 2022), inhibiting glucolipotoxicity (Wagner, 2022), applying antioxidants (Johansen et al., 2005), etc.

By far, there is no treatment that can prevent, halt, or reverse the progression of DM despite the availability of multiple treatment options. However, research into the underlying mechanisms offers potential strategies for preventing, treating, and curing DM.

1.3 Glutaredoxins

1.3.1 Structure, classification and functions of Glutaredoxins

Glutaredoxins (Grxs) were found to belong to the thioredoxin (Trx) protein superfamily and have a classic structural motif called the Trx fold, which consists of a four-stranded β-sheet and three α-helices. A common active site motif, Cys-XX-Cys/Se, has been identified and is able to bind glutathione (GSH) (Martin, 1995; Bushweller et al., 1994). Mammalian Grxs include dithiol/class I Grxs (Cys-X-X-Cys) with two cysteines (Cys) in the active site and monothiol/class II Grxs (Cys-X-X-Ser) with only one Cys in the

active site (Lillig et al., 2008). Dithiol Grxs catalyze cellular redox reactions via both dithiol and monothiol mechanisms (Figure 5).

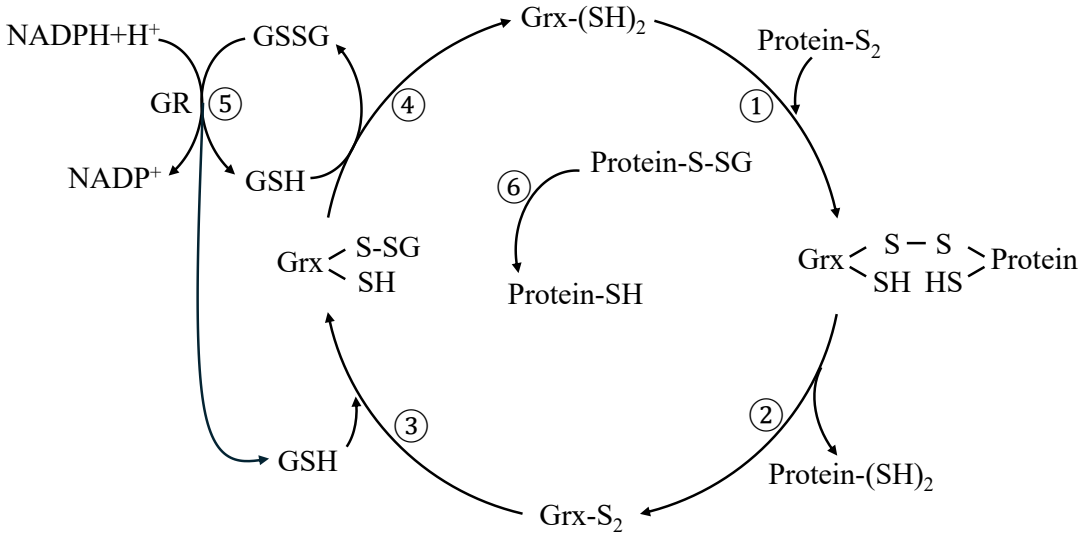

Figure 5 Dithiol and monothiol reaction mechanisms of Grxs. In the dithiol reaction mechanisms, Grxs catalyze the reversible reduction of protein disulfides utilizing both of their active site cysteinyl residues (reactions 1–4). In the monothiol reaction mechanisms, Grxs catalyze deglutathionylation reactions utilizing only the N-terminal active site (reactions 6). Either way, the resulting GSSG is reduced to form GSH by GR using electron transfer from NADPH, which in turn reduces the oxidized Grxs (reactions 5). Modified from (Ogata et al., 2021).

In the dithiol mechanism (also known as disulfide exchange reaction) (Figure 5 (1-4)), the N-terminal active site Cys executes nucleophilic substitution, thereby initiating the formation of a mixed disulfide bond between Grx and the substrate (protein with a disulfide bond) (Figure 5 (1)), which is then reduced by the C-terminal active site Cys, releasing the reduced target protein and oxidized Grx (Grx-S2) (Figure 5 (2)). One of the disulfide bonds is reduced by one molecule of GSH to form Grx-S-SG (Figure 5 (3)), which is then reduced by a second molecule of GSH (Figure 5 (4)) (Begas et al., 2017). The target protein of the monothiol mechanism (i.e., deglutathionylation reaction) is glutathionylated (p-S-SG), and only the N-terminal Cys is involved, generating a reduced target protein and Grx-S-SG (Figure 5 (6)), followed by the reduction of Grx

by a molecule of GSH as in the dithiol mechanism (Figure 5 (4)). Subsequently, the resulting oxidized glutathione (GSSG) is reduced by electron transfer from NADPH via glutathione reductase (GR) (Figure 5(5)) (Fernandes and Holmgren, 2004). In addition, when GSSG is temporarily increased, Grx can catalyze protein glutathionylation at the expense of GSSG (Trnka et al., 2020).

So far, Grx1, 2, 3, and 5 have been described in humans. The dithiol Grx1 is localized in the cytoplasm, mitochondria, and nucleus and can also be secreted into the extracellular space (Pai et al., 2007; Lundberg et al., 2004). In addition to being involved in thiol-disulfide exchange, it also plays a role in cell differentiation, apoptosis, and regulating the proteins and signaling pathways such as ASK-1/Jun kinase kinase (JNKK)/JNK-1, NF-κB, AP-1, glyceraldehyde 3-phosphate dehydrogenase (GAPDH)/Sirtuin-1, protein kinase B-forkhead box (Akt-FoxO), and protein tyrosine phosphatase 1B (PTP1B) (Barrett et al., 1999, p.215; Hirota et al., 2000; Murata et al., 2003; Reynaert et al., 2006; Lekli et al., 2010; Mustafa Rizvi et al., 2021). Besides, studies have shown that Grx1 alleviates high glucose-induced vascular-, cardiac-, and neuro-toxicity (Lekli et al., 2010; Li et al., 2014; Qi et al., 2016; Gorelenkova Miller et al., 2016), and is therefore of great significance in DM and its complications (reviewed in Ref. (Zhou et al., 2024a)).

The dithiol Grx2 includes Grx2a, which is localized in mitochondria and ubiquitously expressed, and Grx2b and Grx2c, which are localized in the nucleus and cytoplasm but exclusively expressed in testis and tumor cells (Lundberg et al., 2001; Lönn et al., 2008; Hudemann et al., 2009). Similar to Grx1, Grx2 has also been shown to regulate signaling pathways such as Ras/Phosphatidylinositol 3-kinase (PI3K)/Akt, JNK/AP-1, NF-κB, and glycogen synthase kinase 3β (GSK-3β) (Daily et al., 2001; Wohua and Weiming, 2019). Overexpression of Grx2 showed reduced sensitivity to apoptosis (Enoksson et al., 2005), as well as protective effects in the heart (Diotte et al., 2009, p.2), kidney (Godoy et al., 2011b, p.6), and nerve (Karunakaran et al., 2007). In contrast,

silencing or knockout of Grx2 led to increased sensitivity to apoptosis *in vitro* (Lillig et al., 2004), cardiac hypertrophy and hypertension (Kanaan et al., 2018), metabolic dysfunction and weight gain (Scalcon et al., 2022), and premature age-dependent cataracts(Wu et al., 2014) *in vivo*. In addition, Grx2 is able to form a 2Grx2-[2Fe–2S]-2GSH dimer. The dimer is inactive but may play a role in iron homeostasis as the deletion of Grx2 leads to a reduction in the mRNA expression of several FeS proteins that function as subunits of complex I, as well as a decrease in bound iron in liver mitochondria (Scalcon et al., 2022). Under oxidative distress conditions, the dimer is activated upon monomerization and has therefore been described as a redox sensor (Lillig et al., 2005; Berndt et al., 2007) (Figure 6).

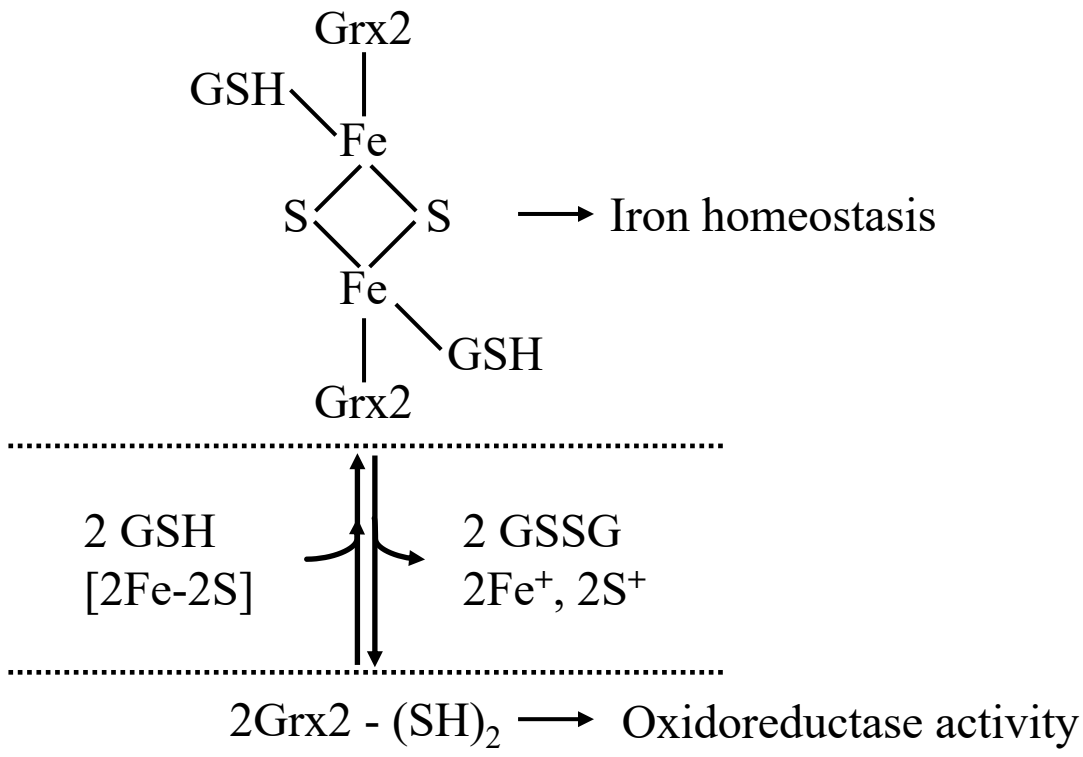

Figure 6 Conversion between 2Grx2-[2Fe-2S]-2GSH dimers and Grx2 monomers and their possible physiological roles. The Grx2 dimer consists of two Grx2 monomers, one [2Fe–2S] cluster, and two GSH with no oxidoreductase activity but may be responsible for the transfer of FeS cluster. Under oxidative distress conditions, the

oxidoreductase activity of Grx2 is activated upon dissociation of [2Fe–2S] cluster and oxidation of GSH.

The monothiol Grx3 is located in the cytosol under reducing conditions. In contrast, under oxidative distress conditions, Grx3 is subject to reversible nuclear aggregation and is strongly correlated with increased cellular ROS production and depletion of reduced GSH (Babichev and Isakov, 2001; Pham et al., 2015). There are three highly conserved domains in Grx3, namely an N-terminal Trx homology domain (HD) and two Grx HDs; each Grx contains an active site C-G-F-S (Isakov et al., 2000; Babichev et al., 2001). Overexpression of Grx3 inhibits the activation of JNK/AP-1 and NF-κB pathways when overexpressed in T cells (Witte et al., 2000), inhibits cellular sensitivity to oxidants and reduces ROS production in Hela cells (Pham et al., 2015). In contrast, the knockdown of Grx3 leads to increased ROS in Jurkat T cells treated with hydrogen peroxide (Pandya et al., 2019) and susceptibility of Hela cells to oxidative distress (Pham et al., 2015). In addition, Grx3 is upregulated in hypertrophic cardiomyopathy (HCM) (Jeong et al., 2006, 2008; Cha et al., 2008) and several cancer types (Cha and Kim, 2009; Ohayon et al., 2010; Qu et al., 2011).

Similar to Grx2, Grx3 can also form a 2Grx3-2[2Fe–2S]-4GSH dimer (Figure 7). Grx3 uses the active sites of its two Grx HDs to bind to two [2Fe–2S] clusters, and the GSH non-covalently binds to Grx3 (Haunhorst et al., 2010). In Hela cells, knockdown of Grx3 was shown to increase cellular iron and decrease activities of several iron-dependent proteins, indicating an important role in iron homeostasis (Haunhorst et al., 2013).

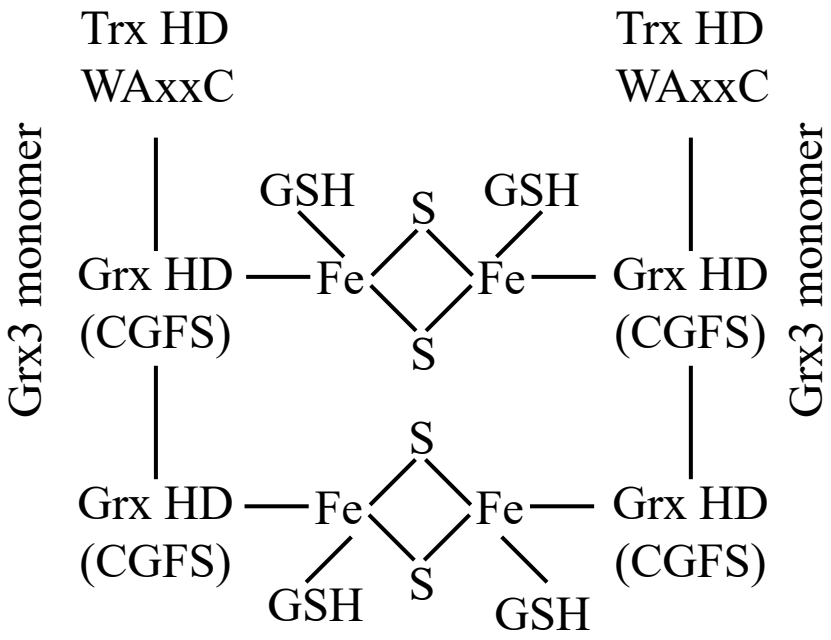

Figure 7 Scheme of Grx3 monomer and 2Grx3-2[2Fe–2S]-4GSH dimer. The Grx3 monomer consists of one Trx HD and two Grx HDs, and the dimer consists of two Grx3 monomers, two [2Fe–2S] clusters, and four GSH molecules.

The monothiol Grx5 is one of the essential components of mitochondrial FeS cluster assembly machinery and cluster trafficking, therefore, it is crucial for various reactions and biological pathways that rely on iron regulation (Lill et al., 2012; Mühlenhoff et al., 2020). The biogenesis of cellular FeS proteins is the most basic and minimal function of mitochondria (Lill and Freibert, 2020). The assembly mechanism mainly consists of three steps, and Grx5 plays a role in the second step, which is responsible for transferring the [2Fe–2S] synthesized de novo on the scaffold protein Isu1 to the target protein under the mediation of the heat shock protein (Hsp) chaperone (Lill and Freibert, 2020; Banci et al., 2014). Deficiency of Grx5 leads to failure of FeS cluster assembly and iron overload in mitochondria, which in turn leads to the inactivation of FeS-dependent proteins. Particularly, in erythrocytes, deficiency of Grx5 impairs heme biosynthesis and reduces cytoplasmic iron, leading to sideroblastic anemia (Wingert et al., 2005; Ye et al., 2010). Similar to Grx3, Grx5 forms a 4Grx5-2[2Fe–2S]-4GSH tetramer with 2[2Fe–2S] (Johansson et al., 2011) (Figure 8).

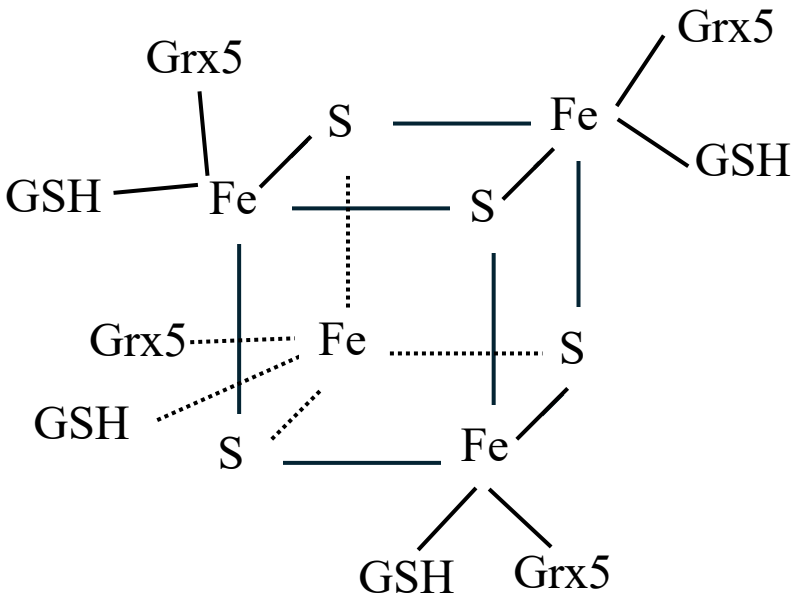

Figure 8 4Grx5-2[2Fe–2S]-4GSH tetramer. The tetramer consists of four Grx5 monomers, two [2Fe–2S] clusters, and four GSH molecules.

In addition, Grx5 plays a role in the maturation of FeS protein by forming clusters with the BolA-like protein family (Nasta et al., 2017). BolA1-Grx5 forms a heterocomplex with the [2Fe–2S] cluster and may work in the electron transfer process but is not suitable for FeS cluster transport, and the [2Fe-2S] BolA3-Grx5 heterocomplex may be preferentially involved in FeS cluster transport (Nasta et al., 2017; Sen et al., 2018).

So far, Grx5 gene mutations have been reported to cause sideroblastic anemia and variant nonketotic hyperglycinemia in multiple cases (Camaschella et al., 2007; Chiong et al., 2007; Baker et al., 2014; Liu et al., 2014; Daher et al., 2019; Feng et al., 2021; Sankaran et al., 2021).

A summary of the characteristics of the human Grxs is given in Table 2.

Table 2 Summary of human Grx family proteins.

hGrx	Active site	Localization	FeS cluster	Reactions
Grx1	CPYC	m, c, n	No	Oxidoreductase, (de-)glutathionylation
Grx2	CSYC	m (Grx2a), c (Grx2b), n (Grx2c)	2Grx2-[2Fe-2S]-2GSH	Oxidoreductase, redox sensor
Grx3	CGFS	c, n	2Grx3-2[2Fe-2S]-4GSH	FeS cluster biogenesis, iron trafficking
Grx5	CGFS	m	4Grx5-2[2Fe-2S]-4GSH	FeS cluster biogenesis FeS cluster trafficking

(hGrx: human Grx, c: cytosol, m: mitochondria, n: nucleus)

1.3.2 Grx5 in pancreatic β cells

1.3.2.1 Grx5 and insulin synthesis and secretion

FeS clusters are involved in the translation of proinsulin in pancreatic β cells, and the possible mechanism is that the FeS cluster enzyme Cdk5-regulatory subunit-associated protein 1-like 1 (Cdkal1) is responsible for the methylthiolation of adenosine in lysine tRNA, which is required for the translation of lysine codons in proinsulin (Wei et al., 2011; Brambillasca et al., 2012). Studies have shown that Cdkal1 is regulated by iron regulatory protein 2 (Irp2). In *Irp2−/−* mice, impaired biosynthesis of the FeS cluster impaired the function of Cdkal1 in the islets, resulting in impaired processing of proinsulin into mature insulin (Santos et al., 2020). In addition, FeS clusters, as part of respiratory chain complexes I, II, III, and IV, participate in ATP synthesis, thus playing an important role in the metabolic coupling mechanism of glucose-stimulated insulin secretion (GSIS) (Marku et al., 2021).

As mentioned in 1.3.1, Grx5 is involved in the assembly and trafficking of the FeS cluster; therefore, we may speculate that Grx5 plays an important role in the synthesis and secretion of insulin. It was shown that in Grx5-deficient human subjects, the

activity and expression of cytoplasmic and mitochondrial FeS protein aconitase were decreased (Camaschella et al., 2007). Our previous study found that, firstly, in db/db diabetic mice, the expression of pancreatic Grx5 mRNA was significantly decreased compared with the control group. It was associated with increased ROS generation, decreased insulin content, and increased blood glucose levels (Petry et al., 2017, 2018). Secondly, Grx5 presented obvious nuclear staining in lean mice, which was consistent with the nuclear localization pattern of the mouse Grxs immunohistochemical detection map described by Godoy et al., while the localization in diabetic mice showed a distinct shift (Godoy et al., 2011a; Petry et al., 2018). Additionally, subsequent studies found that a high-fat diet (HFD) could lead to a decrease in pancreatic islet Grx5 expression, accompanied by increased ROS generation and decreased insulin secretion, and these deviations could be restored by a carbohydrate-rich rescue diet (Petry et al., 2022). The changes in Grx5 expression and insulin secretion observed in MIN6 cells after exposure to FFA *in vitro* were consistent with those in pancreatic islets after an HFD (Petry et al., 2022). These findings provide evidence for a link between Grx5 expression and islet and β cell survival and function, and the impaired FeS cluster may be the underlying mechanism.

1.3.2.2 Grx5 and iron metabolism and ferroptosis

Relevantly, the biosynthesis of FeS clusters in mitochondria is closely related to iron homeostasis since iron is used as a substrate in this process. Impaired assembly and trafficking mechanisms of FeS clusters lead to increased intracellular iron uptake and mitochondrial iron overload through iron starvation responses (Chen et al., 2002; Lill et al., 2012; Stehling and Lill, 2013). Iron overload mediates cytotoxicity via multiple mechanisms, especially in metabolically active pancreatic β cells (Eaton and Qian, 2002; Jomova and Valko, 2011; Marku et al., 2021). Hansen et al. found that IL-1β induces increased expression of the iron transporter divalent metal transporter 1 (DMT1), leading to increased labile iron pool (LIP) and ROS generation in β cells,

while iron chelators or knockdown of DMT1 can protect against IL-1β-induced β cell toxicity (Hansen et al., 2012). In addition, Dmt1 knockout mice are protected from low-dose streptozotocin (STZ) and HFD-induced hyperglycemia, insulin deficiency, and glucose intolerance (Hansen et al., 2012). Cooksey et al. found that pancreatic iron overload caused by targeted deletion of the mouse Hfe gene (*Hfe* −/−) led to a decrease in β cell mass and islet size, resulting in a decrease in insulin secretion capacity (Cooksey et al., 2004).

Possible mechanisms that explain iron toxicity in β cells include (Figure 9): iron accumulation can generate ROS through the Fenton reaction directly or reduce the clearance of ROS by inhibiting the activity of ROS-detoxification enzymes, such as copper-dependent cytochrome c oxidase (CCO) and manganese superoxide dismutase (MnSOD) (Jouihan et al., 2008), leading to a significant increase in ROS generation, and ROS, as described in section 1.2.3.1, leads to β cell dysfunction and apoptosis through multiple pathways; elevated intracellular iron levels impair Cdkal1 by decreasing Irp2, ultimately leading to impaired processing of proinsulin to mature insulin (Camaschella et al., 2007; Santos et al., 2020); iron overload can promote the aggregation and deposition of or form complexes with islet amyloid polypeptide (IAPP) (Mirhashemi, 2011; Mukherjee and Dey, 2013; Seal et al., 2016), thereby leading to β cell failure; in addition, iron accumulation may also contribute to β cell dysfunction and death through ferroptosis.

Ferroptosis is an iron-dependent, non-apoptotic, regulated cell death caused by lipid peroxidation and subsequent plasma membrane disruption, accompanied by the inhibition of oxidoreductases, especially glutathione peroxidase 4 (Gpx4) (Dixon et al., 2012). The inactivation of GSH/Gpx4 consecutively leads to ferroptosis, while an iron restriction is protective (Yang and Stockwell, 2008). Tanaka et al. found that the overexpression of Gpx can protect β cells from high glucose-induced oxidative distress (Tanaka et al., 2002). ML-162 is described as a Gpx4 inhibitor, which can cause tumor

cell death by inducing ferroptosis, which is reversed by the ferroptosis inhibitor ferrostatin-1 (Wang et al., 2022). However, Cheff et al. demonstrated that ML-162 is not a direct inhibitor of Gpx4 but a direct inhibitor of thioredoxin reductase 1 (TXNRD1) (Cheff et al., 2023). Liproxstatin-1 (Lip-1) can inhibit ferroptosis by inhibiting voltage-dependent anion channel 1 (VDAC1) and rescuing Gpx4 levels (Feng et al., 2019).

Moreover, islet function and viability were impaired in the presence of the ferroptosis inducer erastin, which was rescued by pretreatment with the ferroptosis inhibitor ferrostatin-1 (Bruni et al., 2018). Likewise, the antidiabetic drug quercetin can inhibit islet iron deposition and thus inhibit β cell death in STZ-induced diabetic mice (Li et al., 2020). In addition, the increased metabolization of FeS clusters can prevent ferroptosis (Alvarez et al., 2017). Case reports have shown that patients with Grx5 deficiency present with anemia and comorbid DM, but unfortunately, the report did not show blood glucose data for patients after deferoxamine treatment (Camaschella et al., 2007; Liu et al., 2014). Lee et al. found that inhibition of Grx5 makes cancer cells prone to ferroptosis (Lee et al., 2020).

Taken together, these studies and reports lead us to the conclusion that the presence of ferroptosis provides a possible mechanism for β cell death, and the expression and activity of Grx5 may play an important role in it.

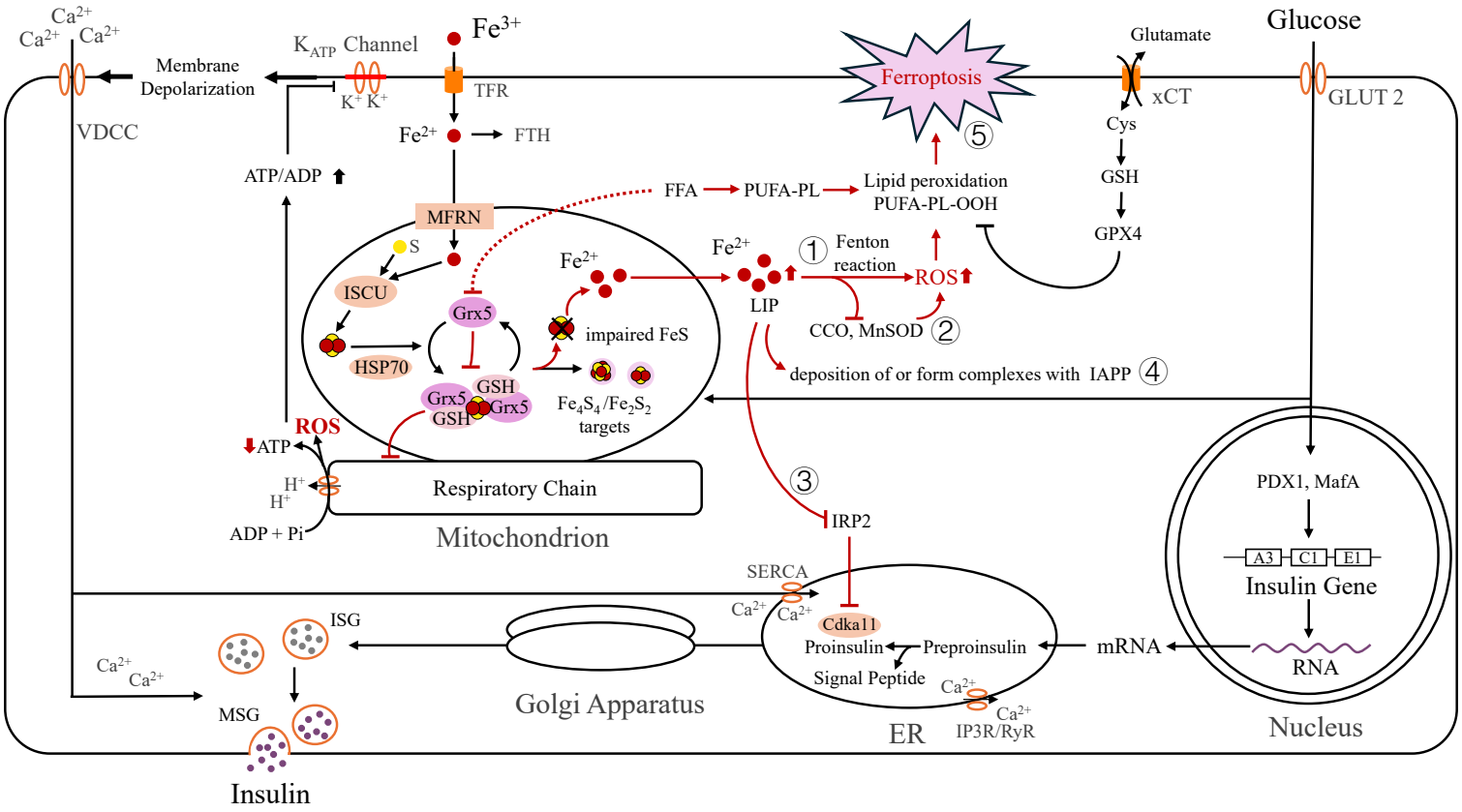

Figure 9 Grx5 and iron metabolism and ferroptosis in β cells. The absence or deficiency of Grx5 may cause impaired assembly and trafficking mechanisms of FeS Cluster, leading to mitochondrial iron overload and increased intracellular iron uptake through the iron starvation response. Iron overload mediates β cell toxicity through multiple mechanisms: 1. promoting ROS generation through the Fenton reaction; 2. reducing ROS clearance by inhibiting CCO and MnSOD, leading to increased ROS generation; 3. impairing Cdkal1 by decreasing Irp2, ultimately leading to impaired processing of proinsulin to mature insulin; 4. promoting the aggregation and deposition of or forming complexes with IAPP; 5. or through ferroptosis.

1.4 Aims of the thesis

The Grx system plays a key role in cellular physiological processes such as cell proliferation, apoptosis, cell signal transduction, and redox regulation. In the pathological conditions with DM, Grxs are differentially expressed in the pancreas as well as cardiovascular, kidney, liver, and eye and are of great significance to DM and its complications, as reviewed in ref. (Zhou et al., 2024a). Our previous study indicated that Grx5 was downregulated in diabetic mice, and subsequent studies revealed that Grx5 was regulated by FFA (Petry et al., 2017, 2018, 2022). Although the existing literature and our previous data suggest that the Grx5 exerts an important role for pancreatic islets and β cells, until now, little is known about the exact mechanisms. Studies have shown that impaired synthesis of FeS clusters can lead to mistranslation of proinsulin, which may induce ER stress, and can also lead to mitochondrial and intracellular iron accumulation, which may lead to increased ROS generation and induce oxidative distress, playing an important role in β cell dysfunction (Sun et al., 2015; Marku et al., 2021). Since Grx5 is a recognized participant in the assembly of the FeS cluster, we can speculate that Grx5 may be a worthwhile novel target protein relevant to β cell survival and function. Meanwhile, ferroptosis may also be involved; correlation between Grx5 and ferroptosis has been reported in cancer cells (Lee et al., 2020). In addition, given the differences between murine and human β cells, we also introduced the use of a human β cell line. Therefore, by using the murine β cell line MIN6, the human β cell line EndoC-βH3, and β cell-specific Grx5 overexpressing mice, the present study was carried out with the following specific aims:

- To analyze the effects of FFA on the metabolic activity of murine and human β cells *in vitro*.
- To address the effects of ferroptosis on β cell function and Grx5.
- To explore the effects of downregulating Grx5 on β cells *in vitro*.

- To study the phenotype and glucose metabolism of β cell-specific Grx5 overexpression mice *in vivo*.
- To investigate the function of pseudoislets formed by aggregation of human β cell line.

2 Materials and Methods

2.1 Materials

2.1.1 Reagents

Reagents used in this thesis are summarized in Table 3.

Table 3 Reagents list

Reagents	Company	Catalog No.
2,2'-Bipyridine (Bpy)	MedChemExpress	HY-D0020
2-mercaptoethanol	Gibco	31350-010
4-hydroxytamoxifen (TAM)	Sigma-Aldrich	H6278-10MG
βCOAT	Human Cell Design	BC-120
βKREBS buffer	Human Cell Design	BK-250
Ammonium iron (II) sulfate hexahydrate	Carl Roth	1L75
BSA	Sigma-Aldrich	9048-46-8
BSA, protease and fatty acid-free	Serva	11945.03
Complete™ Mini, EDTA-free Protease-inhibitor cocktail	Roche	04693159001
Citrate Buffer, pH 6.0, Antigen Retriever	Sigma-Aldrich	C9999
Deferoxamine mesylate (salt) (DFOM)	Sigma-Aldrich	D9533-1G
Dimethyl sulfoxide (DMSO)	Carl Roth	A994.2
DMEM	Gibco	41966-029
Donkey serum	Pan-biotech	P30-0101
Dulbecco's phosphate buffered saline (DPBS)	Lonza	17-512F
EGTA	Sigma-Aldrich	E3889
Eosin G	Roth	7089.2
Ethanol, ≥99.8 %	Carl Roth	64-17-5
FerroOrange (FeO)	BioTracker	SCT210-35nmol
Fetal calf serum (FCS)	Sigma-Aldrich	F2442
Fetal bovine serum (FBS)	Biowest	S1810-500
Ficoll	Sigma-Aldrich	10771
Formaldehyde solution 3.5 -3.7%	Fischar	2652965
D-Glucose	Calbiochem	346351

Glycerol	Sigma	G-5516
Goat serum	Biowest	52000-100
Hanks' Balanced Salt Solution (HBSS)	Gibco	14025050
HCL	Sigma-Aldrich	H7020
Hematoxylin	Sigma-Aldrich	GHS3
Hoechst 33342	Calbiochem	382065
IBMX	Sigma-Aldrich	I-5879
Liperfluo	Dojindo	1448846-35-2
Liproxstatin-1 (Lip-1)	Merck	SML1414
Medium 199	Gibco	11825015
Mito-FerroGreen (MFG)	DoJindo	M489
ML-162	Merck	SML2561
Mounting medium	Dako	S3025
MTT	Abcam	ab146345
NaCl	Carl Roth	3957.1
NP-40-alternative	Millipore	492018-50
Nuclease-Free Water	Qiagen	129114
Oleic acid	Enzo	BMLFA0450010
Optiβ1 medium	Human Cell Design	B003
Optiβ2 medium	Human Cell Design	B004
Paraffin 46-48	Merck	1.07151
Paraformaldehyde	Roth	0335.2
Penicillin-streptomycin	Gibco	15140122
Phosphate buffered saline (PBS 1X)	Lonza	BE17-517Q
Protein assay dye reagent concentrate	BioRad	5000006
ProLong Gold	Invitrogen	P36984
Protease and phosphatase inhibitor cocktail	Thermo Scientific	1861284
Protein standard	Sigma	P0834
Puromycin	InvivoGen	Ant-pr-1
Rotihistol	Carl Roth	6640.1
RPMI Medium 1640 (1X)	Gibco	21875034
Sodium dodecyl sulfate (SDS)	Sigma-Aldrich	71725
Sodium hydroxide solution (NaOH)	Merck	105588
Streptozotocin (STZ)	Millipore	572201
SYBR green supermix	BioRad	1708882
tert-butyl hydroperoxide (t-BHP)	Sigma-Aldrich	458139
Tris base	Merck	108382
Tris Hydrochloride, 1M solution	Fisher BioReagents	BP1758-500
Tris-wash buffer TBS (20x)	Zytomed	ZUC052-500

TBS Tween-20 Buffer (20x)	Thermo scientific	28360
Triton X-100	Roth	3051.3
Trypan blue	Sigma-Aldrich	T6146
Trypsin-EDTA	Gibco	25300054
Tween 20	Merck	8.22184.0050

2.1.2 Buffer recipes

The recipes of all buffers used in this thesis are summarized in Table 4.

Table 4 Buffer recipes

Buffer	**Recipes**	**Stability at °C**
Cell lysis buffer (EndoC-βH3 cells)	10 ml TETG solution, 1 tablet of protease inhibitor	Immediately use
Cell lysis buffer (MIN6 cells)	2 ml NP-40, 60 µl protease inhibitor cocktail	Immediately use
NaOH lysis buffer	5 ml 20% SDS, 2 ml 10 M NaOH, 100ml a. dest	Immediately use
PBS/Donkey/Triton	25 ml PBS,250 µl Donkey serum,125 µl Triton 20%	4 °C
P/FCS	100 ml Medium 199, 50 ml FBS, 850ml a. dest	4 °C
Retrieval buffer	10 ml Citrate Buffer, 90 ml a. dest	4 °C
TETG solution	35 ml a. dest., 1.37 ml NaCl 5M, 500 µl EGTA 0.2 M, 1ml Tris pH8.0 and 1M, 5ml Glycerol, 5ml Triton X-100 10%, fill up to 50ml with a. dest	Room temperature
Tris (0.01 M, pH7.6)	Stock solution: 60.5 g Tris-base in 700 ml a. dest, adjust to pH 7.6 with 2N HCL, fill up to 1000 ml with a. dest, 90 g NaCl Working solution: dilute the stock solution 1:10 with a. dest	Stock solution: Room temperature Working solution: 4 °C
Tris/BSA	100mg BSA, 100ml Tris (0.01M, pH7.6)	4 °C
Tris/Triton	950 ml a. dest, 50 ml Tris (20x), 250 µl Triton x-100	4 °C

Zamboni	20g Paraformaldehyde, 150ml Picric acid (1,2%), 60°C for 2h, neutralize with NaOH (2,5%), fill up to 1000ml with PBS (pH 7.3)	4 °C

2.1.3 Kis

All kits used in this thesis are summarized in Table 5.

Table 5 List of kits

Kits	Company	Catalog No.
Amaxa Cell line Nucleofector Kit V	Lonza	VCA-1003
ATPlite 1 step kit	PerkinElmer	6016736
Fuchsin Substrate Chromogen System	Dako	K0625
Human insulin ELISA kit	Mercodia	10-1113-01
iScript cDNA Synthesis kit	BioRad	1708890
Mouse Grx5 ELISA	CUSABIO	CSB-EL009524MO
Mouse insulin ELISA	DRG	EIA-3439
Mouse insulin ELISA	Mercodia	10-1247-01
RNeasy Mini Kit (50)	Qiagen	74104
Vector red substrate kit	Vector Laboratories	SK-5100

2.1.4 Equipment

All equipment used in this thesis are summarized in Table 6.

Table 6 List of equipment

Equipment	Company
Amaxa Nucleofector	Lonza
Centrifuge Biofuge 13	Heraeus
Centrifuge Biofuge fresco	Heraeus
Centrifuge Universal 320R	Hettich
Fluorescence microscope DM750	Leica
Fluorescence microscope LB30T	Leica

Heating cabinet B 5028	Heraeus
Heating MSZ3034	julabo
Incubator	Heraeus
Microplate Reader Mithra LB940	Berthold
Microscope Leica DMIL LED	Leica
Microwave	Bosch
NanoDrop 1000 Spectrophotometer.	Thermo Scientific
OneTouch Glucometer	LifeScan
Plate centrifuge, perfecctSpin P	Peqlab
Precision scale	Sartorius (Göttingen, Germany)
Shaker	KEUTZ
Shaker MTS2	IKA
StepOne Plus Real-Time PCR	Applied Biosystems
Sterile Benches	Thermo Scientific
Thermal cycler DOPPIO	VWR (Darmstadt, Germany)
Thermostatic water bath	fried Electric
Trinocular live cell microscope AE31	Motic
Vortex mixer 7-2020	Neo lab
Vortex Reax 1R	Heidolph
Vortexer Reax 2000	Heidolph

2.1.5 Software

All Software used in this thesis are summarized in Table 7.

Table 7 Software list

Software	Company
Image J	National Institutes of Health
Leica Application Suite	Leica
Reference Manager	Zotero
Statistical Analysis	GraphPad Prism

2.1.6 Antibodies

All antibodies used in this thesis are listed with host, dilution, company and catalog number and are summarized in Table 8 and Table 9.

2.1.6.1 Primary antibodies

Table 8 List of primary antibodies

Antibody name	Host	Dilution	Company	Catalog No.
Grx5	Rabbit	1:100	Antibodies-online	ABIN7154052
Gpx4	Rabbit	1:200	Invitrogen	PA5-102521
Insulin	Guinea Pig	1:100	Bio-Rad	5330-0104G

2.1.6.2 Secondary antibodies

Table 9 List of secondary antibodies

Antibody name	Host	Dilution	Company	Catalog No.
Donkey anti Guinea pig Alexa Fluor 488	Donkey	1:500	Jackson ImmunoResearch	706-545-148
Donkey anti rabbit Alexa Fluor 568	Donkey	1:500	Invitrogen	A10042
Donkey anti-rabbit RRX	Donkey	1:500	Jackson ImmunoResearch	711-296-152
Goat anti Guinea Pig IgG (H/L)	Goat	1:100	Bio-Rad	AHP863F
Goat Anti-Rabbit IgG (H+L)	Goat	1:100	Jackson ImmunoResearch	111-056-144

2.1.7 Primers

All the primers used in this study are listed in Table 10.

Table 10 List of primers

Primers	Sequences
m Grx5 fwd	GAA GAA GGA CAA GGT GGT GGT CTT C
m Grx5 rev	GCA TCT GCA GAA GAA TGT CAC AGC
m RPL13a fwd	GCG GAT GAA TAC CAA CCC CT
m RPL13a rev	CCA CCA TCC GCT TTT TCT TGT

2.1.8 siRNA duplexes

The sequences of the used siRNA duplexes are listed in Table 11.

Table 11 siRNA duplexes list

siRNA Duplex	Sense sequence	Usage
siGrx5 sens	5'-GGCAAGGUAUUAAAGACUA-3'	Grx5 knockdown
siGrx5 antisens	5'-UAGUCUUUAAUACCUUGCC -3'	
Neg siRNA sens	dTdT 3' overhang	Negative control
Neg siRNA antisens	dTdT 3' overhang	

2.1.9 Cell line and medium

In 1990, Miyazaki, J et al. established the mouse insulinoma, 6th subclone (MIN6) cell line, using insulinomas generated from transgenic mice harboring insulin promoter followed by simian virus 40T (SV40T) antigen gene (Miyazaki et al., 1990). Physiological characteristics of normal β cells, especially insulin secretion in response to increased glucose concentrations, are retained in the MIN6 cell line, which makes it an ideal

model in investigating the function of β cells (Miyazaki et al., 1990; Ishihara et al., 1993). The MIN6 cell line and culture medium are described in detail in Table 12.

Table 12 MIN6 cell line and medium

Cell line name	MIN6
Description	Mouse insulinoma cell
Growth Mode	Adherent
Culture Medium	DMEM (4.5 g/L D-glucose, Gibco) + 20% heat inactivated FBS + 50 μM β-mercaptoethanol+ 1% penicillin/streptomycin
Preservation	Freeze medium: 80% culture medium+ 20% DMSO Cryopreservation: -4 °C (15 min), -20 °C (2.5 h), -80 °C (overnight), liquid nitrogen store

The human β cell line EndoC-βH cell line was developed by the Scharfmann group. In 2011, the EndoC-βH1 cell line was established by obtaining insulinomas from transplantation of the SV40LT-transfected human fetal pancreas into severe combined immunodeficient (SCID) mice, transducing the obtained insulinomas with human telomerase reverse transcriptase (hTERT), transplanting the transduced insulinomas into other SCID mice for amplification and proliferation, and then isolating and *in vitro* propagating (Ravassard et al., 2011; Weir and Bonner-Weir, 2011). However, unlike genuine adult β cells, EndoC-βH1 cells are continuously proliferating. In 2014, the EndoC-βH2 cell line was derived, in which immortalizing transgenes can be removed by CRE lentiviral vector transduction (Scharfmann et al., 2014). Although the proliferation of EndoC-βH2 cells after excision is arrested and the function is enhanced, the viral vector-mediated excision limits the large-scale application of the EndoC-βH2 cell line. In 2015, the group improved the immortalizing transgene excision method by integrating the combining of the tamoxifen-inducible CRE (CRE-ERT2) excision system and antibiotic resistance selection into EndoC-βH2 cells, thereby generating the EndoC-βH3 cell line (Benazra et al., 2015). The insulin expression, storage in secretory granules, and glucose-stimulated secretion of EndoC-βH3 cells after excision are close to

those of real human β cells (Benazra et al., 2015). The EndoC-βH3 cell line and culture medium are described in detail in Table 13.

Table 13 EndoC-βH3 cell line and medium

Cell line name	EndoC-βH3
Description	Human pancreatic β cell
Growth Mode	Adherent
Coat medium	1 vial βcoat (120 µl) + 10 ml DMEM+ 100 µl penicillin/streptomycin
Culture Medium	Optiβ1 medium
Selection	Puromycin:10 µg/ml for 14 days and 5 µg/ml for maintenance
Transgene excision	1 µM 4-hydroxytamoxifen (TAM) for 21 days
Preservation	Freeze medium: 90% heat inactivated FBS + 10% DMSO Cryopreservation: -20 °C (2 h), -80 °C (overnight), liquid nitrogen store

2.1.10 Research animals

The β cell-specific Grx5-overexpressing B6.129-Gt (ROSA) 26Sor$^{em1(INS2\text{-}Grx5)}$ (ROSAINS2-Grx5) mouse on the C57Bl/6 background was created by Cyagen Biosciences GmbH using the CRISPR/Cas method. The Grx5 transgene was inserted into the ROSA26 locus under the control of the INS2 promoter. Heterozygous F1 animals were mated with wild-type (WT) mice to achieve homozygous Glrx5-overexpressing mice in the F2 generation. WT littermates were used as controls. 5 NMRi nu/nu mice were acquired at the age of 10 weeks from Charles River (Sulzfeld, Germany). All mice were given two weeks to adapt to the local animal facility and were provided with tap water and either standard diet (SD) food or HFD food ad libitum. They were housed in a controlled environment with a temperature of 24 ± 2 °C, a light-dark cycle of 14:10 hours, and a relative humidity of 55 ± 10%. All experiments have been designed per the German Animal Welfare law and have been approved by the Regional Administrative Council Giessen, Veterinary Department.

2.2 Methods

2.2.1 Cell culture

2.2.1.1 MIN6 cells

For resuscitation, cryopreserved vials of MIN6 cells were removed from liquid nitrogen and immediately thawed in a 37°C water bath. They were suspended with 10 ml of warm complete medium in a 50-ml Falcon tube and then centrifuged (1200 RPM, 4 minutes). The pellet was resuspended with an appropriate amount of complete culture medium and transferred to a culture flask. The cells were maintained in a humidified 5% CO_2 and 37°C incubator with medium changed every 2 to 3 days.

Passaging was done weekly with 0.5% trypsin-EDTA after washing with 1X D-PBS. Trypsin was inactivated with a complete medium after cells were fully detached. Cells were resuspended in the fresh medium after centrifuging. MIN6 cells used in all experiments were at passage 50-60 with 70-80% confluence.

2.2.1.2 EndoC-βH3 cells

EndoC-βH3 cells were obtained from Human Cell Design and cultured per the manufacturer's instructions in Optiβ1 medium onto βcoat medium-coated culture flasks or plates in humidified 5% CO_2 and 37 °C conditions.

Splitting was carried out every week by trypsinization with 0.05% trypsin-EDTA after washing with D-PBS. The enzymatic reaction was stopped with DMEM containing 20% heat-inactivated FCS. Cells were centrifuged (500 x g, 5 minutes) and resuspended in Optiβ1 medium. 10 µg/ml puromycin was added extemporaneously in the medium for 14 days to select the puromycin-resistant EndoC-βH3 cells, and to allow a better effect of excision of the immortalizing gene, 5 µg/ml puromycin was maintained in the

subsequent culture. 1 µM TAM was added for 21 days, with the medium changed every week to induce the excision of Cre-mediated immortalizing transgenes. Thereafter, TAM was removed from the medium, and all experiments were conducted within the following 14 days.

2.2.1.3 Pseudoislets formation

EndoC-βH3 cells were seeded at a density of 2000 cells/well into 96-well, U-bottom-shaped plates (Biofloat) without coating after the 21-day TAM treatment. Cells were incubated for 48-60 hours in 100 µl/well Optiβ1 medium with 5 µg/ml puromycin. Then the cells attached to each other to form one pseudoislet per well.

2.2.1.4 Determination of cell number

Cells were visualized under a light microscope. Cell number was determined with a hemocytometer. 10 µl of cell suspension was mixed with 90 µl of 0.4% trypan blue solution, then 10 µl of the mixture was applied to the hemocytometer. Cells were counted in the 4 corner squares using a microscope. The total cell number was calculated using the formulas below:

$$\text{Total cell number} = (\text{total cells counted/squares counted}) \times 10000 \text{ dilution factor} \times \text{total sample volume}$$

2.2.2 Preparation of solutions

Oleic acid (OA) was dissolved in absolute ethanol to prepare stock solutions of 150, 225, 450, and 900 mM. The stock OA was complexed to fatty acid-free BSA Fraction V in DMEM to prepare aliquots at concentrations of 2, 3, 6, and 12 mM. The molar FFA:BSA ratio is 5:1. Aliquots were overlayed with nitrogen, incubated overnight at 37 °C on a shaker, sterile filtered (0.22 µm), and stored at -20 °C. For treatment, aliquots

were diluted by a factor of 4 to reach the final fatty acid concentration of 0.5, 0.75, 1.5, and 3 mM. Respective control solutions were prepared to match the same ethanol and BSA concentrations.

The ferroptosis inducer ML-162 and the ferroptosis inhibitor Liproxstatin-1 (Lip-1) were initially dissolved in DMSO at stock concentrations of 4 mM and 5 mM, respectively.

2.2.3 Cell metabolic activity

3-(4,5-dimethylthiazol-2-yl)-2,5-diphenyltetrazolium bromide (MTT) assay was used to evaluate cell metabolic activity. The assay is based on the reduction of MTT reagent to formazan of crystals by metabolically active cells, as MTT can pass through the cell membrane and mitochondrion membrane of viable cells (Mosmann, 1983; Ghasemi et al., 2021).

MIN6 or EndoC-βH3 cells (1×10^4/well) were seeded in 96-well plates in 100 µl of cell culture medium and allowed to settle for 24 hours after seeding. Then, replace the cell culture medium with 100 µl of cell culture medium containing the required concentration of different drugs and incubate for 24 hours or 5 days. It was followed by incubation with 50 µl MTT (2 mg/ml in D-PBS) for 4 hours at 37°C. Formazan crystals were dissolved with 200 µl DMSO. Absorbance was measured at 570 nm and 620 nm (background) using a Multimode Microplate Reader. The cell metabolic activity was calculated by subtracting the absorbance of the blank and normalizing the values to the non-treated control (defined as 100% cell metabolic activity).

2.2.4 Cell staining by fluorescent probes

For live cell staining, MIN6 cells (4×10^4/well) or EndoC-βH3 cells (5×10^4/well) were seeded in 200 µl of culture medium in 48-well plates, and after 24 hours, cells were treated with the required concentration of different drugs and incubated for 24 hours.

2.2.4.1 Determination of lipid peroxidation and mitochondrial Fe^{2+}

Lipid peroxidation was measured by Liperfluo. The detection is based on the specific oxidation of the non-fluorescent Liperfluo reagent by lipid peroxides to the fluorescent Liperfluo oxidized form (Figure 10A). Liperfluo was dissolved with DMSO to prepare a 1 mM stock solution and then diluted with HBSS to prepare a 1 µM working solution. Cells were treated with 250 µM tert-butyl hydroperoxide (t-BHP) for 24 hours as the positive control and 5% ethanol for 1 hour as the negative control.

Mitochondrial iron was measured by Mito-FerroGreen. The measurement is based on the irreversible reaction of the Mito-FerroGreen probe and Fe^{2+} and the enablement of the fluorescent imaging of mitochondria Fe^{2+} in live cells (Figure 10B). Mito-Ferro-Green was dissolved with ethanol to prepare a 1 mM stock solution and then diluted with HBSS to prepare an 8 µM working solution. Cells were treated with 5 mM ammonium iron (II) sulfate hexahydrate (AmmFe) and 100 µM deferoxamine mesylate salt (DFOM) for 1 hour as the positive control and negative control, respectively.

Cells were incubated with Liperfluo (1 µM) or Mito-FerroGreen (8 µM) for 30 minutes at 37°C. Then cells were stained with Hoechst for 5 minutes and fixed with formalin 3.5-3.7% for 15 minutes. Cells were washed with HBSS between each step before fixation and with PBS after fixation. After washing, 500 µl of PBS was added to each well, followed by overnight storage in the dark at 4 °C. The cells were observed under a fluorescence microscope the following day.

2.2.4.2 Determination of intracellular Fe^{2+}

Intracellular iron was measured by FerroOrange. The measurement is based on the irreversible reaction of the FerroOrange probe and Fe^{2+} and the enablement of the fluorescent imaging of intracellular Fe^{2+} in live cells (Figure 10C). FerroOrange was dissolved with DMSO to prepare a 1 mM stock solution and then diluted with HBSS to prepare a 1 μM working solution. Cells were treated with 100 μM AmmFe and 100 μM 2,2'-bipyridine (Bpy) for 30 minutes as the positive control and negative control, respectively.

After treatment, cells were washed 2 times with HBSS and incubated with HBSS for 10 minutes, then cells were stained with FerroOrange (1 μM) for 30 min at 37°C. The cells were observed directly under a fluorescence microscope without washing.

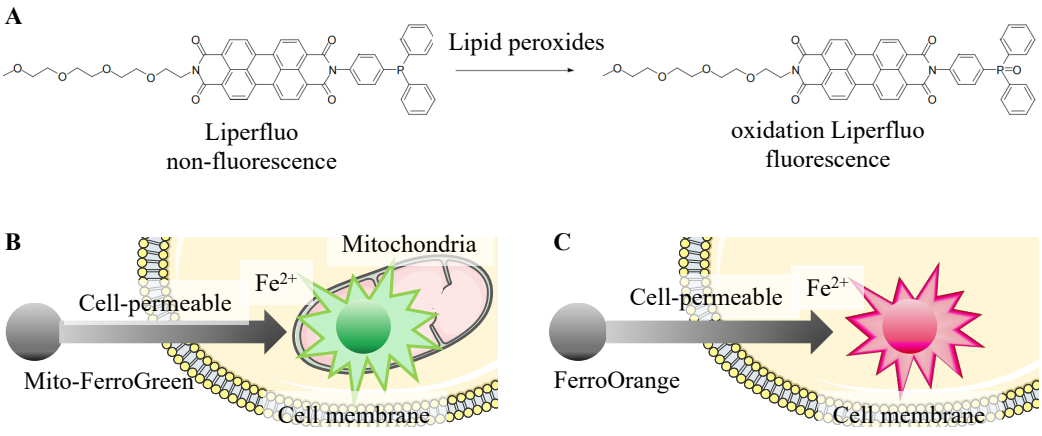

Figure 10 Schematic of the detection of lipid peroxidation, mitochondrial Fe^{2+}, and intracellular Fe^{2+} using Liperfluo, Mito-FerroGreen, and FerroOrange, respectively. (A) Liperfluo, (B) Mito-FerroGreen, (C) FerroOrange. The figure was partly generated according to the product manual using Servier Medical Art, provided by Servier.

2.2.5 Determination of cellular ATP Levels

The ATP luminescence assay is based on the light production caused by the reaction of ATP with added luciferase and luciferin, which is proportional to the ATP

concentration within certain limits. MIN6 cells (4×10^4/well) were seeded into 96-well luminescence plates in reduced culture medium (4% FCS) and allowed to settle for 24 hours. After treatment, cells were lysed with NaOH lysis buffer and incubated for 5 minutes in the dark at room temperature, followed by adding the substrate solution and incubating for 40 minutes at room temperature. The luminescence was measured using a multimode microplate reader.

2.2.6 ELISA

Commercially available enzyme-linked immunosorbent assay (ELISA) kits were used to determine the levels of insulin and Grx5 in cell culture medium or lysates per instructions.

2.2.6.1 Determination of insulin and Grx5 levels in MIN6 cells

MIN6 cells (4×10^5/well) were seeded in 3 ml culture medium into 6-well plates for 24 hours. After treatment, 1 ml of cell culture medium was collected, then cells were washed twice with ice-cold PBS and incubated in a lysis buffer for few seconds on ice. Collect cell lysate with cell scrapers. The cell supernatant was centrifuged at 2000 rpm for 5 min at 4 °C, cell lysis was centrifuged at 12000 rpm for 12 minutes at 4 °C, and supernatant was preserved for analysis. The level of insulin in supernatant and cell lysate was analyzed using a mouse insulin ELISA kit (DRG, Mercodia). Grx5 in cell lysate was analyzed using a mouse Grx5 ELISA Kit (CUSABIO).

The amount of insulin and Grx5 protein was normalized to the total lysate protein as determined by the Bradford protein assay.

2.2.6.2 *In vitro* EndoC-βH3 cells glucose-stimulated insulin secretion

For glucose-stimulated insulin secretion, the excised EndoC-βH3 cells were seeded onto βcoat-coated 6-well plates at a density of 5 x 10^5 cells/well for 24 hours. The pseudoislets formed by EndoC-βH3 cells were seeded for at least 48 hours; the experimental design is shown in Figure 11. The monolayer cells and pseudoislets were incubated overnight in Optiβ2 medium at 37 °C and 5% CO_2 and saturating humidity. A pre-incubation of 60 minutes was conducted using βKREBS buffer containing 0.2% BSA. Subsequently, the βKREBS buffer was replaced with glucose solutions of 0 mM and 20 mM, with or without 45 µM IBMX, and incubated for 1 hour. For insulin secretion measurement, the supernatant was collected. For insulin content measurement, cells or pseudoislets were lysed directly in the culture wells with TETG solution and an anti-protease tablet for 5 min on ice. The lysate was next centrifuged at 3000 rpm for 5 min and stored at 20 °C. Insulin secretion and intracellular content were measured in duplicate using a human insulin ELISA kit (Mercodia).

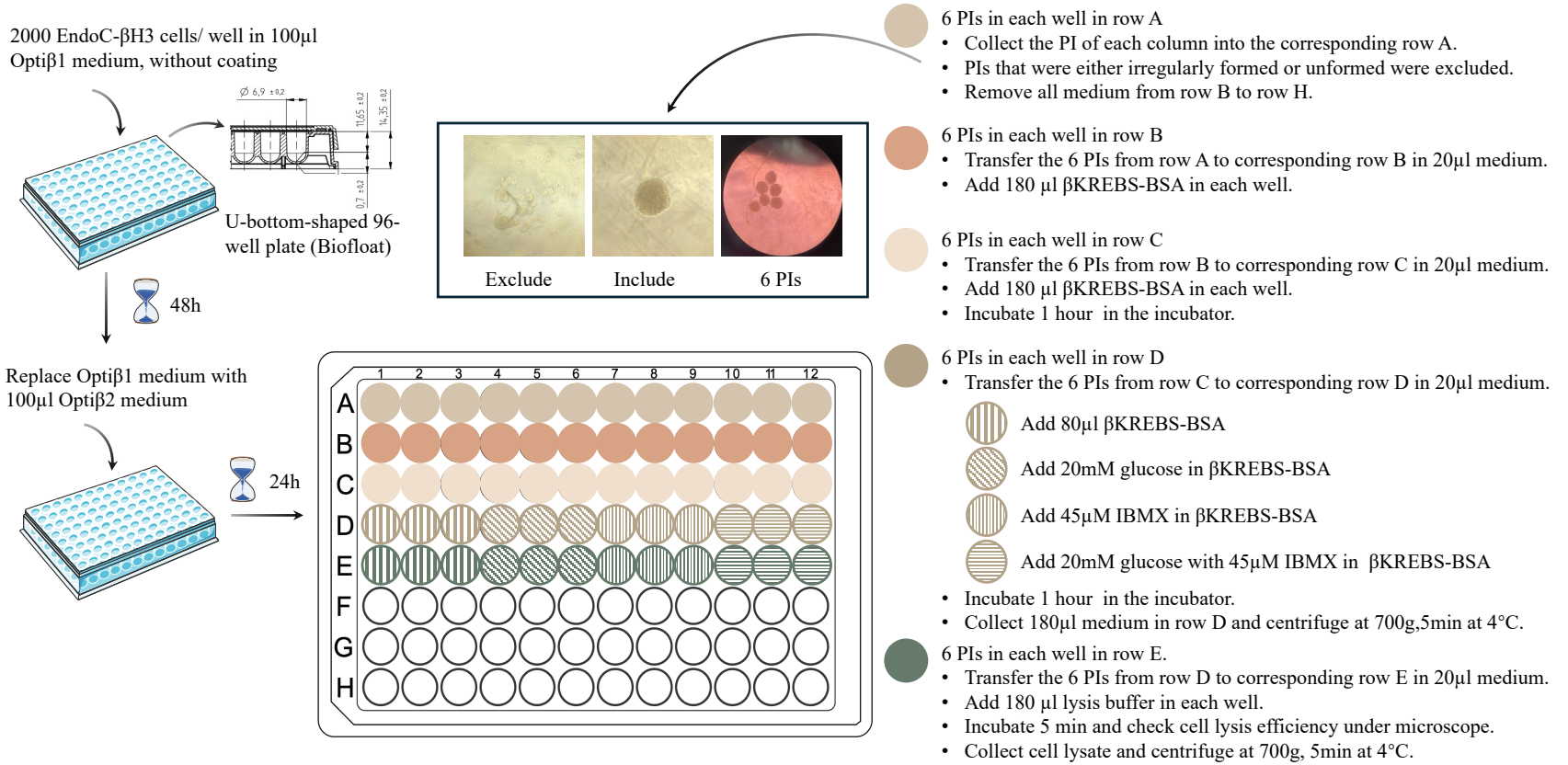

Figure 11 Experimental design of the *in vitro* pseudoislets glucose-stimulated insulin secretion. 1 PI was formed per well, and PIs that were either unformed or irregularly formed were removed; 6 PIs were collected for each column. Following 1 hour of pre-incubation, they were treated with 0 mM glucose, 20 mM glucose, 45 µM IBMX, and 20 mM glucose + 45 µM IBMX diluted in βKREBS-BSA buffer for 1 hour. Afterwards, supernatant and pseudoislet lysate were collected. The figure was partly generated using Servier Medical Art, provided by Servier. PI, pseudoislets.

2.2.7 Bradford protein assay

To determine the total concentration of lysate proteins, the Bradford protein assay was performed. Prior to analysis, different concentrations of standards were prepared, cell lysates were appropriately diluted, and a 1:5 dilution of the Bio-Rad Protein Assay was prepared. Then, 10 µl of standard and cell lysate were added in duplicate to a 96-well plate, followed by 200 µl of Bio-Rad Protein Assay. The absorbance at 595 nm was measured by a Mithras LB 940 Multimode Microplate Reader. The protein concentration was calculated from the standard curve.

2.2.8 Immunocytochemistry

For immunocytochemistry, MIN6 cells (4×10^5/well) were seeded in 3 ml culture medium into 6-well plates and incubated for 24 hours. Following the treatment, the medium was discarded, the cells were washed 3 times with PBS and detached using 0.5% trypsin-EDTA. Trypsin was inactivated by adding FBS (1:5 dilution in PBS). After centrifugation, the supernatant was removed, and the cell pellet was resuspended in PBS to obtain a concentration of 15000–20000 cells in 10-20 µL. The suspension was mixed thoroughly, and 10-20 µL of the cell suspension was dropped on each slide. The slides were allowed to air-dry for 20-40 min. Dry MIN6 cell slides were stored at -20 °C until staining.

2.2.8.1 Insulin and Grx5 staining

Fluorescence staining was used for insulin and Grx5 detection, as described in Table 14.

Table 14 Insulin and Grx5 staining.

Steps	Reagent	Duration
Fixation	Zamboni	15min

Washing	0.1 % Tris buffer containing 0.025% Triton X	3x 15 min
Blocking	1 % goat serum in 0.1 % Tris buffer	20 min
Primary antibody	Primary antibody in 1% donkey serum in 0.3% PBST	Overnight
Washing	Tris/Tween buffer	3x 5 min
Secondary antibody	Secondary antibody in 5% mouse serum in Tris buffer	1 hour
Washing	Tris/Tween buffer	3x 5 min
Nuclei staining	Hoechst	5 min
Washing	Tris buffer	5 min
Preservation	ProLong Gold	-
Embedding	Mounting medium	-
Sealing	Nail polish	-

2.2.8.2 Gpx4 staining

Fluorescence staining was also used for Gpx4 detection, as described in Table 15.

Table 15 Gpx4 staining

Steps	**Reagent**	**Duration**
Fixation	Zamboni	15min
Washing	Tris/Tween buffer	3 x 5 min
Antigen retrieval	Retrieval-buffer at 600 Watt in a microwave	5 min
Blocking	10 % donkey serum in 0.1 % Tris buffer	10 min
Primary antibody	Primary antibody in 1% donkey serum in 0.3% PBST	Overnight
Washing	Tris/Tween buffer	3x 5 min
Secondary antibody	Secondary antibody in 5% mouse serum in Tris	1 hour
Washing	Tris/Tween buffer	3x 5 min
Nuclei staining	Hoechst	5 min
Washing	Tris buffer	5 min
Preservation	ProLong Gold	-
Embedding	Mounting medium	-
Sealing	Nail polish	-

Slides without primary antibodies were used as negative controls. Images were taken with Leica Application Suite v 3.8.0 using a digital microscope camera DFC 420 C.

2.2.9 Cell transfection

Cell transfection was performed by nucleofection with the Amaxa nucleofector. Grx5 siRNA for nucleofection was diluted in RNA-free water to prepare a stock solution of 50 µM and stored at -80 °C. Detached MIN6 cells were resuspended in 100 µl Nucleofector Solution containing 4 µl Grx5 siRNA, then the mixture was transferred into an electroporation cuvette and inserted in the Nucleofector device and pulsed with the program G-16. Afterwards, 500 µl prewarmed RPMI medium containing 10% FCS was immediately added to the electroporation cuvette. Controls are MIN6 cells treated in the same way but with negative siRNA, as well as MIN6 cells that were neither treated with siRNA nor subjected to the nucleofection process. Cells were seeded on 6-well or 96-well plates and cultured for 48 hours before further treatments.

2.2.10 Real-time PCR

2.2.10.1 RNA isolation

The treated MIN6 cells were lysed on the plate by RLT buffer containing 1% β-mercaptoethanol. Total RNA was isolated using the RNeasy Mini Kit (Qiagen) according to the manufacturer's protocol and quantified using a NanoDrop 1000 Spectrophotometer.

2.2.10.2 cDNA synthesis

Total RNA was reversely transcribed into cDNA using the iScript cDNA Synthesis kit (Bio-Rad) according to the manufacturer's protocol. Briefly, 1 µg of RNA was added in a PCR tube, supplemented with RNase-free water to reach a total volume of 15 µl.

Next, 5 µl reaction mix containing 4 µl of 5x iScript Reaction Mix and 1 µl of iScript Reverse Transcriptase was added. The resulting 20 µl complete reaction mixture was incubated in a thermal cycler at 25 °C for 5 minutes for priming, 46 °C for 20 minutes for reverse transcription, and 95 °C for 1 minute for RT inactivation. The resulting cDNA was finally diluted to 200 µl with RNase-free water and subjected to qRT-PCR.

2.2.10.3 Quantitative Real-Time PCR

For gene expression analysis, qRT-PCR was performed in triplicate in the real-time PCR System StepOnePlus (Applied Biosystems) by the SYBR green method. The primer was prepared by mixing it 1:1 with the forward and reverse primers and diluting it 1:10 with RNase-free water. For each qRT-PCR reaction, the master mix containing 3.2 µl RNase-free water, 0.3 µl of primer mix, and 5 µl SYBR green was added to 1.5 µl cDNA dilution or 1.5 µl negative control. The housekeeping gene rpl13a was used for normalization. The qRT-PCR process is described in Table 16.

Table 16 The procedure of qRT-PCR.

Steps		Temp.	Time	Description
Pre-incubation		95 °C	10 min	Activate Taq DNA polymerase
Cycling (40 cycles)	Denaturation	95 °C	10 s	Melt all dsDNA
	Annealing	60 °C	30 s	Promote primer binding to the template
	Extension	72 °C	30 s	Obtain a new dsDNA fragment
Melting Curve		60-95 °C	-	Determine melting temperature of PCR products

Relative gene expression levels were calculated using the 2^-ΔΔCT methods, accordingly to which ΔCT and ΔΔCT are defined by:

$$\Delta CT = CT_{\text{gene of target}} - CT_{rpl13a}$$

$\Delta\Delta CT = \Delta CT_{\text{gene of treated sample}} - \Delta CT_{\text{gene of control sample}}$

2.2.11 Animal experimental design

2.2.11.1 β cell-specific Grx5-overexpressing mice experiment

A total of 38 male C57BL/6J mice were utilized in the experimental design, of which 28 were Grx5-overexpressing mice and 10 were wild-type littermates. Among the 28 overexpressing mice, 6 of them were fed with standard food (SD) throughout the experimental period as a control group; the other Grx5 overexpressing mice and the wild-type littermates had the same dietary changes, as summarized in Figure 12.

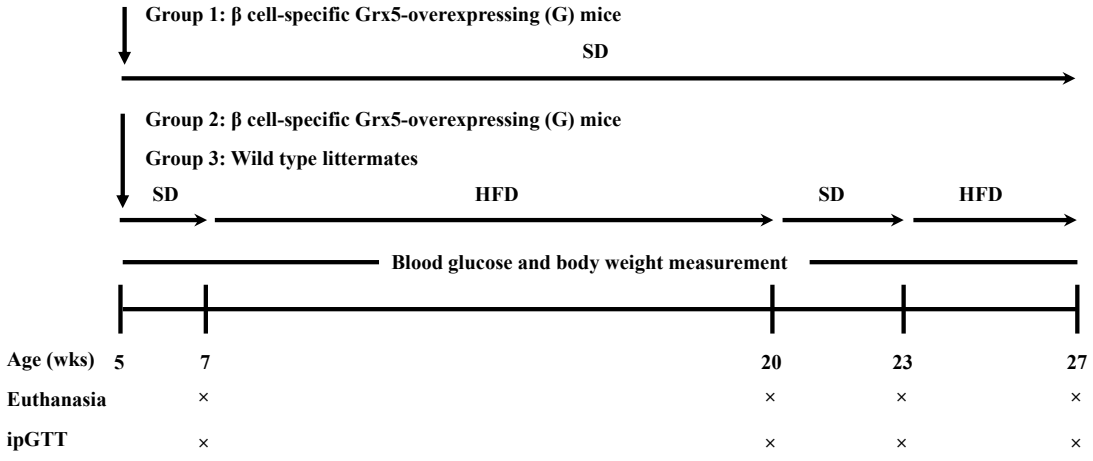

Figure 12 Experimental setup of the Grx5 overexpressing mice experiment. Group 1 is the Grx5 overexpressing mice, which were fed with a standard diet (SD, ca. 3514 kcal/kg, energy from 10% fat, 24% protein, and 66% carbohydrates) throughout the experiment period. Group 2 is the Grx5 overexpressing mice fed with a high-fat diet (HFD, ca. 5389 kcal/kg, energy from 70% fat, 16% protein, and 14% carbohydrates) for 13 weeks to induce an obese phenotype. Then, from 20 to 23 weeks of age, followed by rescue feeding with the SD for 3 weeks to switch from a state of lipotoxicity to glucotoxicity. Afterwards, they were fed with HFD again for the last 4 weeks of the experiment to induce lipotoxic stress again. Group 3 is the wild-type littermates fed with HFD and SD as in group 2. Body weight and fasting blood glucose levels were measured every week. Intraperitoneal glucose tolerance test and euthanasia were carried out in all groups at 7, 20, 23, and 27 weeks of age.

2.2.11.2 Pseudoislets transplantation experiment

5 NMRi nu/nu mice were utilized in the pseudoislets transplantation experiment according to the experimental setup in Figure 13.

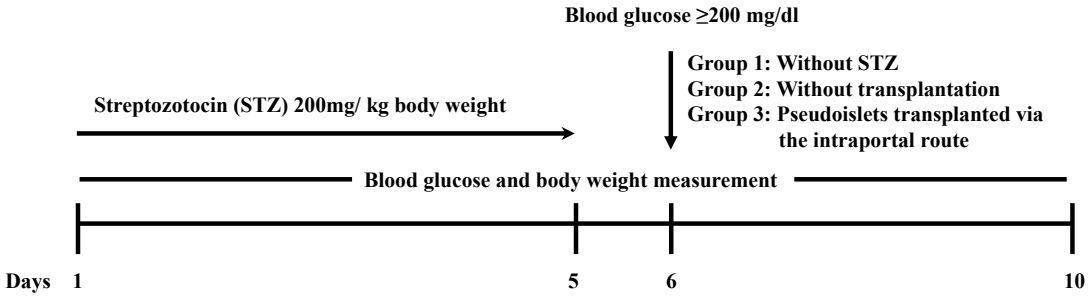

Figure 13 Experimental setup of the pseudoislets transplantation experiment. Four NMRi nu/nu mice were chosen randomly and administered through the intraperitoneal route 200 mg/kg body weight of STZ to induce DM (non-fasting blood glucose of ≥200 mg/dL). Three mice were randomly selected as recipients of pseudoislet transplantation via the intraportal route.

2.2.12 Determination of body weight

Body weights of mice were measured using a weighing machine.

2.2.13 Determination of blood glucose levels

2.2.13.1 Fasting blood glucose

Mice were fasted for approximately 15 hours (from 5:00 PM to 8:00 AM) for the measure of fasting blood glucose (FBG). After puncturing the tail vein with a 26 G needle and discarding the first small drop of blood, a drop of blood was taken, and blood glucose levels were measured with a glucometer (One Touch® Ultra®2, LifeScan).

2.2.13.2 Intraperitoneal glucose tolerance test

Weigh the mouse and prepare the volume of 10% glucose solution (1 mg of glucose/g of body weight) as follows:

Volume of glucose injection (µl) = 10 × body weight (g).

First, fasting blood glucose was measured as described in 2.2.13.1. Then, the mouse was restrained in a head-down position that allowed the viscera to move cranially and expose the abdomen. The needle was inserted at a 30- to 45-degree angle into either the left or right lower abdominal quadrant. Before injecting, aspiration was conducted to ensure the needle had not penetrated a blood vessel, the intestines, or the urinary bladder. Once confirmed, the glucose solution was injected at 0 minutes. The blood glucose levels were measured at 15, 30, 60, 90, and 120 minutes.

2.2.14 Streptozotocin (STZ) injection

The mouse was weighed, and the STZ (200 mg of STZ/kg of body weight) was prepared in 0.1 ml saline. The intraperitoneal injection was then performed as described in section 2.2.13.2.

2.2.15 Pseudoislets transplantation

The preparation of pseudoislets and transplantation are shown in Figure 14. EndoC-βH3 cells (2000/well) were seeded on a U-shaped 96-well plate in 100 µl Optiβ1 medium without coating and incubated for 60 hours to form pseudoislets. For one mouse, 300 pseudoislets were transferred into a 50-ml conical tube. The tube was kept vertical, and the OPTIβ1 medium was replaced with 0.3 ml of Hanks' solution as the pseudoislets were settled. Subsequently, the 300 pseudoislets in 0.3 ml of Hanks' solution were collected in a 1-ml syringe after filling the syringe with 0.1 ml of PFCS. Then, 0.15 ml of Ficoll was added after reducing the total volume in the syringe to 0.05 ml, resulting in a final volume of 0.2 ml in the syringe. The syringe was maintained vertically

throughout the process, and the pseudoislets settled at the cone of the syringe within 2-3 minutes.

Meanwhile, the mouse was subjected to laparotomy after being anesthetized with ketamine (100 mg/kg body weight) and xylazine (20 mg/kg body weight) via intraperitoneal injection. Subsequently, 0.2 ml of the prepared pseudoislets were injected into the portal vein near the liver within 1 minute under magnification after locating the portal vein. Afterwards, the puncture site was covered with sterile gauze and pressed with the index finger for 6 minutes to stop the bleeding, followed by repositioning all viscera and closing the incision. Tramadol (0.2 mg/mouse) was provided in the drinking water after surgery, and the non-fasting blood glucose levels of the mice were measured every day.

After transplantation, the syringe was rinsed in a fresh Petri dish with 1 ml of P/FCS medium, and the remaining pseudoislets were counted under a microscope.

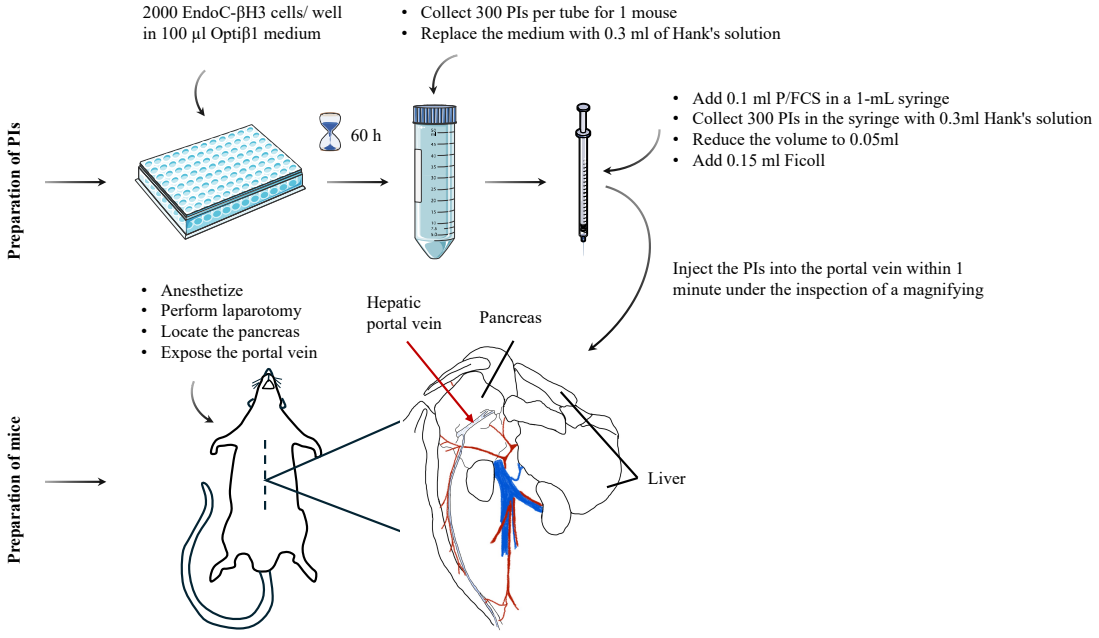

Figure 14 Experimental procedures for the preparation and transplantation of pseudoislets. The figure was partly generated using Servier Medical Art, provided by Servier. The picture of the abdominal viscera of the mouse was generated from The

Anatomy of the Laboratory Mouse, Margaret J. Cook, Laboratory Animals Centre, Carshalton, Surrey, England. PIs, pseudoislets.

2.2.16 Immunohistochemistry

Livers and pancreas were collected at the end of the experiment and fixed with Roti-Histofix 4% formaldehyde solution and stored at 4 °C. Before embedding, organs were washed with 70% ethanol on a shaker overnight at room temperature. Paraffin embedding was performed after being treated with an increasing alcohol series. Slides with a thickness of 5-7 µm were created using a microtome and stored at room temperature. Before staining, paraffin was removed with RotiHistol and a decreasing alcohol series (Table 17). Light microscopy was used for insulin and Grx5 detection, as described in Table 18. Islet morphology was analyzed by hematoxylin and eosin (H&E) staining, as described in Table 19.

Table 17 Deparaffinization

Reagent	Duration
Rotihistol	2 x 5 min
100% ethanol	2 x 5 min
96% ethanol	2 x 5 min
70% ethanol	2 x 5 min
Distilled water	5 min
Retrieval-buffer	Boil at 480 Watt in the microwave for 3 x 5 min, cooled for 30 min at RT

Table 18 Insulin and Grx5 light microscopy staining

Steps	Reagent	Duration
Washing	Tris/Tween buffer	2x 5 min
Blocking	1% goat serum in Tris buffer	20 min
Primary antibody	Primary antibody in 0.1% Tris/BSAbuffer	Overnight
Washing	Tris/Tween buffer	3x 5 min
Secondary antibody	Secondary antibody in 5% mouse serum in Tris buffer	1 hour

Washing	Tris buffer	2x 5 min
Visualization	Vector red (insulin); Fuchsine red (Grx5)	5-10 s
Counterstaining	Hematoxylin	15 s
(Grx5)	Tap water	1 min
	Tris buffer	5 min
Embedding	Mounting medium	-

Table 19 Hematoxylin and Eosin (H&E) Staining

Steps	**Reagent**	**Duration**
Deparaffinization	Rotihistol	5 min
	Rotihistol	5min
	100% ethanol	3 min
	96% ethanol	3 min
	80% ethanol	3 min
	70% ethanol	3 min
	50% ethanol	3 min
Hematoxylin staining	Hematoxylin	10 min
	Tap water	10 min
Eosin staining	Eosin	5 min
	Tap water	2 s
Dehydration	50% ethanol	3 min
	70% ethanol	3 min
	80% ethanol	3 min
	96% ethanol	3 min
	100% ethanol	3 min
	Rotihistol	5 min
	Rotihistol	5min
Embedding	Mounting medium	-

2.3 Statistical Analysis

Unless otherwise stated, all data are presented as mean ± standard error of the mean (SEM). Immunofluorescence images were analyzed by measuring the integrated density (IntDen) using ImageJ. At least three independent experiments were performed. All data analysis was based on GraphPad Prism (Prism 9 Software) using an unpaired

t-test or one- or two-way ANOVA with Tukey or Sidak multiple comparison tests when appropriate. P-values < 0.05 were considered statistically significant.

3 Results

3.1 Metabolic activity of β cells under free fatty acids treatment

3.1.1 Effects of different ratios of OA to BSA on the metabolic activity of MIN6 cells

OA is a commonly used free fatty acid in T2DM research. Apart from the OA concentration, different ratios of OA and BSA complexing will also have different effects. Therefore, we analyzed the effects of different OA to BSA ratios on the metabolic activity of MIN6 cells and found that although there were no statistically significant differences among the 1.5 mM OA groups of different OA to BSA ratios, 1.5 mM OA had different effects on the metabolic activity of MIN6 cells in different OA to BSA ratios compared with the 0 mM OA control group (the 0 mM OA control group solutions were prepared to match the same ethanol and BSA concentrations as the 1.5 mM OA group). Among them, 1.5 mM OA reduced metabolic activity at a 5:1 ratio ($p<0.05$), had no significant effect at a 3:1 ratio, and increased metabolic activity at a 1:1 ratio ($p<0.01$). In addition, when comparing 0 mM OA between different ratios, we found that 0 mM OA at a 1:1 ratio significantly reduced cell metabolic activity ($p<0.05$) (Figure 15). Therefore, in order to minimize the effect of BSA and focus on the effect of OA, a ratio of 5:1 is used in this thesis for simulating pathological conditions.

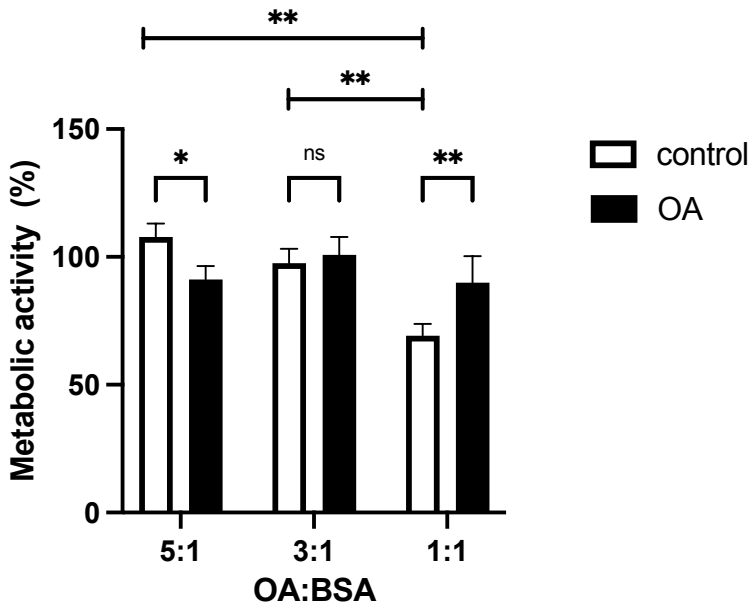

Figure 15 Effects of different ratios of OA to BSA on the metabolic activity of MIN6 cells. MIN6 cells were treated with different ratios of OA to BSA for 24 hours. The control group (0 mM) had the same ethanol and BSA concentrations as the OA group (1.5 mM). Metabolic activity was measured by MTT. From n = 7 independent experiments. Significant differences are indicated (*p<0.05, **p<0.01).

3.1.2 OA reduce the metabolic activity of EndoC-βH3 cells in a dose-dependent manner

Our previous study found that treatment with OA might result in a decrease in metabolic activity in MIN6 cells (Römer et al., 2022). We also analyzed the effect of OA on the metabolic activity of human β cells since it is widely recognized that there are clear differences between human β cells and rodent β cells. Remarkably, we found that OA reduced the metabolic activity of EndoC-βH3 cells in a dose-dependent manner (Figure 16).

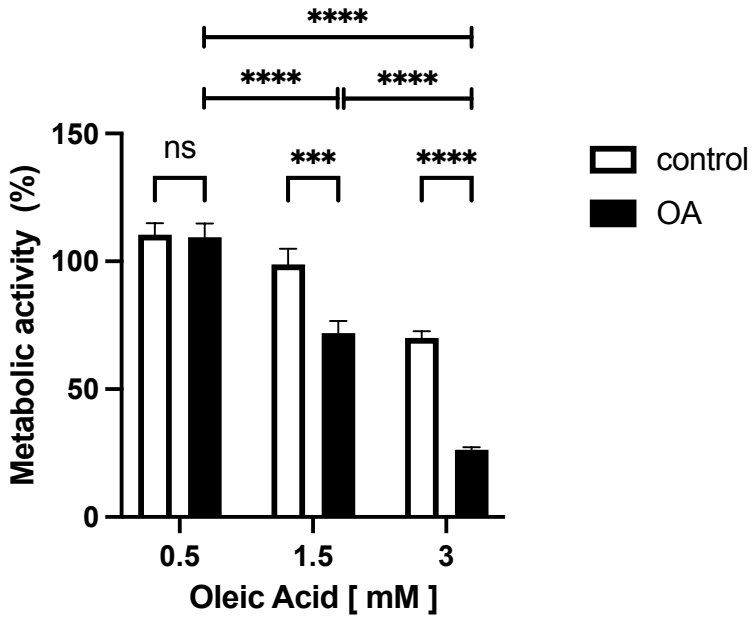

Figure 16 Effects of different concentrations of OA on the metabolic activity of EndoC-βH3 cells. EndoC-βH3 Cells were treated with different concentrations of OA for 48 hours. Metabolic activity was measured by MTT. From n = 6 independent experiments. Significant differences are indicated (***p<0.001, ****p<0.0001).

3.2 Effects of ML-162 and Lip-1 on β cells under free fatty acids treatment

3.2.1 Metabolic activity of MIN6 cells

In the absence of OA, the ferroptosis inducer ML-162 did not decrease the metabolic activity of MIN6 cells, whereas in the presence of OA, ML-162 significantly decreased the cell metabolic activity ($p<0.0001$). ML-162 could further aggravate the OA-induced decrease in cell metabolic activity ($p<0.01$). However, the ferroptosis inhibitor Lip-1 cannot rescue the decrease in cell metabolic activity induced by OA (Figure 17).

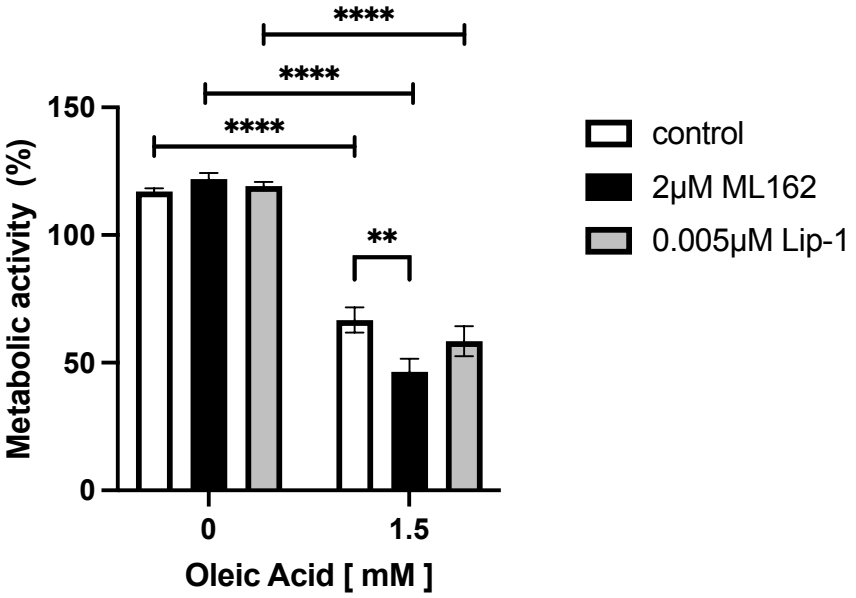

Figure 17 Effects of ferroptosis inducer and inhibitor on MIN6 cells under free fatty acid treatment on metabolic activity. MIN6 cells were treated with ML-162 and Lip-1 with or without OA for 24 hours. Metabolic activity was measured by MTT. From n = 6 independent experiments. Significant differences are indicated (**p<0.01, ****p<0.0001).

3.2.2 ATP content of MIN6 cells

The intracellular ATP level was decreased by 0 mM (p<0.01) and 1.5 mM OA (p<0.001) in comparison to the untreated normal cell group. In the presence of 0 mM OA, Lip-1 could significantly enhance the intracellular ATP level (p<0.001). Lip-1 significantly increased ATP levels in the absence of OA. Moreover, Lip-1 tended to increase ATP levels also in the presence of OA; however, this effect was not significant (Figure 18).

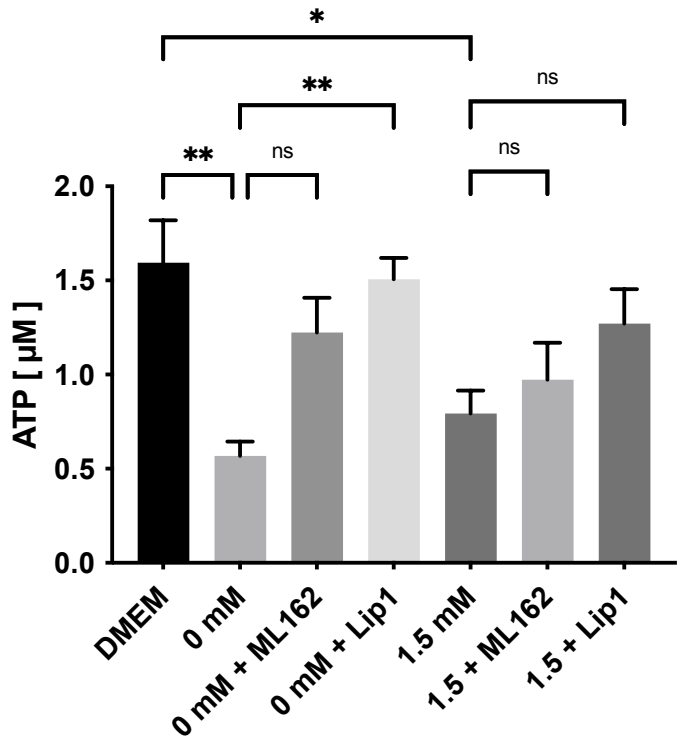

Figure 18 Effects of ML-162 and Lip1-1 on intracellular ATP level of MIN6 cells under fatty acid treatment. MIN6 cells were treated with ML-162 and Lip-1 with or without OA for 24 hours. ATP levels were measured by ATP bioluminescence assay. From n = 6 independent experiments. Significant differences are indicated (**p<0.01, ***p<0.001).

3.2.3 Insulin and Grx5 protein levels of MIN6 cells

The effects of ML-162 and Lip-1 on insulin and Grx5 protein levels in MIN6 cells in the presence of fatty acids were analyzed by immunocytochemistry and ELISA. MIN6 cells were treated with ML-162 or Lip-1 and OA for 24 hours. The staining showed that 3 mM OA significantly reduced insulin ($p<0.01$) and Grx5 ($p<0.01$) protein levels; ML-162 further aggravated the decrease (insulin: $p<0.05$ at 2 µM ML-162, $p<0.01$ at 5 µM ML-162; Grx5: $p<0.05$ at 2 µM ML-162, $p<0.01$ at 5 µM ML-162). By contrast, Lip-1 rescued the reduction of insulin ($p<0.001$) and Grx5 ($p<0.01$) caused by 3 mM OA (Figure 19A, B, C).

The results of ELISA were consistent with quantitative immunocytochemistry analysis in MIN6 cells. Insulin content ($p<0.01$, Figure 20A) and secretion ($p<0.001$, Figure 20B) were decreased by 3 mM OA and further aggravated by ML-162, although not with statistical significance. Furthermore, Lip-1 rescued the decrease in both insulin content ($p<0.01$, Figure 20A) and secretion ($p<0.05$, Figure 20B) caused by 3 mM OA significantly. Consistently, Grx5 levels were also reduced by 3 mM OA ($p<0.01$) and ML-162 ($p<0.01$) and rescued by Lip-1 ($p<0.0001$) (Figure 20C).

Further, long-term treatment (5 days) with lower concentrations of OA, ML-162, and Lip-1 was also conducted, and the results were consistent with the 24-hour treatment. 1.5 mM OA reduced Grx5 levels ($p<0.0001$). Lip-1 significantly rescued the OA-induced reduction of Grx5 ($p<0.0001$), and ML-162 tended to further exacerbate the Grx5 decrease, although the effect was not statistically significant (Figure 20D).

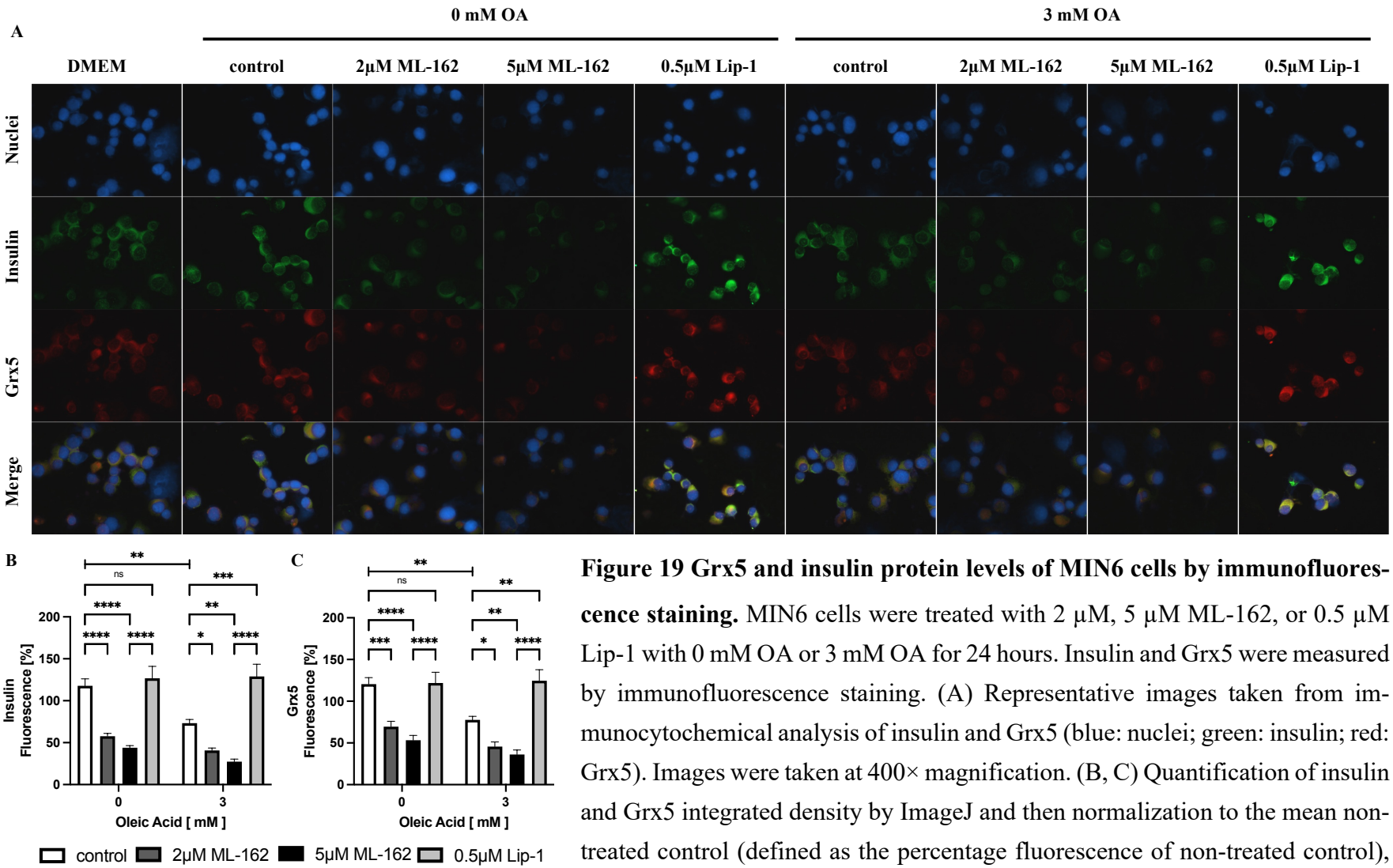

Figure 19 Grx5 and insulin protein levels of MIN6 cells by immunofluorescence staining. MIN6 cells were treated with 2 µM, 5 µM ML-162, or 0.5 µM Lip-1 with 0 mM OA or 3 mM OA for 24 hours. Insulin and Grx5 were measured by immunofluorescence staining. (A) Representative images taken from immunocytochemical analysis of insulin and Grx5 (blue: nuclei; green: insulin; red: Grx5). Images were taken at 400× magnification. (B, C) Quantification of insulin and Grx5 integrated density by ImageJ and then normalization to the mean non-treated control (defined as the percentage fluorescence of non-treated control), from n = 5 independent experiments. Significant differences are indicated (*p<0.05, **p<0.01, ***p<0.001, ****p<0.0001).

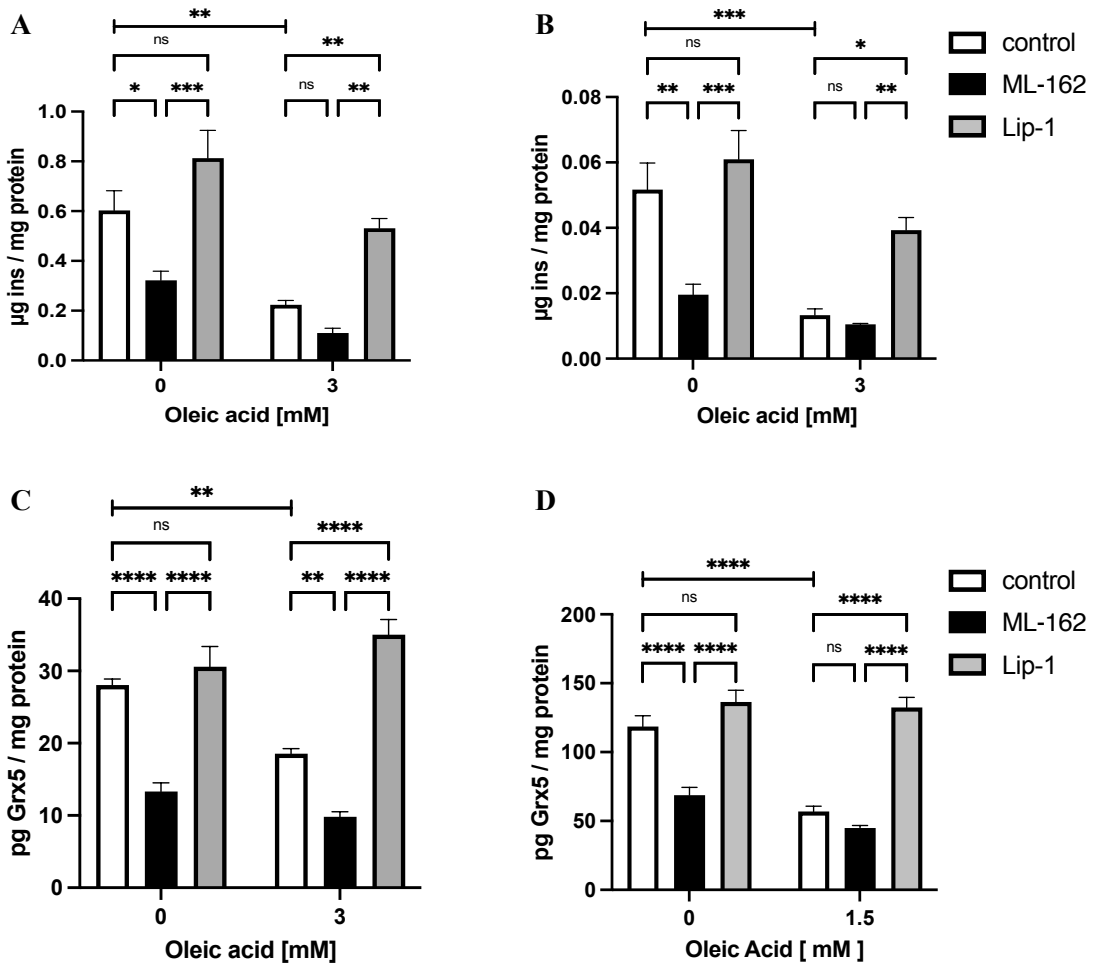

Figure 20 Grx5 and insulin protein levels of MIN6 cells by ELISA. (A, B, C) MIN6 cells were treated with 5 µM ML-162, 0.5 µM Lip-1 with 0 mM OA or 3 mM OA for 24 hours; (A) insulin content, (B) insulin secretion, and (C) Grx5 level were measured by ELISA and normalized by total protein, from n = 3 independent experiments. (D) MIN6 cells were treated with 2 µM ML-162, 0.003 µM Lip-1 with 0 mM OA or 1.5 mM OA for 5 days; Grx5 levels were measured by ELISA and normalized by total protein, from n = 4 independent experiments. Significant differences are indicated (*p<0.05, **p<0.01, ***p<0.001, ****p<0.0001).

3.2.4 Gpx4 levels of MIN6 cells

The effects of ML-162 and Lip-1 on Gpx4 in MIN6 cells under fatty acid treatment were also analyzed by immunocytochemistry. Treatment for 24 hours revealed a significant loss of Gpx4 level by 3 mM OA (p<0.0001), further aggravated by ML-162 (p<0.01 at 2 µM ML-162, p<0.001 at 5 µM ML-162), but different from insulin and

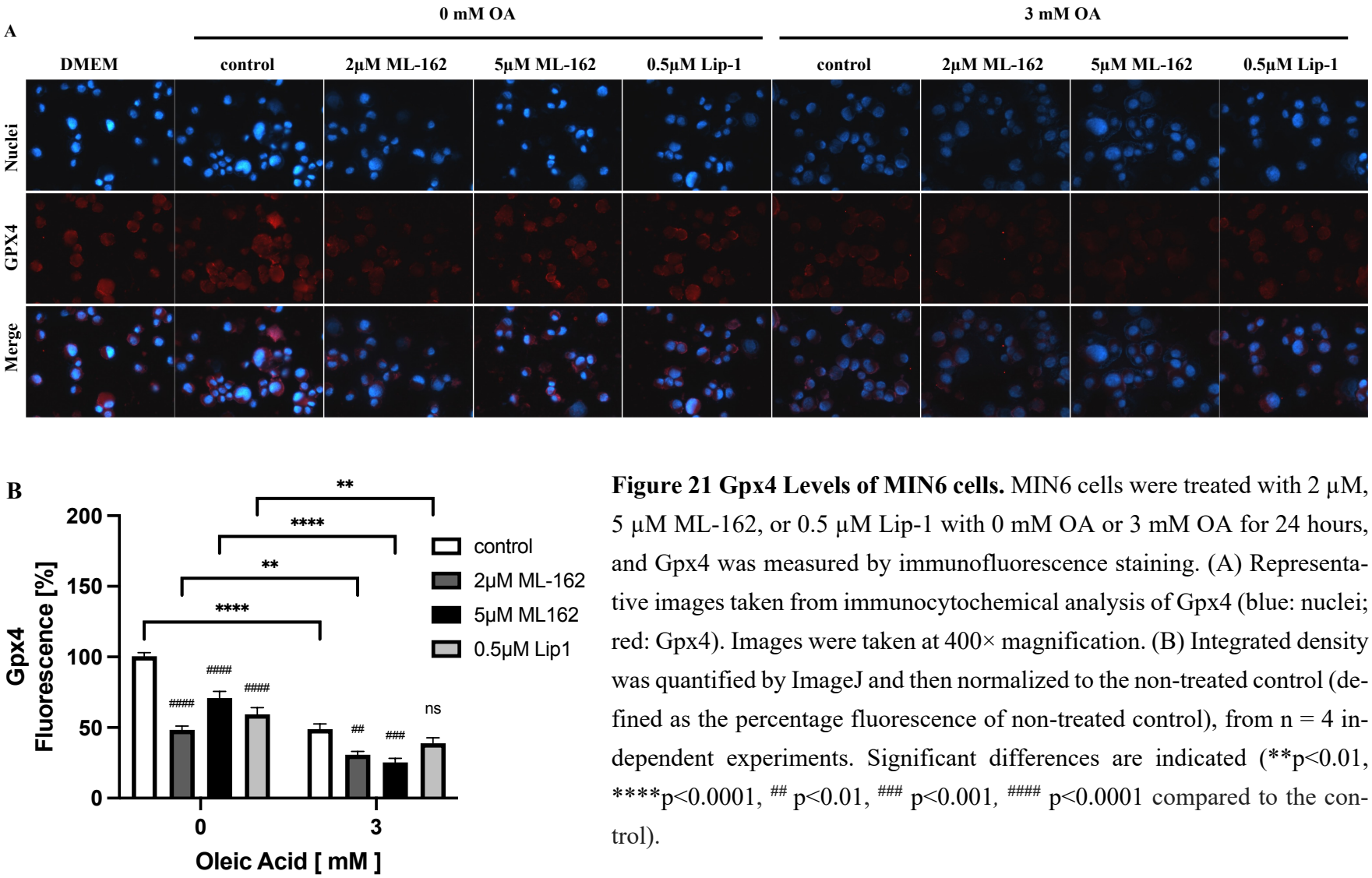

Figure 21 Gpx4 Levels of MIN6 cells. MIN6 cells were treated with 2 μM, 5 μM ML-162, or 0.5 μM Lip-1 with 0 mM OA or 3 mM OA for 24 hours, and Gpx4 was measured by immunofluorescence staining. (A) Representative images taken from immunocytochemical analysis of Gpx4 (blue: nuclei; red: Gpx4). Images were taken at 400× magnification. (B) Integrated density was quantified by ImageJ and then normalized to the non-treated control (defined as the percentage fluorescence of non-treated control), from n = 4 independent experiments. Significant differences are indicated (**p<0.01, ****p<0.0001, $^{\#\#}$ p<0.01, $^{\#\#\#}$ p<0.001, $^{\#\#\#\#}$ p<0.0001 compared to the control).

Grx5, this reduction could not be rescued by Lip-1. In addition, we found that the decrease of ML-162 on Gpx4 was significantly different in the presence or absence of OA ($p<0.01$ at 2 μM ML-162, $p<0.0001$ at 5 μM ML-162). Lip-1 with 3 mM OA significantly reduced Gpx4 levels compared to Lip-1 with 0 mM OA ($p<0.01$) (Figure 21).

3.2.5 Iron metabolism of β cells

Cellular lipid peroxide accumulation and iron metabolism disorders play an important role in ferroptosis. Liperfluo, Mito-FerroGreen, and FerroOrange were used to detect lipid peroxidation, mitochondria, and intracellular Fe^{2+}, respectively.

MIN6 cells were treated with 50 μM ML-162 or 0.5 μM Lip-1 and with 0 mM OA or 3 mM OA for 24 hours. Under the light microscope, treatment with 50 μM ML-162 changed the morphology of MIN6 cells (Figure 22A). The results of Liperfluo staining in MIN6 cells showed that, compared with 0 mM OA, intracellular lipid peroxidation level was significantly increased in the presence of ML-162 ($P < 0.0001$) or 3 mM OA ($P < 0.01$). When MIN6 cells were co-treated with ML-162 or Lip-1 and 3 mM OA, the level of intracellular lipid peroxidation was further enhanced by ML-162 ($P < 0.01$) and reduced by Lip-1 ($P < 0.01$) compared to treatment with 3 mM OA alone. And regardless of the presence or absence of 3 mM OA, there was a significant difference in the intracellular lipid peroxidation level between ML-162 and Lip-1 treated MIN6 cells ($P < 0.0001$ at 0 mM OA, $P < 0.0001$ at 3 mM OA) (Figure 22B).

Patterns of Fe^{2+} changes in mitochondria are consistent with lipid peroxidation. The application of Mito-FerroGreen revealed that mitochondrial Fe^{2+} was significantly upregulated in MIN6 cells treated with ML-162 ($P < 0.01$) or 3 mM OA ($P < 0.05$) compared with cells treated with 0 mM OA. Similarly, compared with 3 mM OA alone, mitochondrial Fe^{2+} was higher when MIN6 cells were cotreated with ML-162 and 3 mM OA ($P < 0.01$) but lower with the combination of Lip-1 and 3 mM OA ($P < 0.05$).

Finally, in addition to the consistently clear differences in mitochondrial Fe^{2+} between ML-162 and Lip-1 treated cells ($P < 0.01$ at 0 mM OA, $P < 0.0001$ at 3 mM OA), we also found that mitochondrial Fe^{2+} was significantly higher in MIN6 cells treated with ML-162 and 3 mM OA than in ML-162 and 0 mM OA ($P < 0.01$) (Figure 22C).

We further verified these effects using EndoC-βH3 cells. They were treated with 50 μM ML-162 or 0.5 μM Lip-1 combined with either 0 mM OA or 3 mM OA for 24 hours. Consistent with the changes observed in MIN6 cells, lipid peroxidation was enhanced in the presence of ML-162 ($P < 0.0001$). 3 mM OA also supported the accumulation of lipid peroxides ($P < 0.05$), which was aggravated by ML62 ($P < 0.0001$) and reduced by Lip-1 ($P < 0.01$) (Figure 22E).

Regarding the changes in mitochondrial Fe^{2+} in EndoC-βH3 cells, although we only performed one independent experiment, we could observe that the trend of changes in mitochondrial Fe^{2+} in EndoC-βH3 cells was exactly the same as in MIN6 cells (Figure 22F).

However, there are different findings when using FerroOrange to detect changes in intracellular Fe^{2+}. Intracellular Fe^{2+} increased significantly in MIN6 cells treated with 3 mM OA ($P < 0.01$) but conversely decreased in MIN6 cells treated with ML-162 ($P < 0.01$). When MIN6 cells were co-treated with ML-162 or Lip-1 and 3 mM OA, intracellular Fe^{2+} levels were further reduced by ML-162 ($P < 0.0001$) and increased by Lip-1 ($P < 0.001$). Intracellular Fe^{2+} was significantly higher in cells treated with Lip-1 and 3 mM OA than in in cells treated with Lip-1 and 0 mM OA ($P < 0.0001$). Nevertheless, intracellular Fe^{2+} levels were significantly different between ML-162 and Lip1-treated MIN6 cells ($P < 0.0001$ at 0 mM OA, $P < 0.0001$ at 3 mM OA) (Figure 22D).

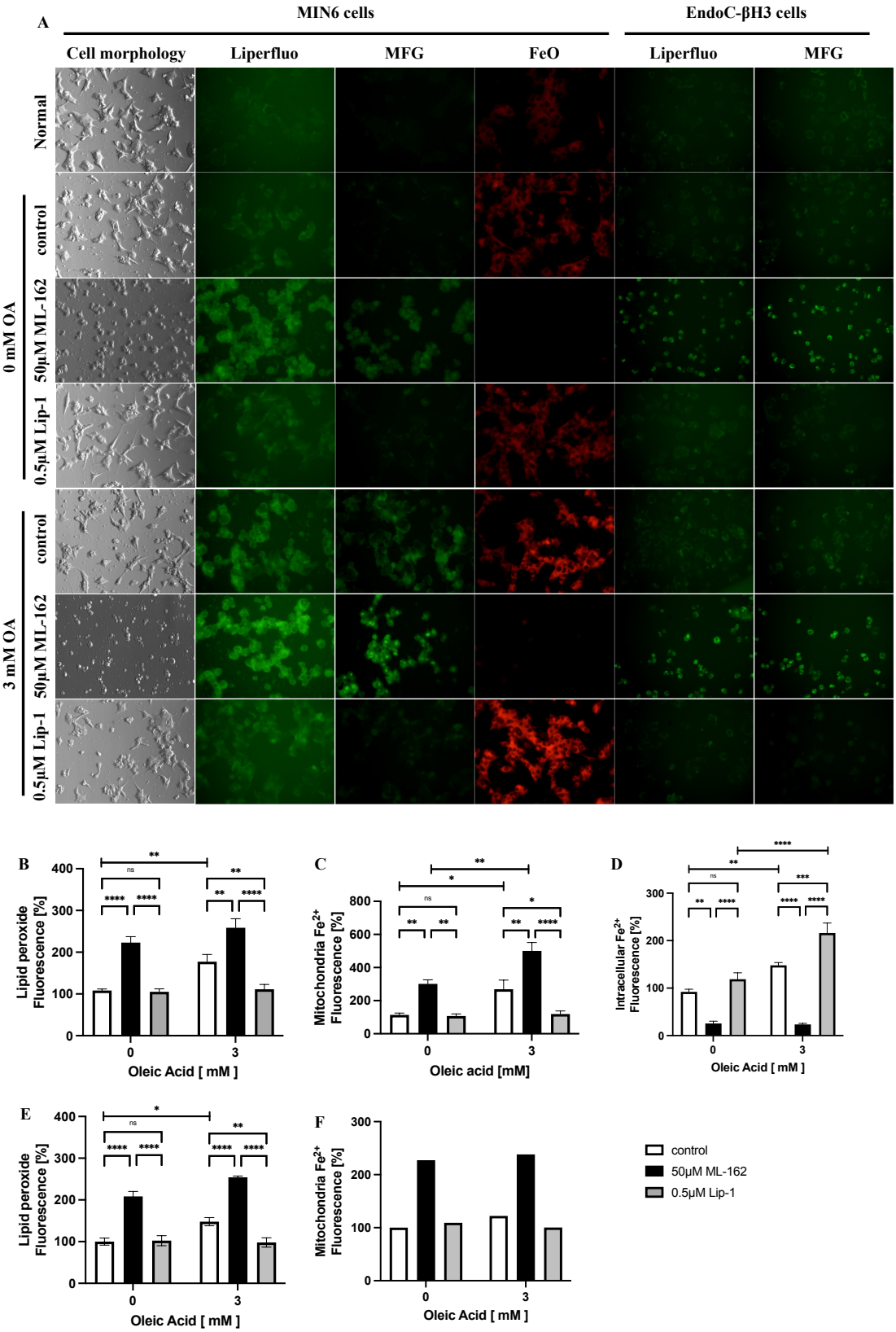

Figure 22 Iron metabolism of β cells. MIN6 cells and EndoC-βH3 cells were treated with 50 μM ML-162 or 0.5 μM Lip-1 with 0 mM OA or 3 mM OA for 24 hours. (A) Representative images were taken under fluorescence microscopy at 400× magnification (Liperfluo, Mito-FerroGreen, and FerroOrange) or light microscopy at 200×

magnification (cell morphology). (B) Quantification of MIN6 cells lipid peroxidation integrated density, from n = 4 independent experiments. (C) Quantification of MIN6 cells mitochondria Fe^{2+} integrated density, from n = 3 independent experiments. (D) Quantification of MIN6 cells intracellular Fe^{2+} integrated density, from n = 4 independent experiments. (E) Quantification of EndoC-βH3 cells lipid peroxidation integrated density, from n = 3 independent experiments. (F) Quantification of EndoC-βH3 cells mitochondria Fe^{2+} integrated density, from n = 1 experiment. All integrated density was normalized to the non-treated control (defined as the percentage fluorescence of the non-treated control). Significant differences are indicated (*p<0.05, **p<0.01, ***p<0.001, ****p<0.0001). Abbreviations: MFG, Mito-FerroGreen; FeO, FerroOrange.

Therefore, we further determined the effects of different concentrations of ML-162 and Lip-1 on intracellular Fe^{2+}. MIIN6 cells were treated with a series of concentrations of ML-162 and Lip-1 for 24 hours. The results showed that ML-162 reduced intracellular iron in a dose-dependent manner, reaching the lowest level at 50 μM ($P < 0.0001$) (Figure 23B), while Lip1 gradually increased intracellular iron until a decrease was observed after reaching a concentration of 0.5 μM (Figure 23C).

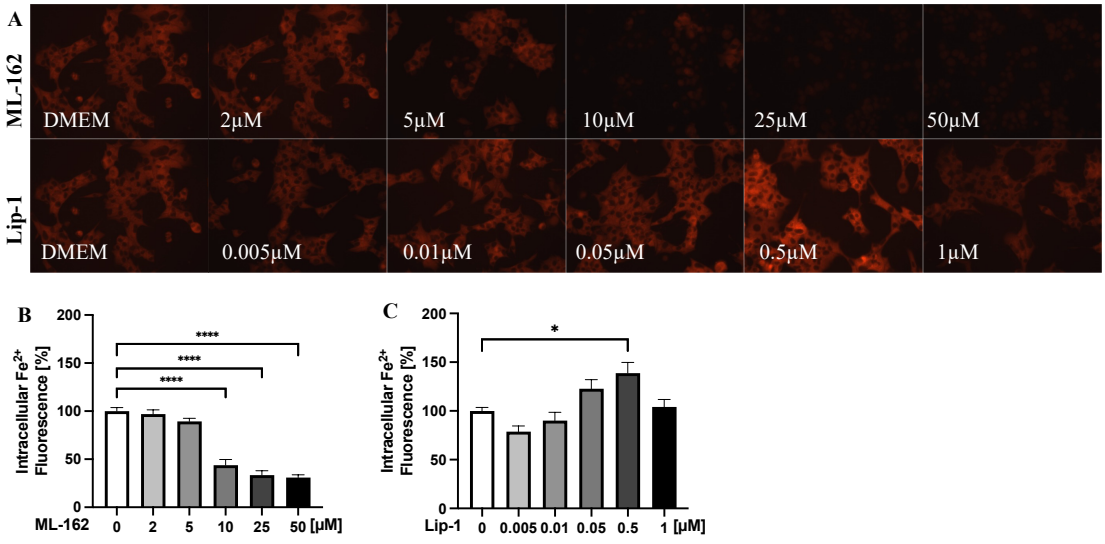

Figure 23 Effect of a concentration series of ML-162 and Lip-1 on intracellular Fe^{2+}. MIN6 cells were treated with 2 μM, 5 μM, 10 μM, 25 μM and 50 μM ML-162 or 0.005 μM, 0.01 μM, 0.05 μM, 0.5 μM and 1 μM Lip-1 for 24 hours. (A) Representative images taken under fluorescence microscopy at 400× magnification. (B) Quantification

of MIN6 cells intracellular Fe^{2+} integrated density under ML-162 treatment and (C) Lip-1 treatment by ImageJ and then normalization to the non-treated control (defined as the percentage fluorescence of the non-treated control), from n = 3 independent experiments. Significant differences are indicated (*p<0.05, ***p<0.001).

3.3 Grx5 downregulation under free fatty acids treatment

Grx5 knockdown was achieved using siRNA by nucleofection in MIN6 cells to further investigate the role of Grx5 in β cells. The controls were untransfected cells and cells transfected with negative siRNA. In addition, all cells were treated with different concentrations of OA and corresponding controls.

3.3.1 Grx5 downregulation *in vitro*

The results showed that the level of Grx5 mRNA in transfected cells was significantly lower than that in untransfected cells (p<0.01 at 0 mM, p<0.01 at 1.5 mM, and p<0.001 at 3 mM) (Figure 24A). And the level of Grx5 protein in transfected cells was significantly lower than that in untransfected cells, as well (p<0.0001 at 0 mM, p<0.0001 at 1.5 mM, and p<0.001 at 3 mM) (Figure 24B). Consistent with the previous results (see 3.2.3), the level of Grx5 protein was reduced by OA in a dose-dependent manner in cells with or without transfection (Figure 24B).

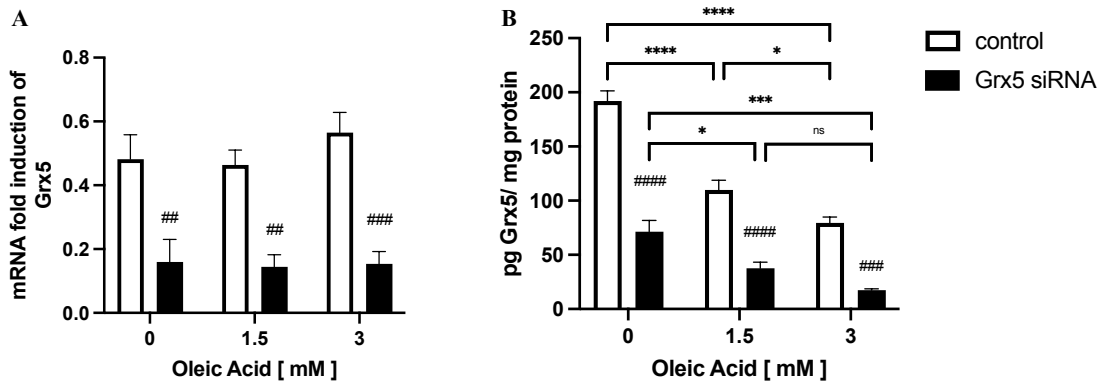

Figure 24 Knockdown of Grx5 *in vitro* using siRNA. MIN6 cells were treated with 0 mM, 1.5 mM, or 3 mM OA for 24 hours after transfection. (A) Fold change in mRNA expression of Grx5, relative to non-transfected, non-treated MIN6 cells, from n = 4 independent experiments. (B) Grx5 level was measured by ELISA and normalized by total protein, from n = 3 independent experiments. Significant differences are indicated (*p<0.05, ***p<0.001, ****p<0.0001, $^{\#\#}$p<0.01, $^{\#\#\#}$p<0.001, $^{\#\#\#\#}$p<0.0001; $^{\#}$ indicates significance for the untransfected cells).

3.3.2 Effects on metabolic activity

Grx5 knockdown resulted in reduced cell metabolic activity in MIN6 cells (p<0.0001 at 0 mM, p<0.01 at 1.5 mM, and p<0.0001 at 3 mM) (

Figure 25).

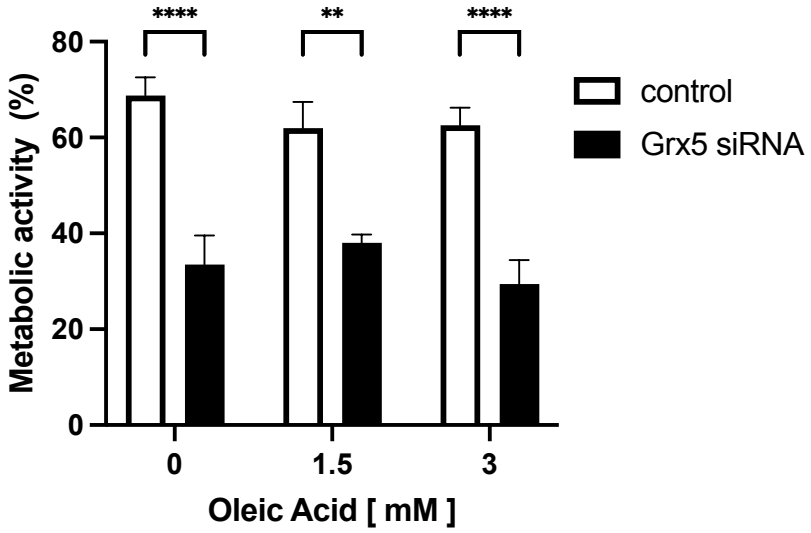

Figure 25 The metabolic activity of MIN6 cells with Grx5 knockdown. MIN6 cells were treated with 0 mM, 1.5 mM, or 3 mM OA for 24 hours after transfection. Cell metabolic activity was measured by MTT, defined as the percentage of the non-transfected, non-treated control. From n = 5 independent experiments. Significant differences are indicated (**p<0.01, ****p<0.001).

3.3.3 Effects on insulin content and secretion

Next, insulin content and secretion were analyzed in MIN6 cells after the knockdown of Grx5. As shown in Figure 26, Grx5 knockdown led to a significant decrease in insulin content in MIN6 cells when compared to the untransfected cells ($p<0.01$ at 0 mM, $p<0.001$ at 1.5 mM, and $p<0.05$ at 3 mM) (Figure 26A). Similarly, insulin secretion was significantly reduced when Grx5 was knocked down ($p<0.0001$ at 0 mM, $p<0.0001$ at 1.5 mM, and $p<0.01$ at 3 mM) (Figure 26B). In addition, consistent with the changes in Grx5 protein levels, both insulin content and insulin secretion decreased significantly with increasing OA concentrations.

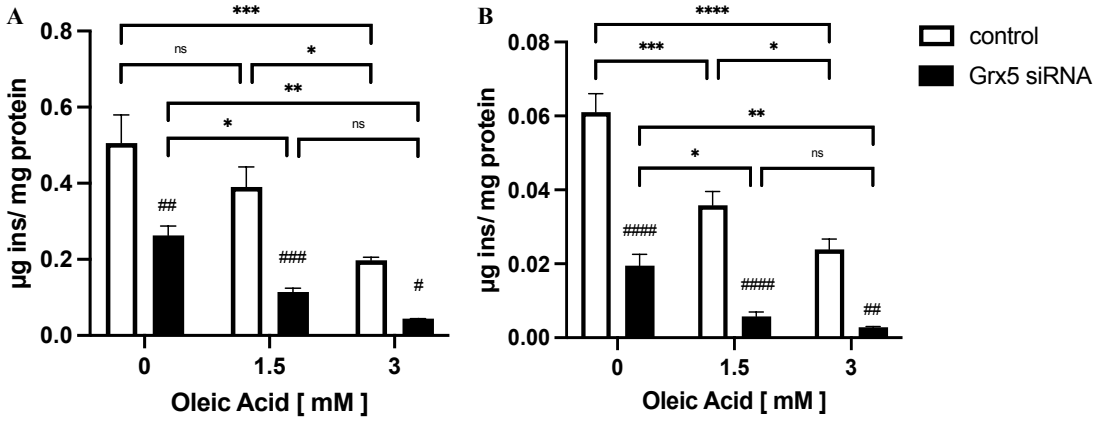

Figure 26 Insulin content and secretion of MIN6 cells with Grx5 knockdown. MIN6 cells were treated with 0 mM, 1.5 mM, or 3 mM OA for 24 hours after transfection. Insulin content and secretion of MIN6 cells with Grx5 knockdown. (A) Insulin content and (B) insulin secretion were measured by ELISA and normalized by total protein, from n = 3 independent experiments. Significant differences are indicated (*$p<0.05$, **$p<0.01$, ***$p<0.001$, ****$p<0.0001$, $^{\#}p<0.05$, $^{\#\#}p<0.01$, $^{\#\#\#}p<0.001$, $^{\#\#\#\#}p<0.0001$; $^{\#}$ indicates significance for the untransfected cells).

3.3.4 Effects on iron metabolism

Furthermore, to investigate the effect of Grx5 knockdown on the iron metabolism of MIN6 cells, Liperfluo, Mito-FerroGreen, and FerroOrange were used as live labels on normal and transfected MIN6 cells.

The results of Liperfluo labeling showed that compared with untransfected cells, Grx5 knockdown triggered intracellular peroxidation ($p<0.05$ at 0 mM, $p<0.001$ at 1.5 mM, and $p<0.0001$ at 3 mM). In addition, the level of intracellular lipid peroxidation was also increased with rising OA concentrations (Figure 27B).

The alterations in mitochondrial Fe^{2+} measured by Mito-FerroGreen were compatible with lipid peroxidation. In cells with Grx5 knockdown, mitochondrial Fe^{2+} was significantly increased ($p<0.01$ at 0 mM, $p<0.01$ at 1.5 mM, and $p<0.001$ at 3 mM). And the accumulation of mitochondrial Fe^{2+} was also enhanced by OA in a dose-dependent manner (Figure 27C).

However, different from the changes in mitochondrial Fe^{2+}, although intracellular Fe^{2+} also increased with the increase of OA concentrations, Grx5 knockdown reduced intracellular Fe^{2+} levels ($p<0.05$ at 0 mM, $p<0.05$ at 1.5 mM, and $p<0.001$ at 3 mM) (Figure 27D).

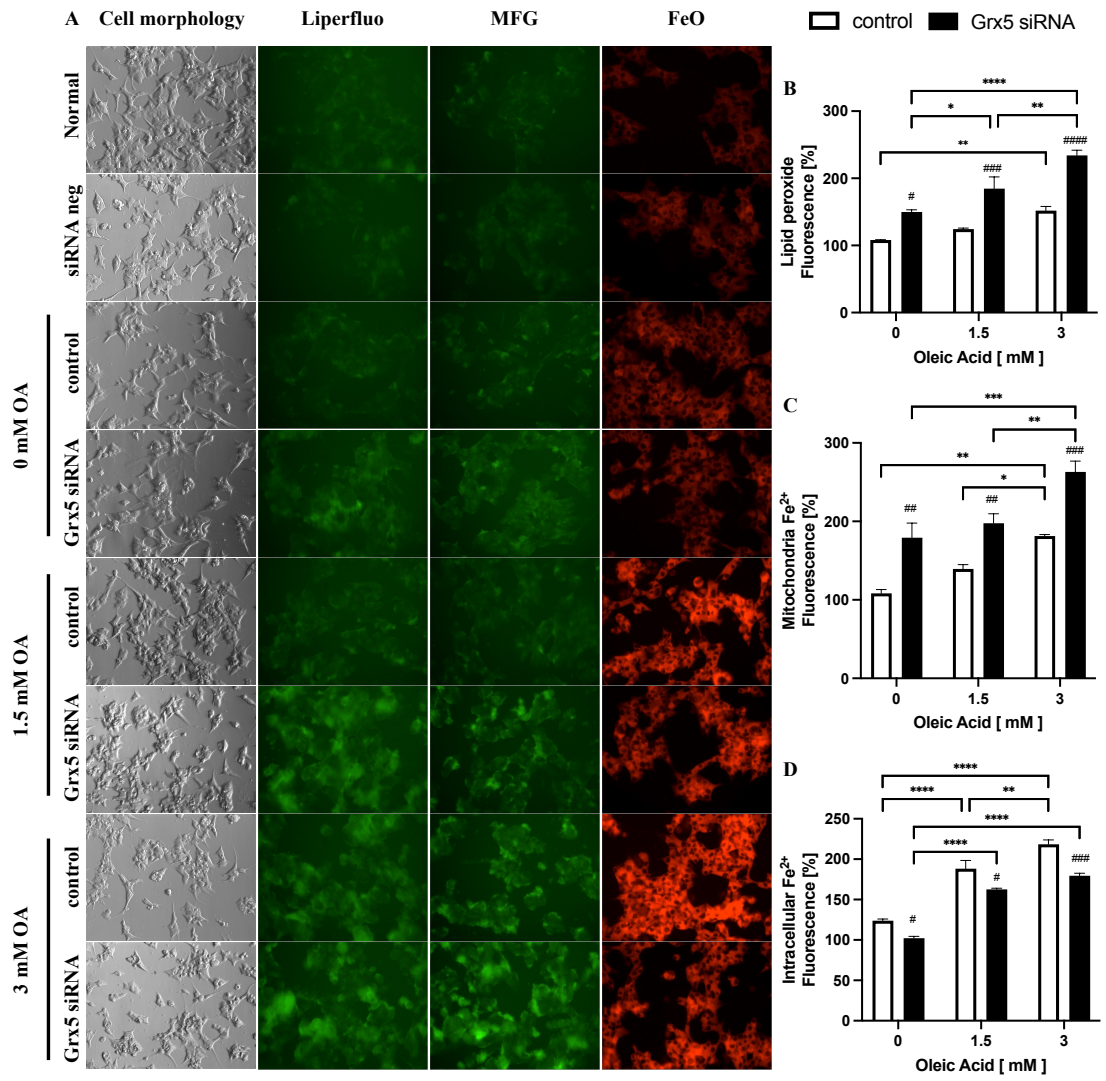

Figure 27 Iron metabolism of MIN6 cells with Grx5 knockdown. MIN6 cells were treated with 0 mM, 1.5 mM, or 3 mM OA for 24 hours after transfection. (A) Representative images were taken under fluorescence microscopy at 400× magnification (Liperfluo, Mito-FerroGreen, and FerroOrange) or light microscopy at 200× magnification (cell morphology). (B) Quantification of MIN6 cells lipid peroxidation integrated density, from n = 3 independent experiments. (C) Quantification of MIN6 cells mitochondria Fe^{2+} integrated density, from n = 3 independent experiments. (D) Quantification of MIN6 cells intracellular Fe^{2+} integrated density, from n = 3 independent experiments. All integrated density was normalized to the non-treated control (defined as the percentage fluorescence of the non-treated control). Significant differences are indicated (*p<0.05, **p<0.01, ***p<0.001, ****p<0.0001, $^{\#}$p<0.05, $^{\#\#}$p<0.01, $^{\#\#\#}$p<0.001, $^{\#\#\#\#}$p<0.0001; $^{\#}$ indicates significance for the untransfected cells). Abbreviations: MFG, Mito-FerroGreen; FeO, FerroOrange.

3.4 Intraportal transplantation of pseudoislets

3.4.1 Glucose-stimulated insulin secretion of EndoC-βH3 cell monolayers and pseudoislets *in vitro*

The insulin secretion level of EndoC-βH3 cell monolayers and pseudoislets was increased 2.1- and 4.6-fold compared to the basal group when exposed to high glucose (20 mM) (Figure 28B, D). When cAMP was increased by the phosphodiesterase inhibitor IBMX upon exposure to high glucose concentrations, insulin secretion of EndoC-βH3 cell monolayers was not only enhanced compared to the basal condition ($p<0.0001$) but also higher than the 20 mM glucose condition alone ($p<0.0001$) (Figure 28B), but insulin secretion of EndoC-βH3 pseudoislets was increased 4.95-fold compared to the control and 1.42-fold compared to the 20 mM glucose alone, although not significant (Figure 28D). There were no significant changes in insulin content in either monolayer cells or pseudoislets (Figure 28A, C).

Insulin secretion capacity was then calculated to compare the difference between monolayer cells and pseudoislets. The results showed that the insulin secretion capacity of pseudoislets was significantly increased compared to monolayer cells ($p<0.01$ at 45 μM IBMX and $p<0.05$ at 20 mM glucose with 45 μM IBMX) (Figure 28E).

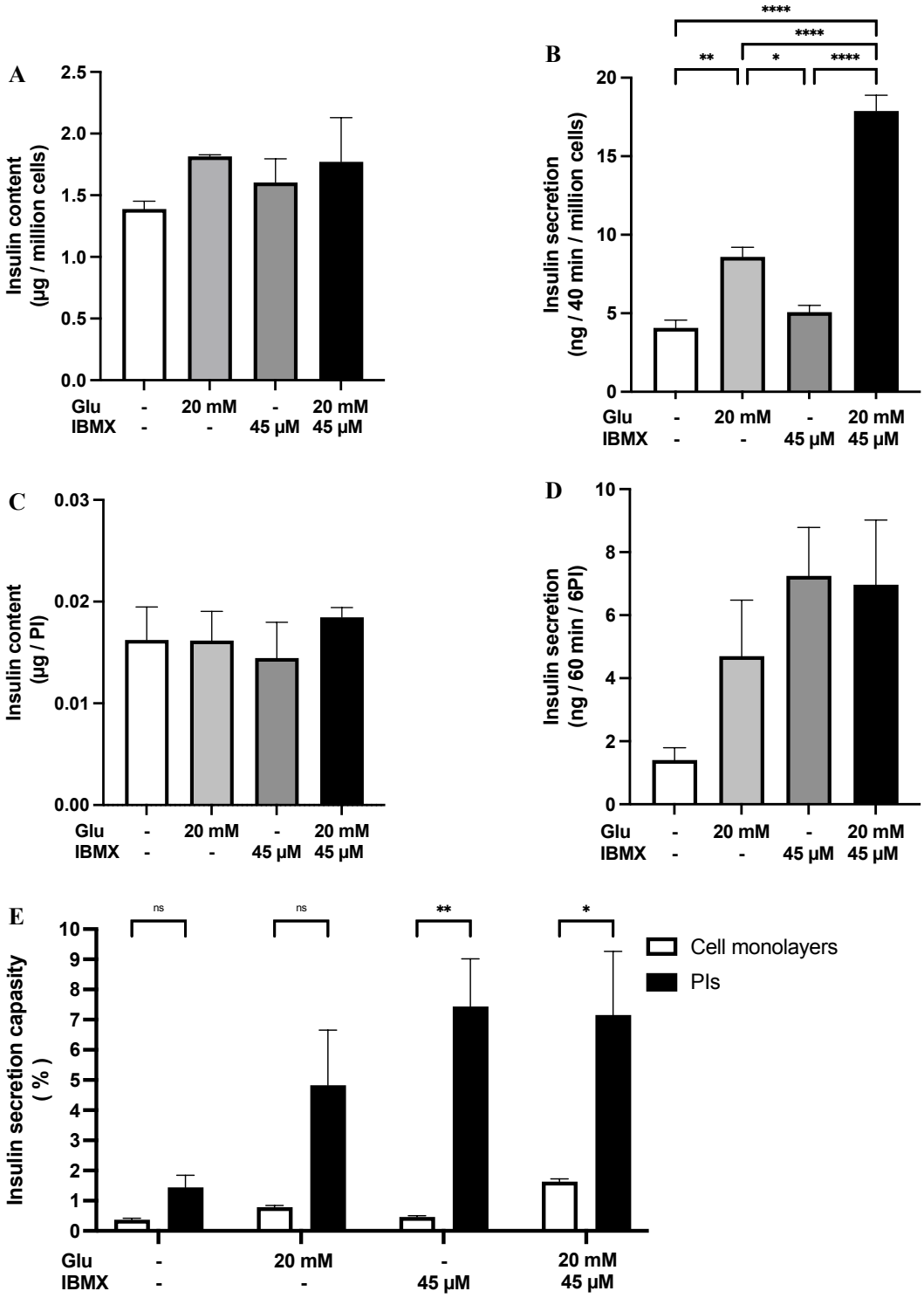

Figure 28 Glucose-stimulated insulin secretion in EndoC-βH3 cell monolayers and pseudoislets. (A, B) Glucose-stimulated insulin content (A) and insulin secretion (B) of EndoC-βH3 cell monolayers. (C, D) Glucose-stimulated insulin content (C) and insulin secretion (D) of EndoC-βH3 pseudoislets. (E) Insulin secretion capacity is given as the proportion of insulin secreted into the incubation medium in relation to the insulin

content. From n=3 independent experiments. Significant differences are indicated (*p<0.05, **p<0.01, ***p<0.001, ****p<0.0001).

3.4.2 Transplantation of pseudoislets formed by EndoC-βH3 cells via the portal vein route into diabetic mice

Next, after the transplantation of pseudoislets formed by EndoC-βH3 cells into STZ-induced diabetic mice via the portal vein route, it was found that blood glucose decreased significantly after transplantation (p<0.0001) (Figure 29A). Liver and islets were then collected for further study. First, by HE staining, we found that the pseudoislets in the liver (Figure 29B) were morphologically similar to those in the pancreas (Figure 29C). Then, immunohistological insulin staining showed that pseudoislets in the liver had the potential of producing insulin (Figure 29E), although the staining intensity was lower than that of pancreatic islets (Figure 29D). Finally, in contrast to native islets (Figure 29F), immunohistological Grx5 staining of pseudoislets in the liver was negative (Figure 29G).

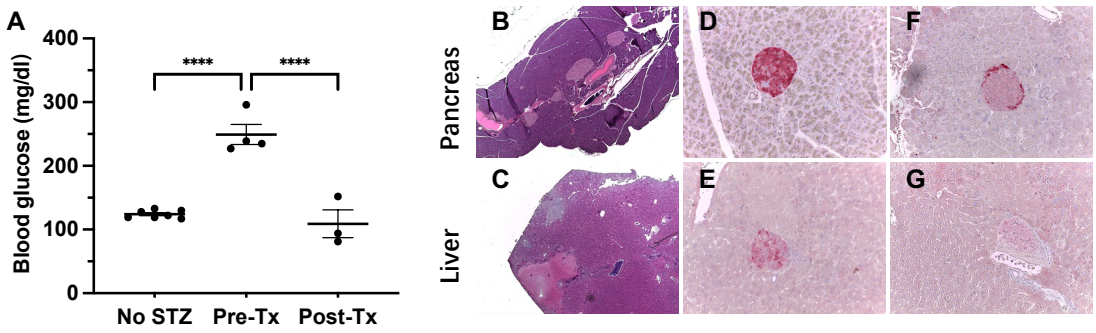

Figure 29 Blood glucose levels of transplanted NMRi nu/nu mice. Comparison of morphology, insulin, and Grx5 expression of transplanted EndoC-βH3 pseudoislets and native pancreatic islets. (A) Blood glucose levels of non-diabetic (no streptozotocin, STZ) and STZ-induced diabetic NMRi nu/nu mice before (pre) and after (post) intraportal transplantation of EndoC-βH3 pseudoislets. (B, C) Representative images of HE staining of the (B) pancreas and (C) liver. (D, E) Representative images of insulin staining of native (D) pancreatic islets and (E) transplanted pseudoislets in the

liver. (F, G) Representative images of Grx5 staining of native (F) pancreatic islets and (G) transplanted pseudoislets in the liver. From n = 3-7 mice. Significant differences are indicated (****$p<0.0001$).

3.5 Grx5 overexpressing mice had unexpectedly higher blood glucose than wild-type littermates after induction of DM by HFD

To gain insights into the potential importance of Grx5 for pancreatic β cell function, we examined mice with β cells specifically overexpressing of Grx5, particularly with HFD feeding. Our group had previously observed that HFD reduced pancreatic islet Grx5 expression in wild-type mice (Petry et al., 2022).

3.5.1 Fasting blood glucose and body weight

Three groups of mice were fed according to Figure 12; fasting blood glucose and body weight were measured every week. As shown in Figure 30, all mice gained weight with age, and mice fed with HFD gained more weight than mice fed with SD (Figure 30A). There was no significant difference in the body weight among the three groups of mice at 7 weeks of age. But compared with body weight at 7 weeks of age, the mean body weight of Grx5 overexpressing mice fed with SD increased approximately 1.6-fold, that of WT mice fed with HFD increased 2.2-fold, and that of Grx5 overexpressing mice fed with HFD increased 2.1-fold at 27 weeks of age. In addition, WT mice with HFD had higher body weight than Grx5 overexpressing mice with HFD, and the difference was significant ($p<0.05$) at 27 weeks of age. When the diet was changed to SD from 20 to 23 weeks of age, both WT mice ($p<0.01$) and Grx5 overexpressing mice ($p<0.05$) showed a decrease in body weight. Then, when the diet was switched to HFD after 23 weeks of age, the body weight of WT ($p<0.0001$) and Grx5 overexpressing mice ($p<0.05$) was increased again (Figure 30B).

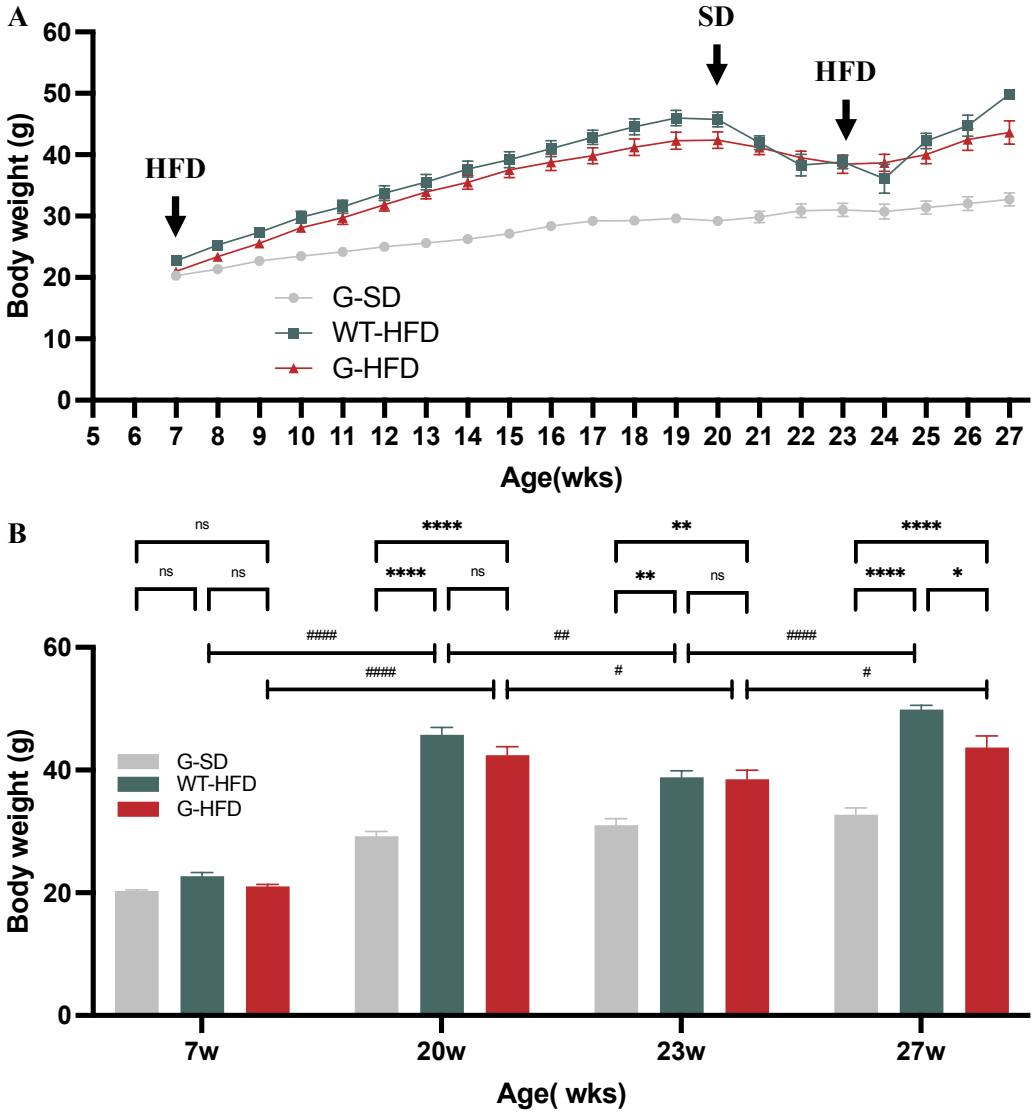

Figure 30 Body weight data of Grx5 overexpressing and WT mice fed with HFD or SD. Body weight of Grx5 overexpressing and WT mice fed with HFD or standard diet (SD). (A) Weekly body weight data of mice from 5 weeks to 27 weeks of age. (B) Body weight data of mice at 7, 20, 23, and 27 weeks of age, from n = 3-22 per timepoint. Significant differences are indicated (*p<0.05, **p<0.01, ****p<0.0001, $^{\#}$p<0.05, $^{\#\#}$p<0.01, $^{\#\#\#\#}$p<0.0001). G-SD, Grx5 overexpressing mice with a standard diet; WT-HFD, wild-type littermates with a high-fat diet; G-HFD, Grx5 overexpressing mice with a high-fat diet.

Fasting blood glucose levels of HFD-fed Grx5 overexpressing mice were generally elevated as opposed to the other two groups (Figure 31A).

Compared to HFD-fed WT mice, at 7 weeks of age, fasting blood glucose level was significantly higher in HFD-fed Grx5 overexpressing mice ($p<0.05$); then, after 13 weeks of HFD feeding, fasting blood glucose level was increased in both HFD-fed WT ($p<0.0001$) and HFD-fed Grx5 overexpressing mice ($p<0.0001$) and was even higher in HFD-fed Grx5 overexpressing mice, although not significantly. When the diet was changed to SD from 20 to 23 weeks of age, WT mice showed a significant decrease in blood glucose ($p<0.0001$), whereas the decrease in Grx5 overexpressing mice was not significant. But similar to the changes in body weight, when the diet was switched back to HFD after 23 weeks of age, the fasting blood glucose of WT ($p<0.0001$) and Grx5 overexpressing mice ($p<0.01$) was increased. Differently, HFD-fed Grx5 overexpressing mice had higher blood glucose than the WT mice, although not in a significant way (Figure 31B).

Subsequently, when compared to the SD-fed Grx5 overexpressing mice, HFD-fed Grx5 overexpressing mice had higher fasting blood glucose levels ($p<0.01$ at 20 weeks of age, $p<0.001$ at 27 weeks of age). Interestingly, from 20 weeks of age to 23 weeks of age, although all three groups of mice were fed SD, the blood glucose level of both Grx5 overexpressing mice fed with SD throughout the experimental ($p<0.0001$) and Grx5 overexpressing mice fed with SD for 3 weeks ($p<0.0001$) was higher than that of WT mice fed SD only for 3 weeks (Figure 31B).

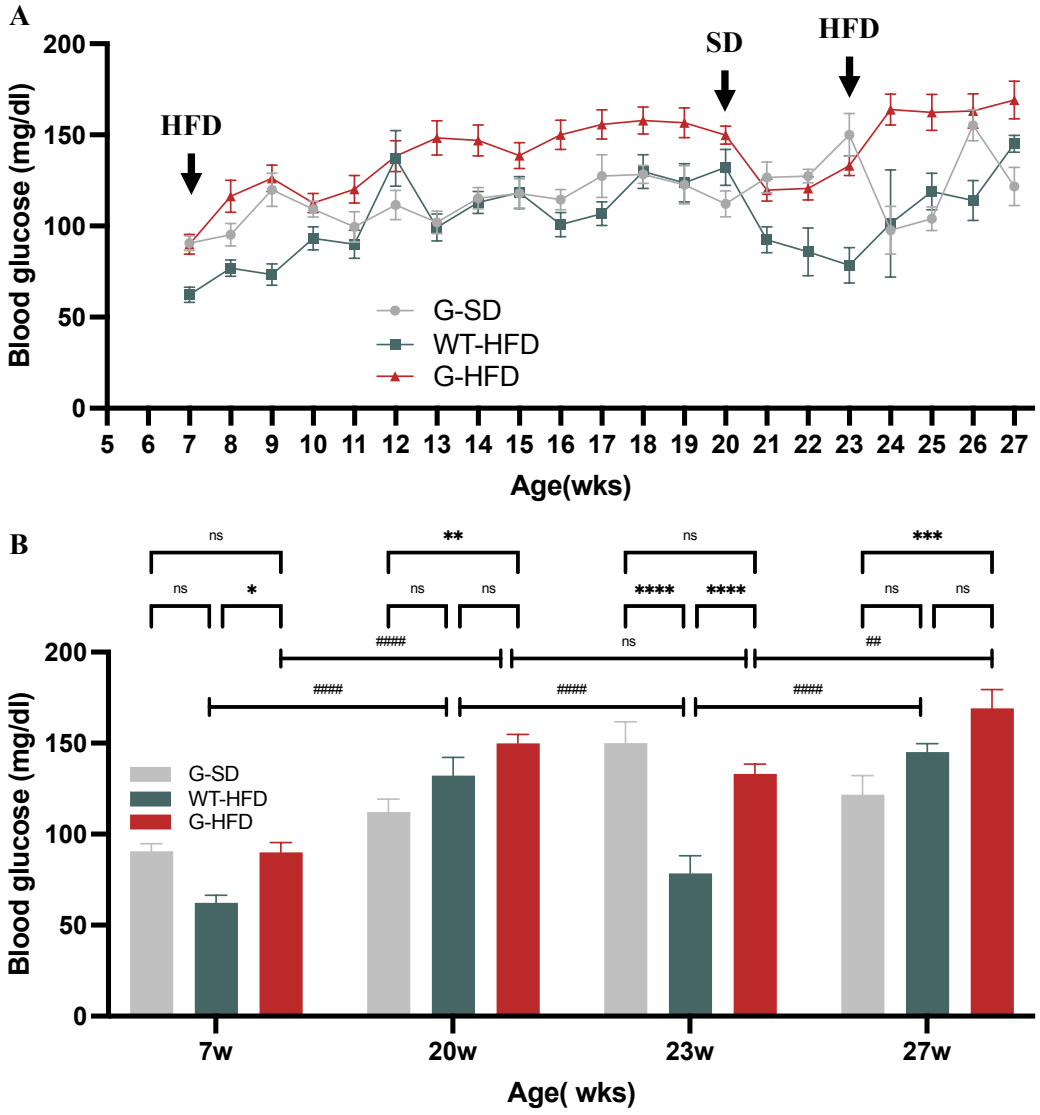

Figure 31 Fasting blood glucose levels of Grx5 overexpressing and WT mice fed with HFD or SD. (A) Weekly fasting blood glucose data of mice from 5 weeks to 27 weeks of age. (B) Fasting blood glucose data of mice at 7, 20, 23, and 27 weeks of age, from n = 3-22 per timepoint. Significant differences are indicated (*p<0.05, **p<0.01, ***p<0.001, ****p<0.0001, $^{\#\#}$p<0.01, $^{\#\#\#\#}$p<0.0001). G-SD, Grx5 overexpressing mice with a standard diet, WT-HFD, wild-type littermates with a high-fat diet, G-HFD, Grx5 overexpressing mice with a high-fat diet.

3.5.2 Glucose tolerance test

In addition to fasting blood glucose and body weight, the intraperitoneal glucose tolerance test (ipGTT) was performed at 7, 19, 23, and 27 weeks of age.

The area under the ipGTT curve (AUC) of Grx5 overexpressing mice was significantly higher than that of WT mice at 7 weeks of age ($p<0.0001$) (Figure 32A, B). Then at 19 weeks of age, Grx5 overexpressing mice exhibited significantly impaired glucose tolerance, specifically, although basal plasma glucose levels were similar and blood glucose concentrations increased to a maximum at 30 min after intraperitoneal glucose injection in the three groups, blood glucose levels were higher in HFD-fed and SD-fed Grx5 overexpressing mice than in HFD-WT mice at all time points after glucose injection, and HFD-fed Grx5 overexpressing mice were higher than SD-fed Grx5 overexpressing mice, with the area under the curve showing statistical significance (HFD-fed Grx5 overexpressing mice vs HFD-WT mice: $p<0.0001$, SD-fed Grx5 overexpressing mice vs HFD-WT mice: $p<0.0001$, HFD-fed Grx5 overexpressing mice vs SD-fed Grx5 overexpressing mice: $p<0.0001$) (Figure 32C, D).

Next, after 3 weeks of SD diet from 20 weeks of age, the ipGTT blood glucose levels of HFD-fed Grx5 overexpressing mice were close to SD-fed Grx5 overexpressing mice, but both were significantly higher than HFD-WT mice, and this was reflected in the AUC data (HFD-fed Grx5 overexpressing mice vs HFD-WT mice: $p<0.0001$; SD-fed Grx5 overexpressing mice vs HFD-WT mice: $p<0.0001$) (Figure 32E, F).

Subsequently, after 4 weeks of an HFD diet from 23 weeks of age, the HFD-fed Grx5 overexpressing mice (44963±2437) showed a significant 76% increase in the AUC compared with the HFD-fed WT mice (25541±2914) ($p<0.0001$) and a 13.1% increase in the AUC compared with the SD-fed Grx5 overexpressing mice (39746±1843) ($p<0.001$). The SD-fed Grx5 overexpressing mice showed a significant 56% increase compared with the HFD-fed WT mice ($p<0.0001$) (Figure 32G, H).

Besides, we also interpreted these data as 2-hour-ipGTT blood glucose levels. At 7 weeks of age, there was no significant difference in 2-hour-ipGTT blood glucose concentrations among the three groups. However, SD-fed ($p<0.05$ at 19 weeks of age, $p<0.0001$ at 23 weeks of age, $p<0.001$ at 27 weeks of age) and HFD-fed ($p<0.0001$ at 19 weeks of age, $p<0.0001$ at 23 weeks of age, $p<0.0001$ at 27 weeks of age) Grx5 overexpressing mice both had significantly higher blood glucose levels than HFD-WT mice at 7, 19, 23, and 27 weeks of age. Additionally, the 2-hour blood glucose concentrations of HFD-fed Grx5 overexpressing mice varied with diet switching: 125±18 mg/dl at 7 weeks of age, increasing to 352±73 mg/dl after 13 weeks of HFD ($p<0.001$), decreasing to 245±56 mg/dl after switching to SD ($p<0.001$), and increasing to 344±71 mg/dl when switching to HFD again ($p<0.001$) (Figure 32I).

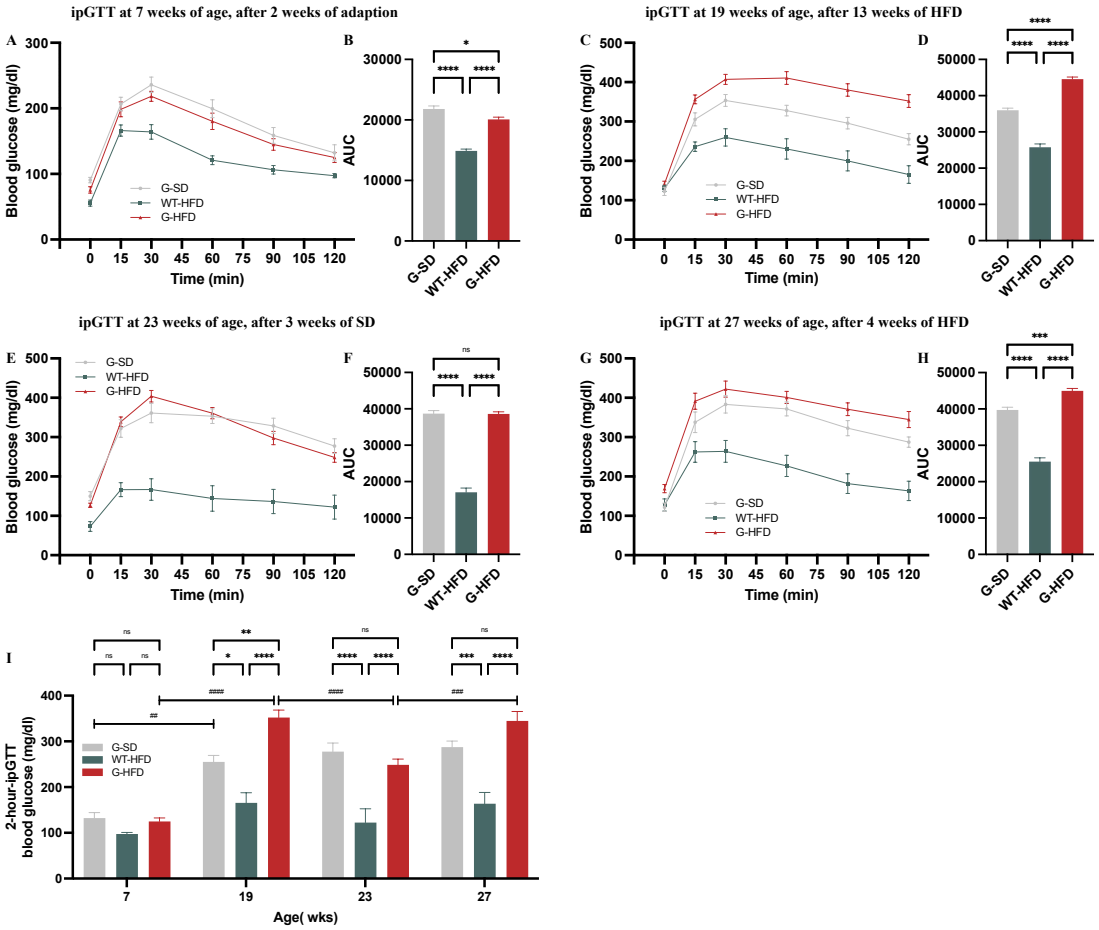

Figure 32 Glucose tolerance test of Grx5 overexpressing and WT mice fed with HFD or SD. Intraperitoneal glucose tolerance test (ipGTT) data and related area under curve (AUC) at 7 (A, B), 19 (C, D), 23 (E, F), and 27 (G, H) weeks of age. (I) 2-hour-ipGTT blood glucose level, from n = 5-20 per timepoint. Significant differences are indicated (*p<0.05, **p<0.01, ***p<0.001, ****p<0.0001, $^{\#\#}$p<0.01, $^{\#\#\#}$p<0.001, $^{\#\#\#\#}$p<0.0001). G-SD, Grx5 overexpressing mice with a standard diet; WT-HFD, wild-type littermates with a high-fat diet; G-HFD, Grx5 over-expressing mice with a high-fat diet.

4 Discussion

4.1 Cytotoxicity of OA in pancreatic β cells

FFAs exert dual effects on β cell function and survival, which can be either beneficial or detrimental depending on factors such as saturation, carbon chain length, glucose abundance, as well as concentration and treatment duration. FFAs are regulated by extracellular factors like growth factors, hormones, inflammatory mediators, and FFA receptor 1 (FFAR1) (Sharma and Alonso, 2014). The detrimental effects of excess lipids accumulated in non-adipose tissues mediated by elevated FFA levels are referred to as lipotoxicity (Lee et al., 1994), which is thought to contribute to insulin resistance (Ferrannini et al., 1983; Love et al., 2024) and β cell dysfunction (Zhou and Grill, 1994; Plötz and Lenzen, 2024; Wang et al., 2024), thereby playing a critical role in the onset and progression of T2DM.

According to the length of the carbon chain, FFAs are categorized as short chain (SCFA) (C⩽5), medium chain (MCFA) (C=6-12), long chain (LCFA) (C=13-21), and very long chain (VLCFA) (C⩾22) FFAs. Depending on the presence of double bonds, FFAs are categorized as saturated (SFAs, no double bond), monounsaturated (MUFAs, one double bond), and polyunsaturated FFAs (PUFAs, two or more double bonds) (Basson et al., 2020). On the one hand, it is generally believed that LCSFAs like palmitic acid (PA) have a pro-apoptotic effect on β cells. Numerous studies have demonstrated that PA causes loss of β cell function and mass in isolated β cells, β cell lines, and pancreatic islets in both rodents (Maedler et al., 2003; Thörn et al., 2010; Baldwin et al., 2012; Liu et al., 2019; Guo et al., 2024; Liu et al., 2024) and humans (Maedler et al., 2003; El-Assaad et al., 2003; Lai et al., 2008; Ladrière et al., 2010; Nemecz et al., 2018; Plötz et al., 2019). On the other hand, the pro-apoptotic effect of LCUFAs, such as OA, on β cells remains controversial. Some studies have shown that OA, in addition to its unclear pro-apoptotic effects, can prevent the detrimental effects of PA on β cells and pancreatic

islets (Maedler et al., 2003; Busch et al., 2005; Welters et al., 2006; Diakogiannaki et al., 2007; Bellini et al., 2018; Nemecz et al., 2018; Liu et al., 2019). Conversely, other studies have shown that OA can also be detrimental (Kharroubi et al., 2004; Lai et al., 2008; Plötz et al., 2017, 2019; Römer et al., 2022). Besides, it is generally accepted that both SFAs and UFAs with a chain length of fewer than 16 carbon atoms are well tolerated by β cells (Welters et al., 2004; Tuei et al., 2011). The toxicity of FFAs increased along with the increase in chain length, but more rapidly for SFAs than for UFAs (Plötz et al., 2019; Oshima et al., 2020; von Hanstein et al., 2023; Plötz and Lenzen, 2024). Despite the ongoing controversy on the effect of OA on β cells, it was shown that the level of OA is elevated in subjects with T2DM compared with healthy individuals and is associated with an increased risk of DM (Clore et al., 2002; Yi et al., 2007; Liu et al., 2010; Grapov et al., 2012; Sergeant et al., 2016; Lu et al., 2016). A recent case-control study further demonstrated that LCFAs and UFAs may increase the risk of DM by increasing oxidative distress and homeostatic model assessment for insulin resistance (HOMA-IR) (Shiri et al., 2024).

The detrimental effects on β cells caused by long-term exposure to high levels of glucose concentration are defined as glucotoxicity (Robertson et al., 2003). The synergistic harmful effects of glucotoxicity and lipotoxicity are collectively termed glucolipotoxicity (Prentki and Corkey, 1996; Poitout and Robertson, 2002). Whether lipotoxicity increases with increasing glucose concentration is also up for debate. Early studies suggested that glucose-induced malonyl-CoA formation inhibited carnitine palmitoyltransferase I (CPT-1), thereby reducing FA oxidation and leading to the accumulation of LC-CoA in the cytoplasm, which contributes to lipotoxicity (Prentki and Corkey, 1996; Poitout and Robertson, 2002; Prentki et al., 2002). In other words, these data suggest that FFAs are only harmful in the context of concomitant glucotoxicity (Poitout and Robertson, 2002) or are more harmful (El-Assaad et al., 2003). However, Sargsyan E and Bergsten P found that lipotoxicity was also evident at low glucose concentrations, and high glucose only exacerbated FA-induced apoptosis in INS-1E cells but not in

healthy human islets or MIN6 cells (Sargsyan and Bergsten, 2011). They proposed that this may be due to the limited inhibition of FA oxidation by high glucose in human islets and MIN6 cells, potentially related to the lower activity of acetyl-CoA carboxylase (ACC), which catalyzes malonyl-CoA synthesis, in healthy human islets rather than in INS-1E cells (Sargsyan and Bergsten, 2011). ACC gene polymorphism is independently associated with obesity and T2DM (Riancho et al., 2011). This may also support findings that those with a family history of T2DM are more sensitive to the harmful effects on insulin secretion caused by fat infusion than control subjects (Storgaard et al., 2003; Kashyap et al., 2003). In addition, glucolipotoxicity is also related to the saturation and chain length of FFAs, as well as the interaction with stearoyl-CoA-desaturase (SCD) (von Hanstein et al., 2023). In EndoC-βH1 cells, high glucose exacerbated the toxic effects of SFAs, but only when the chain length of SFAs exceeded C18, likely due to the reduced desaturation of FAs by SCD at a chain length of C18 (von Hanstein et al., 2023). In contrast, this exacerbation was not observed in MUFA (von Hanstein et al., 2023). Furthermore, our research group found that Grx5 protein level was reduced significantly when treated with PA and high glucose, but not with glucose alone, and this reduction correlated with decreased insulin secretion (Petry et al., 2022).

Naturally, the concentration and duration of FFA exposure are also critical determinants of lipotoxicity. Lipidomics analysis revealed that OA is one of the most common FFAs in physiology, constituting a major component of FFAs (80.3 nmol/ml ± 9.331) (Quehenberger et al., 2010). The total serum FFA concentration in individuals with DM is approximately 3.5 to 15 mM, with OA concentration ranging from 0.74 to 3.9 mM (Kish-Trier et al., 2016; Sergeant et al., 2016; de Oliveira et al., 2020; Navina et al., 2011). However, there is considerable variability in the concentrations used in existing literature to induce lipotoxicity (Römer et al., 2021). Under physiological conditions, approximately every two FFA molecules are bound to one albumin molecule (2:1), but this ratio can exceed 5:1 under pathological conditions (Kleinfeld et al., 1996).

Therefore, as a common FFA in DM research, the preparation of OA involves dissolving and complexing. In this study, we observed differences in the effects of OA at the same concentration but with varying OA-to-BSA ratios (Figure 15), which is consistent with our previous study (Römer et al., 2022). The cytotoxicity of OA on β cells depends on its unbound fraction. At the same concentration, the unbound OA concentration increases with a higher OA-to-BSA ratio and decreases with a lower ratio (Cnop et al., 2001). Therefore, to minimize the influence of BSA and emphasize the effects of OA, we chose an OA:BSA ratio of 5:1 to simulate diabetic conditions in pancreatic β cells. Furthermore, it is generally accepted that a short-term acute increase in FFA will increase β cell mass and insulin secretion, while long-term chronic increases will lead to lipotoxicity, resulting in β cell dysfunction and cell death (Paolisso et al., 1995; Carpentier et al., 1999; Oh et al., 2018).

Plötz, T et al. suggested that a 2-day treatment with 500 μM OA resulted in an increase in caspase-3 activity, propidium iodide (PI) staining, and annexin V staining in human EndoC-βH1 cells, pseudoislets, isolated human islets, and rat islets, indicating that OA is the main physiologically toxic FFA in human β cells and does not protect against the PA-induced toxicity (Plötz et al., 2017). This is consistent with the results of this thesis, where we found that OA reduced the metabolic activity of EndoC-βH3 cells in a concentration-dependent manner (Figure 16).

As mentioned earlier (section 1.2.3), the mechanisms by which lipotoxicity leads to β cell dysfunction and death include oxidative distress, ER stress, inflammation, and mitochondrial dysfunction. However, the relative contributions of these mechanisms vary depending on the chain length and saturation of FFAs. Among these, the MUFA OA may be involved in promoting the formation of lipid droplets and the generation of peroxisomal hydrogen peroxide (H_2O_2) (Plötz et al., 2019), as well as reducing the level of Grx5 in β cells (Petry et al., 2017, 2018, 2022). Peroxisomal β-oxidation is considered a key molecular mechanism mediating β cell lipotoxicity (Elsner et al.,

2011). The inactivation of its product, H_2O_2 (rather than reducing equivalents), usually requires the expression of catalase (Dansen and Wirtz, 2001). However, pancreatic islets exhibit low expression levels of classical antioxidant enzymes such as catalase ((Lenzen et al., 1996; Gehrmann et al., 2010), which makes β cells vulnerable towards peroxisomal H_2O_2 generation, leading to elevated ROS generation and increased vulnerability of β cells to lipotoxicity. Additionally, our previous studies have shown that reduced Grx5 expression is associated with impaired insulin secretion and β cell loss under diabetic conditions, suggesting that Grx5 may have a protective effect on β cells (Petry et al., 2017, 2018, 2022). Based on the role of Grx5 in mitochondria, it is reasonable to postulate that OA-induced Grx5 deficiency may be a potential mechanism for lipotoxicity-induced dysfunction in β cells.

4.2 Deficiency of Grx5 and iron metabolism in pancreatic β cells

In this study, we investigated the effects of OA treatment and Grx5 deficiency on iron homeostasis in β cells. While iron is essential for β cell function and survival, excess iron can lead to β cell dysfunction and apoptosis through multiple pathways (Guo et al., 2024). Our findings demonstrate that OA treatment in β cells reduced cell metabolic activity, insulin content, and insulin secretion, as well as Grx5 and Gpx4 levels. Moreover, OA treatment led to increased mitochondrial Fe^{2+} accumulation, intracellular Fe^{2+} levels, and lipid peroxidation. Similarly, Grx5 knockdown resulted in decreased cell metabolic activity, insulin content, and secretion, combined with mitochondrial Fe^{2+} overload, reduced intracellular Fe^{2+} levels, and elevated lipid peroxidation.

Grx5 knockdown directly reduced insulin content and secretion, which is a novel finding. Given that Grx5 plays a critical role in the assembly and transport of FeS clusters (Lill et al., 2012; Lill and Freibert, 2020; Mühlenhoff et al., 2020), which are essential for proinsulin translation in pancreatic β cells (Wei et al., 2011; Brambillasca et al., 2012), it is plausible that Grx5 deficiency disrupts FeS cluster biosynthesis, leading to

impaired proinsulin processing. Furthermore, the ferroptosis inducer ML-162 exacerbated the reduction in Grx5, while the ferroptosis inhibitor Lip-1 partially rescued it. Correspondingly, insulin content and insulin secretion were also regulated by ML-162 and Lip-1. These findings suggested that ferroptosis might be involved in the effects of Grx5 deficiency, further linking Grx5 levels to β cell function and insulin regulation.

Ferroptosis is well-acknowledged to be iron-dependent and characterized by the accumulation of lipid peroxides (Riegman et al., 2020). Gpx4 is the only Gpx isoform capable of using GSH as a cofactor to reduce lipid peroxides in lipid membranes to their corresponding alcohols, thereby playing a key role in inhibiting ferroptosis (Yang et al., 2014). In MIN6 cells, OA treatment significantly reduced Gpx4 levels, impairing the ability of cells to clear lipid peroxides and exacerbating the spread of lipid oxidation chain reactions, potentially inducing ferroptosis. As expected, cellular lipid peroxides were increased by OA treatment in both MIN6 cells and EndoC-βH3 cells. Notably, the ferroptosis inducer ML-162 markedly inhibited the expression of Gpx4 and increased cellular lipid peroxidation regardless of the presence or absence of OA, but it was more pronounced in the presence of OA. In contrast, the ferroptosis inhibitor Lip-1 failed to rescue OA-induced reductions in Gpx4 levels but partially reduced intracellular lipid peroxidation. This suggests that Lip-1 may partially alleviate lipid peroxidation through other Gpx4-independent mechanisms in β cells. Various pathways of ferroptosis independent of Gpx4 have been described, including NADPH/ferroptosis suppressor protein 1 (FSP1)/coenzyme Q10 (CoQ10), P53-mediated lipoxygenase and calcium-independent phospholipase A2β (iPLA2β) pathway, nitric oxide synthase (iNOs)/NO pathway, dihydroorotate dehydrogenase (DHODH) pathway, GTP cyclohydrolase 1 (GCH1)/tetrahydrobiopterin (BH_4) pathway, ferritin and prominin2 pathway, and sterol regulatory element-binding protein 1 (SREBP1)/SCD1/MUFA pathway (Ma et al., 2022).

Lipid peroxidation initiates through enzymatic and non-enzymatic mechanisms. The enzymatic lipid peroxidation is mediated by lipoxygenases (LOX), cyclooxygenases (COX), and cytochrome P450 (CYP), while the non-enzymatic lipid peroxidation is described as a process by which free radicals attack lipids, particularly PUFAs, generating lipid peroxides and hydroperoxide derivatives (Yin et al., 2011). The process includes initiation, propagation, and termination, with lipid hydroperoxides (LOOH) as the primary product (Yin et al., 2011). The initial step is usually accomplished by free iron through the Fenton reaction to generate hydroxyl and peroxide radicals (Gaschler and Stockwell, 2017). While moderate amounts of lipid peroxides are essential for cell signal transduction and immune response, excessive lipid peroxides damage cells by destroying the lipid bilayer structure of the cell membrane, increasing membrane permeability, and reducing bilayer thickness, causing cell membrane damage (Wong-Ekkabut et al., 2007; Gaschler and Stockwell, 2017). The elevated level of lipid peroxides is closely related to the severity of membrane damage and the reactive end products such as malondialdehyde (MDA) and 4-hydroxy-2-nonenal (4-HNE) produced during the decomposition of lipid peroxides (Wong-Ekkabut et al., 2007; Ayala et al., 2014; Schaur et al., 2015; Gaschler and Stockwell, 2017). In fact, lipid peroxidation biomarkers in the plasma of patients with T2DM are significantly higher than those in healthy subjects and are correlated with disease progression (Turk et al., 2002; Martín-Timón et al., 2014). Consistent with oxidative distress, increased lipid peroxidation also plays a critical role in the onset and progression of β cell dysfunction and insulin resistance (Shabalala et al., 2022). Furthermore, we found that OA treatment increased β cell sensitivity to ferroptosis, as ML-162 exacerbated the reduction in β cell metabolic activity in the presence of OA but was not evident in the absence of OA, despite studies suggesting that OA may inhibit ferroptosis (Yang et al., 2016; Magtanong et al., 2019). This is also consistent with the observed OA-induced decline in Gpx4 levels and increase in lipid peroxidation.

Next, we found that OA treatment increased the accumulation of mitochondrial Fe^{2+} and intracellular Fe^{2+} in MIN6 cells. Mitochondrial Fe^{2+}overload was partially alleviated by the ferroptosis inhibitor Lip-1 and aggravated by the ferroptosis inducer ML-162. This was also verified in the human β cell line Endoc-βH3 cells. In addition, considering the important role of Grx5 in the assembly and transport of FeS clusters, we can speculate that the inhibition of Grx5 is closely related to ferroptosis. Grx5 knockdown in MIN6 cells significantly reduced metabolic activity, insulin content, and secretion, accompanied by increased intracellular lipid peroxides and mitochondrial Fe^{2+}, which were further aggravated by OA treatment. Consistent with our findings, a study showed that inhibition of Grx5 predisposed therapy-resistant cancer cells to ferroptosis (Lee et al., 2020). Actually, dysregulated iron metabolism is directly linked to DM, as patients with T2DM exhibit significantly higher body iron levels than healthy controls (Rajpathak et al., 2009), and iron overload increases the risk of T2DM or GDM (Forouhi et al., 2007; McElduff, 2017; Rawal et al., 2017; Sun et al., 2020). Exposure to high concentrations of iron can cause oxidative damage and trigger insulin secretion dysfunction in MIN6 cells (Blesia et al., 2021), and accumulation of free iron leads to mitochondrial dysfunction through multiple pathways, resulting in defects in insulin synthesis and secretion (Figure 9) (Blesia et al., 2021). Notably, β cells are more susceptible to iron-induced damage than α or δ cells (Shirasuga et al., 1989), making them particularly vulnerable to ferroptosis. Studies have shown that ferroptosis inducers erastin and RLS3 decrease GSIS and viability in human islets (Bruni et al., 2018), while the ferroptosis inhibitor ferrostatin-1 (Fer-1) protects against these effects (Bruni et al., 2018; Miotto et al., 2020). Similarly, high glucose, proinflammatory cytokines, H_2O_2, and STZ-induced cell death in RIN-5F rat insulinoma cells were found together with an increased abundance of ROS, lipid peroxides, and iron and decreased Gpx4 expression. High glucose, H_2O_2, and STZ-induced cell death could be rescued by Fer-1 (Stancic et al., 2022). The significant increase in mitochondrial Fe^{2+} is also associated with the decrease in mitochondrial Grx5 levels, which impair FeS cluster synthesis,

leading to abnormal accumulation of unutilized free iron in the mitochondria (Ye et al., 2010).

In contrast to the increase in mitochondrial iron, ferroptosis inducer ML-162 significantly decreased intracellular Fe^{2+}, and ferroptosis inhibitor Lip-1 significantly increased it in cells treated with OA. The effects of different ML-162 and Lip-1 concentrations on intracellular Fe^{2+} were examined in MIN6 cells. ML-162 reduced intracellular Fe^{2+} in a concentration-dependent manner, while Lip-1 increased intracellular Fe^{2+} in a concentration-dependent manner, reaching a peak at 0.5 μM and decreasing at 1 μM. In Grx5 knockdown MIN6 cells, we observed decreased intracellular Fe^{2+} levels, which increased dose-dependently following OA treatment.

Cellular iron homeostasis is regulated by iron regulatory proteins 1 and 2 (IRPs 1 and 2) and hypoxia-inducible factors 1 and 2 (HIF1 and 2) (Lane et al., 2015). IRPs regulate post-transcriptional processes through mRNA binding, rapidly responding to changes in intracellular iron levels. Under low intracellular iron conditions, IRPs bind to iron response elements (IREs) in the 5′ untranslated region (UTR) of specific mRNAs (e.g., ferritin heavy chain (FTH1), ferritin light chain (FTL), ferroportin 1 (FPN1), etc.), thereby inhibiting mRNA translation to reduce iron storage, and bind to IREs in the 3′ UTR of specific mRNAs (e.g., transferrin receptor protein 1 (TfR1), DMT1-I, etc.), thereby increasing mRNA stability to promote iron uptake. Conversely, under high intracellular iron conditions, the binding activity of IRP-IRE decreases, the translation of mRNAs with IREs located in the 5′ UTR increases, and the degradation rate of mRNAs located in the 3′ UTR is faster, resulting in reduced protein translation (Hentze and Kühn, 1996; Hentze et al., 2010). HIFs regulate iron metabolism-related genes through gene transcription to adapt to long-term hypoxia or iron deficiency conditions (Cassavaugh and Lounsbury, 2011).

Mitochondria serve as the central hub of iron metabolism and homeostasis, containing up to 20-50% of total cellular iron (Rauen et al., 2007; Jhurry et al., 2012; Paul et al., 2017). Iron is imported into mitochondria via three potential pathways: the hypothesized endosomal "kiss-and-run" mechanism (Sheftel et al., 2007), in which the endosome containing transferrin (Tf) directly contacts the mitochondrial outer membrane (OMM); direct iron uptake from LIP driven by the mitochondrial membrane potential ($\Delta\Psi m$) (Lawen and Lane, 2013); and uptake from cytosol, which may involve directed transfer by protein–protein contacts (Lawen and Lane, 2013). Once inside mitochondria, iron is utilized for storage (Arosio and Levi, 2010), heme synthesis (Ponka, 1997), and FeS cluster biosynthesis (Muckenthaler et al., 2008; Rouault, 2012). Therefore, any imbalance in any of these pathways can lead to the destruction of intracellular iron homeostasis.

IRP1 is a bifunctional protein that regulates cellular iron homeostasis via the FeS biosynthesis machinery. When IRP1 acquires a 4Fe-4S cluster, it is converted into aconitase, losing its IRE-binding activity (Rouault, 2006). IRP2, independent of the formation of FeS clusters, is regulated by iron-regulated proteasome degradation (Guo et al., 1995). Under iron-replete conditions, IRP2 is degraded, while iron storage proteins are upregulated. Conversely, iron depletion upregulates IRP2 and downregulates iron storage proteins (Rouault, 2006). In Grx5-knockdown HeLa cells, reduced mitochondrial aconitase activity and significantly elevated IRP2 levels indicated mitochondrial iron overload and cytosolic iron depletion (Ye et al., 2010). Disruption of cellular iron homeostasis has also been observed in patients with GLRX5 mutations (Ye et al., 2010). Consistent with these findings, Grx5 knockdown in MIN6 cells leads to mitochondrial iron overload, accompanied by reduced cytosolic free iron levels and disrupted cellular iron homeostasis.

Mitochondrial iron overload leads to mitochondrial dysfunction, swelling, ROS accumulation, and impaired energy metabolism, potentially triggering ferroptosis (Kumfu

et al., 2012; Khamseekaew et al., 2017). Therefore, we hypothesize that Grx5-deficient cells exhibit impaired mitochondrial FeS synthesis and are unable to correctly assess mitochondrial iron status, leading to increased iron import or decreased iron export from the mitochondria, resulting in mitochondrial iron overload and concomitant cytosolic iron deficiency. Indeed, Grx5 deficiency may activate the IRE binding activity of IRP1 to respond to cytoplasmic iron depletion (Ye et al., 2010), potentially upregulating iron-starvation responses and increasing intracellular free iron, thereby triggering ferroptosis. Therefore, Grx5 deficiency may play a role in the initiation stage of ferroptosis.

4.3 Overexpression of Grx5 *in vivo* did not protect against FFA-induced hyperglycemia

According to previous studies of our group, Grx5 mRNA levels are significantly reduced in db/db- mice (Petry et al., 2017). We also observed a loss of Grx5 in pancreatic islets, accompanied by increased ROS generation, elevated serum FFA, and impaired glucose tolerance in an HFD-induced diabetic mouse model (Petry et al., 2022). These findings suggested that the loss of Grx5 is closely associated with impaired β cell function and disrupted glucose metabolic homeostasis. Given its essential role in FeS cluster assembly and mitochondrial function, Grx5 is a key regulator of iron metabolism. We can speculate that its downregulation may contribute to mitochondrial dysfunction by altering iron homeostasis, thereby exacerbating β cell impairment in DM. Studies have shown that *in vitro* overexpression of Grx5 can protect osteoblasts from H_2O_2-induced apoptosis and ROS formation (Linares et al., 2009). However, the effects of Grx5 overexpression *in vivo* are relatively unknown. Therefore, in this study, we aimed to study the phenotype and glucose metabolism of homozygous, β cell-specific Grx5-overexpressing mice under HFD conditions. We found that under HFD conditions, Grx5-overexpressing mice exhibited slightly lower body weight, but consistently higher fasting blood glucose levels compared to WT littermates. Notably, although the body weight of SD-fed Grx5-overexpressing mice was lower than that of HFD-fed WT littermates,

the fasting blood glucose levels of the overexpressing mice were higher after WT littermates were also switched to SD. Despite our previous findings showing that switching from HFD to an SD restored islet Grx5 levels (Petry et al., 2022), the current results indicate that Grx5 overexpression *in vivo* failed to protect β cell function under metabolic stress induced by HFD effectively.

Long-term HFD feeding has been widely demonstrated to be detrimental to pancreatic β cells, involving multiple mechanisms that induce oxidative distress, ER stress, and increased inflammatory responses, ultimately leading to β cell dysfunction and impaired glucose tolerance (Lee et al., 2011; Wu et al., 2013; Abebe et al., 2017; Gupta et al., 2017; Petry et al., 2022; Yi et al., 2020). Additionally, it is important to consider that both T2DM and HFD-induced mouse models are highly complex diseases involving multiple tissues and overlapping and complex pathogenic mechanisms (Heydemann, 2016). While Grx5 downregulation plays a crucial role in β cell dysfunction, it is important to acknowledge that Grx5 deficiency is not the only factor contributing to this pathological process. In β cells subjected to HFD or OA treatment, multiple mitochondrial proteins beyond Grx5 are significantly affected (Lowell and Shulman, 2005; Römer et al., 2021). Furthermore, Grx5 is essential for maintaining iron homeostasis (section 1.3.2.2). Our findings suggest that Grx5 deficiency leads to the accumulation of mitochondrial free iron, which in turn contributes to β cell dysfunction. However, overexpression of Grx5 does not appear to provide additional protective effects. This may be because Grx5 is not an iron chelator but rather a scaffold protein that facilitates iron distribution in FeS cluster assembly. These findings imply that Grx5 deficiency may be a contributing factor to mitochondrial dysfunction but cannot be regarded as a central regulatory switch for its reversal. Future studies should explore the molecular pathways regulated by Grx5, particularly its interactions with other redox-sensitive proteins and signaling cascades, to better understand its role in β cell function and glucose metabolism.

In conclusion, while Grx5 plays a critical role in maintaining β cell function and glucose homeostasis, its overexpression *in vivo* may not be sufficient to protect β cells under the complex metabolic stress induced by HFD.

4.4 EndoC-βH3 pseudoislets are suitable for intraportal transplantation in diabetic mice

Next, based on the employing of human β cell line EndoC-βH3 cells in our study, we further investigated the function of pseudoislets formed by EndoC-βH3 cells. Islet transplantation remains one of the most promising therapeutic strategies for T1DM, emphasizing the need for future research. Although rodent-derived pseudoislets have been widely used to study islet function and transplantation, significant differences in structure, function, and metabolic properties between human and rodent islets highlight the necessity for research based on human islets. The establishment of the EndoC-βH3 cell line provides an alternative method to study human islets.

Studies have confirmed the benefits of cell-cell interactions for β cell function (Lecomte et al., 2016). Also, Cornell et al. found that cell-cell contact can improve glucose-induced ATP production by regulating metabolic flux, thereby increasing pseudoislets GSIS (Cornell et al., 2022). As expected, in this study, we found that pseudoislets formed by EndoC-βH3 cell aggregation increased GSIS compared with monolayer cells *in vitro*. Additionally, our transplantation experiments demonstrated that EndoC-βH3 pseudoislets could be successfully transplanted into the liver of STZ-induced diabetic mice via the intraportal route. Although immunohistological staining showed lower insulin intensity in pseudoislets compared to native islets, the recipient mice exhibited significantly reduced blood glucose levels, indicating that these pseudoislets retained functional insulin secretion *in vivo*. Additionally, we performed Grx5 immunohistochemical staining on both native islets and transplanted pseudoislets. The results showed that Grx5 was predominantly localized at the periphery of native islets, while

pseudoislets were negative for Grx5 staining, which indicates that the specific localization of Grx5 in native islets may be related to its functional role in β cells, and its absence in pseudoislets may reflect functional limitations during *in vitro* culture or transplantation.

Comprehensive analysis of EndoC-βH cell karyotyping, chromatin structural conformation, cis-regulatory networks, histone marks, genotyping, and gene expression information highlighted that the EndoC-βH cell line was a valid model for studying β cells (Lawlor et al., 2019). Tsonkova et al. further confirmed that pseudoislets derived from EndoC-βH cells were responsive to cytokines, glucolipotoxicity, and ER stress, providing strong evidence for their application in DM research (Tsonkova et al., 2018). The latest EndoC-βH5 cell exhibits enhanced physiological behavior, including responsiveness to GLP-1 and GIP, and expression of the glucagon receptor (Blanchi et al., 2023). These advancements significantly improve the experimental reproducibility and physiological relevance of pseudoislet models.

In summary, the transplantation of EndoC-βH3 pseudoislets was technically feasible and provided a new direction for β cell replacement therapy. By integrating multi-omics analyses and gene-editing technologies, future research may uncover additional targets to improve graft function and survival, thereby advancing the field of islet transplantation.

4.5 Conclusion

In conclusion, we provide a comprehensive investigation into the molecular mechanisms underlying β cell dysfunction under lipotoxic conditions, with a particular focus on the roles of Grx5, iron metabolism, and β cell survival and function.

We demonstrated that OA exposure reduced β cell metabolic activity and impaired β cell function, with a significant reduction in Grx5 protein levels. For the first time, we

provided evidence that the downregulation of Grx5 was associated with decreased insulin content and insulin secretion and a potential involvement with ferroptosis, as indicated by mitochondrial iron overload and lipid peroxidation accumulation. Grx5 is a mitochondrial enzyme that forms part of the machinery involved in the biogenesis and assembly of FeS cluster (Lill et al., 2015). Thereby, Grx5 exerts essential tasks for the mitochondria function as well as for the cellular iron homeostasis (Rodríguez-Manzaneque et al., 2002; Kühn, 2015). We found that Grx5 levels in β cells were decreased by exposure to OA, which is consistent with previous studies from our group (Petry et al., 2022). In addition, our results showed that knockdown of Grx5 expression by siRNA in MIN6 cells led to mitochondrial iron overload accompanied by depletion of cytoplasmic free iron and decreased cellular metabolic activity. These findings align with reports in various cell models showing that Grx5 deficiency leads to an increased susceptibility to oxidative distress and a cellular iron overload (Linares et al., 2009; Rodríguez-Manzaneque et al., 1999; Wingert et al., 2005; Ye et al., 2010). A human subject suffering from a Grx5 deficiency was reported to present anemia, a type 2/3c DM, hepatosplenomegaly, and cirrhosis of the liver due to a cellular iron overload (Camaschella et al., 2007). The disease could be markedly ameliorated by the application of iron chelators. The same observation was made in a murine model of cellular iron overload (Cooksey et al., 2010), leading to the speculation that the iron overload may be the main pathological factor behind the Grx5 deficiency. Ferroptosis is an iron-dependent, non-apoptotic, regulated cell death caused by lipid peroxidation and subsequent plasma membrane disruption, accompanied by the inhibition of oxidoreductases, especially Gpx4 (Dixon et al., 2012). Iron accumulation and lipid peroxidation are two key signals that initiate membrane oxidative damage during ferroptosis (Dixon et al., 2012). In addition, Grx5 deficiency has been reported to activate IRP1/IRE binding activity and upregulate IRP2 levels in response to cytoplasmic depletion, which may ultimately upregulate the iron starvation response and increase intracellular free iron

(Ye et al., 2010). Therefore, we speculate that Grx5 deficiency may play an important role in the initial stage of ferroptosis.

However, in vivo experimental results showed that β cell-specific Grx5 overexpression failed to prevent HFD-induced hyperglycemia despite a slight decrease in body weight. This suggests that although Grx5 deficiency causes β cell dysfunction, it is not the only determinant of β cell failure in diabetes, because multiple mitochondrial proteins and metabolic pathways are affected under lipotoxic conditions (Lowell and Shulman, 2005; Römer et al., 2021).

In conclusion, this thesis provides evidence that the detrimental effects of OA on the β cell in diabetes are mediated by a decrease in Grx5, leading to an impaired iron metabolism and promoting ferroptosis.

5 Summary

Diabetes mellitus is a chronic metabolic disorder characterized by progressive β cell dysfunction and insulin resistance, leading to hyperglycemia and associated complications. Grx5, a mitochondrial enzyme of the group of thioredoxin proteins, plays a crucial role in the biogenesis of FeS clusters, which are essential for maintaining cellular iron homeostasis.

This thesis explored the complex interplay between free fatty acids, Grx5 deficiency, and iron metabolism in pancreatic β cells, emphasizing their roles in β cell survival and dysfunction *in vitro*, and investigated the phenotype and glucose metabolism of β cell-specific Grx5 overexpressing mice *in vivo*. Additionally, human EndoC-βH3 cells were aggregated into pseudoislets and transplanted into streptozotocin-induced diabetic mice to assess their functionality and therapeutic potential.

Our findings demonstrated that oleic acid treatment in β cells led to reduced metabolic activity, insulin content, and secretion, accompanied by increased mitochondrial iron accumulation and decreased levels of Grx5 and Gpx4. In addition, ferroptosis inducer ML-162 reduced insulin content and secretion, Grx5 levels, and increased lipid peroxidation and mitochondrial free iron accumulation. Cell metabolic activity was only reduced in the presence of oleic acid, and the reduction of Gpx4 and mitochondrial iron accumulation was more evident in the presence of oleic acid. Notably, the ferroptosis inhibitor Liproxstatin-1 was able to alleviate the oleic acid -induced reduction in insulin and Grx5 levels, as well as the associated lipid peroxidation and mitochondrial free iron overload. This suggests that exposure to oleic acid increases susceptibility to ferroptosis, an iron-dependent form of cell death characterized by lipid peroxidation.

We further investigated the essential role of Grx5 in maintaining β cell survival and function using Grx5 knockdown MIN6 cells. Notably, we demonstrated that Grx5

knockdown in MIN6 cells led to reduced insulin content and secretion, increased lipid peroxidation, and mitochondrial free iron overload. This was accompanied by cytoplasmic free iron depletion and decreased cell metabolic activity. These results indicate that Grx5-deficient cells exhibit impaired iron homeostasis, which is known to impair insulin secretion and may play an important role in the initial stage of ferroptosis.

Despite the strong link between Grx5 downregulation and β cell dysfunction, our *in vivo* studies revealed that Grx5 overexpression does not provide significant protection against high fat diet-induced metabolic stress. This may be due to the fact that Grx5 is not the only mitochondrial protein affected by lipotoxicity and that Grx5 is not an iron chelator but rather a scaffold protein that facilitates iron distribution in FeS cluster assembly. Therefore, while Grx5 deficiency contributes to β cell dysfunction, it cannot be regarded as a central regulatory switch for its reversal.

Eventually, we explored the potential of EndoC-βH3 pseudoislets as a model for studying human islet function and transplantation. Pseudoislets formed by EndoC-βH3 cells exhibited improved glucose-stimulated insulin secretion and could be successfully transplanted into diabetic mice, resulting in lower blood glucose levels. However, the lack of Grx5 in pseudoislets compared with native islets suggests potential functional limitations that warrant further investigation.

In conclusion, we propose that exposure to oleic acid leads to decreased Grx5 levels, impairing iron metabolism, promoting lipid peroxidation and eventually causing β cell dysfunction. However, Grx5 overexpression *in vivo* fails to reverse high fat diet-induced hyperglycemia. Additionally, we highlighted the potential of pseudoislet transplantation as a therapeutic strategy for diabetes.

6 Zusammenfassung

Diabetes mellitus ist eine chronische Stoffwechselstörung, die durch eine fortschreitende β-Zell-Dysfunktion und Insulinresistenz gekennzeichnet ist, was zu Hyperglykämie und damit verbundenen Komplikationen führt. Grx5, ein mitochondriales Enzym aus der Gruppe der Thioredoxin-Proteine, spielt eine entscheidende Rolle bei der Biogenese von FeS-Clustern, die für die Aufrechterhaltung der zellulären Eisenhomöostase essenziell sind. In dieser Arbeit wurde das komplexe Zusammenspiel zwischen freien Fettsäuren, Grx5-Defizienz und Eisenstoffwechsel in pankreatischen β-Zellen untersucht, wobei deren Bedeutung für das Überleben und die Dysfunktion von β-Zellen in vitro herausgearbeitet wurde. Des Weiteren wurden der Phänotyp und Glukosestoffwechsel von β-zellspezifischen Grx5-überexprimierenden Mäusen in vivo analysiert. Zusätzlich wurden menschliche EndoC-βH3-Zellen zu Pseudoinseln aggregiert und in STZ-induzierte diabetische Mäuse transplantiert, um ihre Funktionalität und ihr therapeutisches Potenzial zu beurteilen.

Die Ergebnisse zeigten, dass die Behandlung mit Ölsäure in β-Zellen zu einer verminderten metabolischen Aktivität, einem reduzierten Insulingehalt und einer verringerten Insulinsekretion führte, begleitet von einer mitochondrialen Eisenakkumulation und erniedrigten Proteingehalten von Grx5 und Gpx4. Die Behandlung mit dem Ferroptose-Induktor ML-162 führe zu einer Abnahme des Insulingehalts und der Insulinsekretion, des Grx5-Spiegels, zu einer erhöhten Lipidperoxidation und einer Akkumulation freien Eisens in den Mitochondrien. Die zelluläre metabolische Aktivität wurde jedoch nur in Gegenwart von Ölsäure reduziert. Die Abnahme von Gpx4 und der mitochondrialen Eisenakkumulation war in Anwesenheit von Ölsäure deutlicher ausgeprägt. Bemerkenswerterweise konnte der Ferroptose-Inhibitor Lip-1 die ölsäureinduzierte Reduktion der Insulin- und Grx5-Spiegel sowie die damit verbundene Lipidperoxidation und

mitochondriale freie Eisenüberladung abschwächen. Dies legt nahe, dass eine Ölsäure-Exposition die Suszeptibilität für Ferroptose erhöht.

In weiteren Untersuchungen analysierten wir die essenzielle Rolle von Grx5 für das Überleben und die Funktion von β-Zellen mittels Grx5-knockdown MIN6-Zellen. Dabei konnten wir zeigen, dass der Grx5-Knockdown in MIN6-Zellen zu verringertem Insulin-Gehalt und Sekretion, erhöhter Lipidperoxidation und mitochondrialer freier Eisenüberladung führte. Dies ging einher mit einer Depletion von zytosolischem freiem Eisen und verminderter zellulärer metabolischer Aktivität. Diese Ergebnisse deuten darauf hin, dass Grx5-defiziente Zellen eine gestörte Eisenhomöostase aufweisen, was eine wichtige Rolle in der Initialphase der Ferroptose spielen könnte.

Trotz des starken Zusammenhangs zwischen Grx5-Herunterregulierung und β-Zell-Dysfunktion zeigten unsere In-vivo-Studien, dass eine Grx5-Überexpression keinen signifikanten Schutz gegen durch fettreiche Diät induzierten metabolischen Stress bietet. Dies könnte darauf zurückzuführen sein, dass Grx5 nicht das einzige mitochondriale Protein ist, das von Lipotoxizität betroffen ist, und dass Grx5 kein Eisenchelator, sondern ein Gerüstprotein ist, dass die Eisenverteilung bei der FeS-Cluster-Assemblierung erleichtert. Daher trägt zwar ein Grx5-Mangel zur β-Zell-Dysfunktion bei, kann jedoch nicht als zentraler regulatorischer Schalter für deren Umkehrung betrachtet werden.

Abschließend untersuchten wir das Potenzial von EndoC-βH3-Pseudoinseln als Modell zur Erforschung humaner Inselzellfunktion und Transplantation. Die aus EndoC-βH3-Zellen gebildeten Pseudoinseln zeigten eine verbesserte glukose-stimulierte Insulinsekretion (GSIS) und konnten erfolgreich in diabetische Mäuse transplantiert werden, was zu niedrigeren Blutzuckerspiegeln führte. Das im Vergleich zu nativen Inseln geringere Grx5-Vorkommen in Pseudoinseln deutet jedoch auf potenzielle funktionelle Einschränkungen hin, die weitere Untersuchungen erfordern.

Zusammenfassend deuten unsere Daten darauf hin, dass Ölsäure zu einem verminderten Grx5-Gehalt der β-Zelle führt, wodurch es zu einer Eisenumverteilung, Lipidperoxidation und schließlich β-Zell-Dysfunktion kommt. Allerdings kann eine Grx5-Überexpression in vivo die durch fettreiche Diät induzierte Hyperglykämie nicht umkehren. Zudem unterstreichen wir das Potenzial der Pseudoinsel-Transplantation als therapeutische Strategie bei Diabetes.

7 Reference

Abebe, T., Mahadevan, J., Bogachus, L., et al. (2017) Nrf2/antioxidant pathway mediates β cell self-repair after damage by high-fat diet-induced oxidative stress. *JCI insight*, 2 (24): e92854, 92854. doi:10.1172/jci.insight.92854.

Akil, A.A.-S., Yassin, E., Al-Maraghi, A., et al. (2021) Diagnosis and treatment of type 1 diabetes at the dawn of the personalized medicine era. *Journal of Translational Medicine*, 19 (1): 137. doi:10.1186/s12967-021-02778-6.

Akshintala, D., Chugh, R., Amer, F., et al. (2019) *Nonalcoholic Fatty Liver Disease: The Overlooked Complication of Type 2 Diabetes*. Available at: https://www.ncbi.nlm.nih.gov/books/NBK544043/.

Alberti, K.G. and Zimmet, P.Z. (1998) Definition, diagnosis and classification of diabetes mellitus and its complications. Part 1: diagnosis and classification of diabetes mellitus provisional report of a WHO consultation. *Diabetic Medicine: A Journal of the British Diabetic Association*, 15 (7): 539–553. doi:10.1002/(SICI)1096-9136(199807)15:7<539::AID-DIA668>3.0.CO;2-S.

Alejandro, E.U., Gregg, B., Blandino-Rosano, M., et al. (2015) Natural history of β-cell adaptation and failure in type 2 diabetes. *Molecular Aspects of Medicine*, 42: 19–41. doi:10.1016/j.mam.2014.12.002.

Almgren, P., Lehtovirta, M., Isomaa, B., et al. (2011) Heritability and familiality of type 2 diabetes and related quantitative traits in the Botnia Study. *Diabetologia*, 54 (11): 2811–2819. doi:10.1007/s00125-011-2267-5.

Alvarez, S.W., Sviderskiy, V.O., Terzi, E.M., et al. (2017) NFS1 undergoes positive selection in lung tumours and protects cells from ferroptosis. *Nature*, 551 (7682): 639–643. doi:10.1038/nature24637.

American Diabetes Association (2009) Diagnosis and classification of diabetes mellitus. *Diabetes Care*, 32 Suppl 1 (Suppl 1): S62–S67. doi:10.2337/dc09-S062.

American Diabetes Association Professional Practice Committee (2024) 9. Pharmacologic Approaches to Glycemic Treatment: Standards of Care in Diabetes-2024. *Diabetes Care*, 47 (Suppl 1): S158–S178. doi:10.2337/dc24-S009.

Arosio, P. and Levi, S. (2010) Cytosolic and mitochondrial ferritins in the regulation of cellular iron homeostasis and oxidative damage. *Biochimica Et Biophysica Acta*, 1800 (8): 783–792. doi:10.1016/j.bbagen.2010.02.005.

Ashcroft, F.M. and Rorsman, P. (2012) Diabetes mellitus and the β cell: the last ten years. *Cell*, 148 (6): 1160–1171. doi:10.1016/j.cell.2012.02.010.

Ashcroft, S.J. (1980) Glucoreceptor mechanisms and the control of insulin release and biosynthesis. *Diabetologia*, 18 (1): 5–15. doi:10.1007/BF01228295.

Atkinson, M.A., Campbell-Thompson, M., Kusmartseva, I., et al. (2020) Organisation of the human pancreas in health and in diabetes. *Diabetologia*, 63 (10): 1966–1973. doi:10.1007/s00125-020-05203-7.

Ayala, A., Muñoz, M.F. and Argüelles, S. (2014) Lipid peroxidation: production, metabolism, and signaling mechanisms of malondialdehyde and 4-hydroxy-2-nonenal. *Oxidative Medicine and Cellular Longevity*, 2014: 360438. doi:10.1155/2014/360438.

Babichev, Y. and Isakov, N. (2001) "Tyrosine phosphorylation of PICOT and its translocation to the nucleus in response of human T cells to oxidative stress." In Mackiewicz, A., Kurpisz, M. and Żeromski, J. (eds.) *Advances in Experimental Medicine and Biology*. Progress in Basic and Clinical Immunology. Boston,MA: Springer. pp. 41–45.

Babichev, Y., Witte, S., Altman, A., et al. (2001) "The Human PICOT Protein Possesses A Thioredoxin-like Homology Domain and A Tandem Repeat of A Novel Domain Which Is Highly Conserved during Evolution." In *Protein Modules in Cellular Signalling*. Series A: Life Sciences. Amsterdam: IOS Press OHM. pp. 104–113.

Baekkeskov, S., Aanstoot, H.J., Christgau, S., et al. (1990) Identification of the 64K autoantigen in insulin-dependent diabetes as the GABA-synthesizing enzyme glutamic acid decarboxylase. *Nature*, 347 (6289): 151–156. doi:10.1038/347151a0.

Baker, P.R., Friederich, M.W., Swanson, M.A., et al. (2014) Variant non ketotic hyperglycinemia is caused by mutations in LIAS, BOLA3 and the novel gene GLRX5. *Brain : a Journal of Neurology*, 137 (Pt 2): 366–379. doi:10.1093/brain/awt328.

Baldwin, A.C., Green, C.D., Olson, L.K., et al. (2012) A role for aberrant protein palmitoylation in FFA-induced ER stress and β-cell death. *American Journal of Physiology. Endocrinology and Metabolism*, 302 (11): E1390-1398. doi:10.1152/ajpendo.00519.2011.

Banci, L., Brancaccio, D., Ciofi-Baffoni, S., et al. (2014) [2Fe-2S] cluster transfer in iron-sulfur protein biogenesis. *Proc Natl Acad Sci U S A*, 111 (17): 6203–6208. doi:10.1073/pnas.1400102111.

Bansod, H., Wanjari, A. and Dumbhare, O. (2023) A Review on Relationship Between Charcot Neuroarthropathy and Diabetic Patients. *Cureus*, 15 (12): e50988. doi:10.7759/cureus.50988.

Barrett, W.C., DeGnore, J.P., König, S., et al. (1999) Regulation of PTP1B via glutathionylation of the active site cysteine 215. *Biochemistry*, 38 (20): 6699–6705. doi:10.1021/bi990240v.

Basile, G., Qadir, M.M.F., Mauvais-Jarvis, F., et al. (2022) Emerging diabetes therapies: Bringing back the β-cells. *Molecular Metabolism*, 60: 101477. doi:10.1016/j.molmet.2022.101477.

Basson, A.R., Chen, C., Sagl, F., et al. (2020) Regulation of Intestinal Inflammation by Dietary Fats. *Frontiers in Immunology*, 11: 604989. doi:10.3389/fimmu.2020.604989.

Begas, P., Liedgens, L., Moseler, A., et al. (2017) Glutaredoxin catalysis requires two distinct glutathione interaction sites. *Nature Communications*, 8: 14835. doi:10.1038/ncomms14835.

Bellini, L., Campana, M., Rouch, C., et al. (2018) Protective role of the ELOVL2/docosahexaenoic acid axis in glucolipotoxicity-induced apoptosis in rodent beta cells and human islets. *Diabetologia*, 61 (8): 1780–1793. doi:10.1007/s00125-018-4629-8.

Benazra, M., Lecomte, M.-J., Colace, C., et al. (2015) A human beta cell line with drug inducible excision of immortalizing transgenes. *Molecular Metabolism*, 4 (12): 916–925. doi:10.1016/j.molmet.2015.09.008.

Berndt, C., Hudemann, C., Hanschmann, E.-M., et al. (2007) How does iron-sulfur cluster coordination regulate the activity of human glutaredoxin 2? *Antioxid Redox Signal*, 9 (1): 151–157. doi:10.1089/ars.2007.9.151.

Bjornstad, P., Cherney, D. and Maahs, D.M. (2014) Early diabetic nephropathy in type 1 diabetes: new insights. *Current Opinion in Endocrinology, Diabetes, and Obesity*, 21 (4): 279–286. doi:10.1097/MED.0000000000000074.

Blanchi, B., Taurand, M., Colace, C., et al. (2023) EndoC-βH5 cells are storable and ready-to-use human pancreatic beta cells with physiological insulin secretion. *Molecular Metabolism*, 76: 101772. doi:10.1016/j.molmet.2023.101772.

Blesia, V., Patel, V.B., Al-Obaidi, H., et al. (2021) Excessive Iron Induces Oxidative Stress Promoting Cellular Perturbations and Insulin Secretory Dysfunction in MIN6 Beta Cells. *Cells*, 10 (5): 1141. doi:10.3390/cells10051141.

Bloomgarden, Z.T. (2005) Diabetic nephropathy. *Diabetes Care*, 28 (3): 745–751. doi:10.2337/diacare.28.3.745.

Boden, G. (2009) Endoplasmic reticulum stress: another link between obesity and insulin resistance/inflammation? *Diabetes*, 58 (3): 518–519. doi:10.2337/db08-1746.

Bonner-Weir, S., Sullivan, B.A. and Weir, G.C. (2015) Human Islet Morphology Revisited: Human and Rodent Islets Are Not So Different After All. *The Journal of Histochemistry and Cytochemistry: Official Journal of the Histochemistry Society*, 63 (8): 604–612. doi:10.1369/0022155415570969.

Bottazzo, G.F., Florin-Christensen, A. and Doniach, D. (1974) Islet-cell antibodies in diabetes mellitus with autoimmune polyendocrine deficiencies. *Lancet (London, England)*, 2 (7892): 1279–1283. doi:10.1016/s0140-6736(74)90140-8.

Boulton, A.J.M. (2008) The diabetic foot: grand overview, epidemiology and pathogenesis. *Diabetes/Metabolism Research and Reviews*, 24 Suppl 1: S3-6. doi:10.1002/dmrr.833.

Brambillasca, S., Altkrueger, A., Colombo, S.F., et al. (2012) CDK5 regulatory subunit-associated protein 1-like 1 (CDKAL1) is a tail-anchored protein in the endoplasmic reticulum (ER) of insulinoma cells. *The Journal of Biological Chemistry*, 287 (50): 41808–41819. doi:10.1074/jbc.M112.376558.

Bratanova-Tochkova, T.K., Cheng, H., Daniel, S., et al. (2002) Triggering and augmentation mechanisms, granule pools, and biphasic insulin secretion. *Diabetes*, 51 Suppl 1: S83-90. doi:10.2337/diabetes.51.2007.s83.

Bril, F. and Cusi, K. (2016) Nonalcoholic Fatty Liver Disease: The New Complication of Type 2 Diabetes Mellitus. *Endocrinology and Metabolism Clinics of North America*, 45 (4): 765–781. doi:10.1016/j.ecl.2016.06.005.

Browning, D.J., Stewart, M.W. and Lee, C. (2018) Diabetic macular edema: Evidence-based management. *Indian Journal of Ophthalmology*, 66 (12): 1736–1750. doi:10.4103/ijo.IJO_1240_18.

Bruni, A., Pepper, A.R., Pawlick, R.L., et al. (2018) Ferroptosis-inducing agents compromise in vitro human islet viability and function. *Cell Death Dis*, 9 (6): 595. doi:10.1038/s41419-018-0506-0.

Burrack, A.L., Martinov, T. and Fife, B.T. (2017) T Cell-Mediated Beta Cell Destruction: Autoimmunity and Alloimmunity in the Context of Type 1 Diabetes. *Frontiers in Endocrinology*, 8: 343. doi:10.3389/fendo.2017.00343.

Busch, A.K., Gurisik, E., Cordery, D.V., et al. (2005) Increased fatty acid desaturation and enhanced expression of stearoyl coenzyme A desaturase protects pancreatic beta-cells from lipoapoptosis. *Diabetes*, 54 (10): 2917–2924. doi:10.2337/diabetes.54.10.2917.

Bushweller, J.H., Billeter, M., Holmgren, A., et al. (1994) The nuclear magnetic resonance solution structure of the mixed disulfide between Escherichia coli glutaredoxin(C14S) and glutathione. *Journal of Molecular Biology*, 235 (5): 1585–1597. doi:10.1006/jmbi.1994.1108.

Camaschella, C., Campanella, A., De Falco, L., et al. (2007) The human counterpart of zebrafish shiraz shows sideroblastic-like microcytic anemia and iron overload. *Blood*, 110 (4): 1353–1358. doi:10.1182/blood-2007-02-072520.

Cao, S.S. and Kaufman, R.J. (2014) Endoplasmic reticulum stress and oxidative stress in cell fate decision and human disease. *Antioxidants & Redox Signaling*, 21 (3): 396–413. doi:10.1089/ars.2014.5851.

Cardozo, A.K., Ortis, F., Storling, J., et al. (2005) Cytokines downregulate the sarcoendoplasmic reticulum pump Ca2+ ATPase 2b and deplete endoplasmic reticulum Ca2+, leading to induction of endoplasmic reticulum stress in pancreatic beta-cells. *Diabetes*, 54 (2): 452–461. doi:10.2337/diabetes.54.2.452.

Carpentier, A., Mittelman, S.D., Lamarche, B., et al. (1999) Acute enhancement of insulin secretion by FFA in humans is lost with prolonged FFA elevation. *The American Journal of Physiology*, 276 (6): E1055-1066. doi:10.1152/ajpendo.1999.276.6.E1055.

Cassavaugh, J. and Lounsbury, K.M. (2011) Hypoxia-mediated biological control. *Journal of Cellular Biochemistry*, 112 (3): 735–744. doi:10.1002/jcb.22956.

Cha, H., Kim, J.M., Oh, J.G., et al. (2008) PICOT is a critical regulator of cardiac hypertrophy and cardiomyocyte contractility. *J Mol Cell Cardiol*, 45 (6): 796–803. doi:10.1016/j.yjmcc.2008.09.124.

Cha, M.-K. and Kim, I.-H. (2009) Preferential overexpression of glutaredoxin3 in human colon and lung carcinoma. *Cancer Epidemiology*, 33 (3–4): 281–287. doi:10.1016/j.canep.2009.08.006.

Chaudhury, A., Duvoor, C., Reddy Dendi, V.S., et al. (2017) Clinical Review of Antidiabetic Drugs: Implications for Type 2 Diabetes Mellitus Management. *Frontiers in Endocrinology*, 8: 6. doi:10.3389/fendo.2017.00006.

Cheff, D.M., Huang, C., Scholzen, K.C., et al. (2023) The ferroptosis inducing compounds RSL3 and ML162 are not direct inhibitors of GPX4 but of TXNRD1. *Redox Biology*, 62: 102703. doi:10.1016/j.redox.2023.102703.

Chen, O.S., Hemenway, S. and Kaplan, J. (2002) Inhibition of Fe-S cluster biosynthesis decreases mitochondrial iron export: evidence that Yfh1p affects Fe-S cluster synthesis. *Proceedings of the National Academy of Sciences of the United States of America*, 99 (19): 12321–12326. doi:10.1073/pnas.192449599.

Cheung, N., Mitchell, P. and Wong, T.Y. (2010) Diabetic retinopathy. *Lancet (London, England)*, 376 (9735): 124–136. doi:10.1016/S0140-6736(09)62124-3.

Chiong, M.A., Procopis, P., Carpenter, K., et al. (2007) Late-onset nonketotic hyperglycinemia with leukodystrophy and an unusual clinical course. *Pediatric Neurology*, 37 (4): 283–286. doi:10.1016/j.pediatrneurol.2007.05.016.

Chiu, H.K., Tsai, E.C., Juneja, R., et al. (2007) Equivalent insulin resistance in latent autoimmune diabetes in adults (LADA) and type 2 diabetic patients. *Diabetes Research and Clinical Practice*, 77 (2): 237–244. doi:10.1016/j.diabres.2006.12.013.

Choukem, S.-P., Sobngwi, E., Boudou, P., et al. (2013) β- and α-cell dysfunctions in africans with ketosis-prone atypical diabetes during near-normoglycemic remission. *Diabetes Care*, 36 (1): 118–123. doi:10.2337/dc12-0798.

Clore, J.N., Allred, J., White, D., et al. (2002) The role of plasma fatty acid composition in endogenous glucose production in patients with type 2 diabetes mellitus. *Metabolism: Clinical and Experimental*, 51 (11): 1471–1477. doi:10.1053/meta.2002.35202.

Cnop, M., Hannaert, J.C., Hoorens, A., et al. (2001) Inverse relationship between cytotoxicity of free fatty acids in pancreatic islet cells and cellular triglyceride accumulation. *Diabetes*, 50 (8): 1771–1777. doi:10.2337/diabetes.50.8.1771.

Colagiuri, S., Falavigna, M., Agarwal, M.M., et al. (2014) Strategies for implementing the WHO diagnostic criteria and classification of hyperglycaemia first detected in pregnancy. *Diabetes Research and Clinical Practice*, 103 (3): 364–372. doi:10.1016/j.diabres.2014.02.012.

Cooksey, R.C., Jones, D., Gabrielsen, S., et al. (2010) Dietary iron restriction or iron chelation protects from diabetes and loss of beta-cell function in the obese (ob/ob lep-/-) mouse. *American Journal of Physiology. Endocrinology and Metabolism*, 298 (6): E1236-1243. doi:10.1152/ajpendo.00022.2010.

Cooksey, R.C., Jouihan, H.A., Ajioka, R.S., et al. (2004) Oxidative stress, beta-cell apoptosis, and decreased insulin secretory capacity in mouse models of hemochromatosis. *Endocrinology*, 145 (11): 5305–5312. doi:10.1210/en.2004-0392.

Cornell, D., Miwa, S., Georgiou, M., et al. (2022) Pseudoislet Aggregation of Pancreatic β-Cells Improves Glucose Stimulated Insulin Secretion by Altering Glucose Metabolism and Increasing ATP Production. *Cells*, 11 (15): 2330. doi:10.3390/cells11152330.

Cucca, F., Lampis, R., Congia, M., et al. (2001) A correlation between the relative predisposition of MHC class II alleles to type 1 diabetes and the structure of their proteins. *Human Molecular Genetics*, 10 (19): 2025–2037. doi:10.1093/hmg/10.19.2025.

Cusi, K. (2020a) A diabetologist's perspective of non-alcoholic steatohepatitis (NASH): Knowledge gaps and future directions. *Liver International : Official Journal of the International Association For the Study of the Liver*, 40 Suppl 1: 82–88. doi:10.1111/liv.14350.

Cusi, K. (2020b) Time to Include Nonalcoholic Steatohepatitis in the Management of Patients With Type 2 Diabetes. *Diabetes Care*, 43 (2): 275–279. doi:10.2337/dci19-0064.

Daher, R., Mansouri, A., Martelli, A., et al. (2019) GLRX5 mutations impair heme biosynthetic enzymes ALA synthase 2 and ferrochelatase in Human congenital

sideroblastic anemia. *Molecular Genetics and Metabolism*, 128 (3): 342–351. doi:10.1016/j.ymgme.2018.12.012.

Daily, D., Vlamis-Gardikas, A., Offen, D., et al. (2001) Glutaredoxin protects cerebellar granule neurons from dopamine-induced apoptosis by activating NF-kappa B via Ref-1. *J Biol Chem*, 276 (2): 1335–1344. doi:10.1074/jbc.M008121200.

Dansen, T.B. and Wirtz, K.W. (2001) The peroxisome in oxidative stress. *IUBMB life*, 51 (4): 223–230. doi:10.1080/152165401753311762.

Diakogiannaki, E., Dhayal, S., Childs, C.E., et al. (2007) Mechanisms involved in the cytotoxic and cytoprotective actions of saturated versus monounsaturated long-chain fatty acids in pancreatic beta-cells. *The Journal of Endocrinology*, 194 (2): 283–291. doi:10.1677/JOE-07-0082.

Dillmann, W.H. (2019) Diabetic Cardiomyopathy. *Circulation Research*, 124 (8): 1160–1162. doi:10.1161/CIRCRESAHA.118.314665.

Diotte, N.M., Xiong, Y., Gao, J., et al. (2009) Attenuation of doxorubicin-induced cardiac injury by mitochondrial glutaredoxin 2. *Biochim Biophys Acta*, 1793 (2): 427–438. doi:10.1016/j.bbamcr.2008.10.014.

Dixon, S.J., Lemberg, K.M., Lamprecht, M.R., et al. (2012) Ferroptosis: an iron-dependent form of nonapoptotic cell death. *Cell*, 149 (5): 1060–1072. doi:10.1016/j.cell.2012.03.042.

Dolenšek, J., Rupnik, M.S. and Stožer, A. (2015) Structural similarities and differences between the human and the mouse pancreas. *Islets*, 7 (1): e1024405. doi:10.1080/19382014.2015.1024405.

Donath, M.Y. and Shoelson, S.E. (2011) Type 2 diabetes as an inflammatory disease. *Nature Reviews. Immunology*, 11 (2): 98–107. doi:10.1038/nri2925.

Eaton, J.W. and Qian, M. (2002) Molecular bases of cellular iron toxicity. *Free Radical Biology & Medicine*, 32 (9): 833–840. doi:10.1016/s0891-5849(02)00772-4.

El-Assaad, W., Buteau, J., Peyot, M.-L., et al. (2003) Saturated fatty acids synergize with elevated glucose to cause pancreatic beta-cell death. *Endocrinology*, 144 (9): 4154–4163. doi:10.1210/en.2003-0410.

Elsner, M., Gehrmann, W. and Lenzen, S. (2011) Peroxisome-generated hydrogen peroxide as important mediator of lipotoxicity in insulin-producing cells. *Diabetes*, 60 (1): 200–208. doi:10.2337/db09-1401.

Enoksson, M., Fernandes, A.P., Prast, S., et al. (2005) Overexpression of glutaredoxin 2 attenuates apoptosis by preventing cytochrome c release. *Biochem Biophys Res Commun*, 327 (3): 774–779. doi:10.1016/j.bbrc.2004.12.067.

Fasanmade, O.A., Odeniyi, I.A. and Ogbera, A.O. (2008) Diabetic ketoacidosis: diagnosis and management. *African Journal of Medicine and Medical Sciences*, 37 (2): 99–105.

Feng, W.-X., Zhuo, X.-W., Liu, Z.-M., et al. (2021) Case Report: A Variant Non-ketotic Hyperglycinemia With GLRX5 Mutations: Manifestation of Deficiency of Activities of the Respiratory Chain Enzymes. *Frontiers in Genetics*, 12: 605778. doi:10.3389/fgene.2021.605778.

Feng, Y., Madungwe, N.B., Imam Aliagan, A.D., et al. (2019) Liproxstatin-1 protects the mouse myocardium against ischemia/reperfusion injury by decreasing VDAC1 levels and restoring GPX4 levels. *Biochemical and Biophysical Research Communications*, 520 (3): 606–611. doi:10.1016/j.bbrc.2019.10.006.

Fernandes, A.P. and Holmgren, A. (2004) Glutaredoxins: glutathione-dependent redox enzymes with functions far beyond a simple thioredoxin backup system. *Antioxidants & Redox Signaling*, 6 (1): 63–74. doi:10.1089/152308604771978354.

Ferrannini, E., Barrett, E.J., Bevilacqua, S., et al. (1983) Effect of fatty acids on glucose production and utilization in man. *The Journal of Clinical Investigation*, 72 (5): 1737–1747. doi:10.1172/JCI111133.

Forouhi, N.G., Harding, A.H., Allison, M., et al. (2007) Elevated serum ferritin levels predict new-onset type 2 diabetes: results from the EPIC-Norfolk prospective study. *Diabetologia*, 50 (5): 949–956. doi:10.1007/s00125-007-0604-5.

Fox, C.S., Coady, S., Sorlie, P.D., et al. (2004) Trends in cardiovascular complications of diabetes. *JAMA*, 292 (20): 2495–2499. doi:10.1001/jama.292.20.2495.

Frandsen, C.S., Dejgaard, T.F. and Madsbad, S. (2016) Non-insulin drugs to treat hyperglycaemia in type 1 diabetes mellitus. *The Lancet. Diabetes & Endocrinology*, 4 (9): 766–780. doi:10.1016/S2213-8587(16)00039-5.

Fu, Z., Gilbert, E.R. and Liu, D. (2013) Regulation of Insulin Synthesis and Secretion and Pancreatic Beta-Cell Dysfunction in Diabetes. *Current diabetes reviews*, 9 (1): 25–53.

Galicia-Garcia, U., Benito-Vicente, A., Jebari, S., et al. (2020) Pathophysiology of Type 2 Diabetes Mellitus. *International Journal of Molecular Sciences*, 21 (17): 6275. doi:10.3390/ijms21176275.

Gaschler, M.M. and Stockwell, B.R. (2017) Lipid peroxidation in cell death. *Biochemical and Biophysical Research Communications*, 482 (3): 419–425. doi:10.1016/j.bbrc.2016.10.086.

Gehrmann, W., Elsner, M. and Lenzen, S. (2010) Role of metabolically generated reactive oxygen species for lipotoxicity in pancreatic β-cells. *Diabetes, Obesity & Metabolism*, 12 Suppl 2: 149–158. doi:10.1111/j.1463-1326.2010.01265.x.

Genco, R.J. and Borgnakke, W.S. (2020) Diabetes as a potential risk for periodontitis: association studies. *Periodontology 2000*, 83 (1): 40–45. doi:10.1111/prd.12270.

Ghasemi, M., Turnbull, T., Sebastian, S., et al. (2021) The MTT Assay: Utility, Limitations, Pitfalls, and Interpretation in Bulk and Single-Cell Analysis. *International Journal of Molecular Sciences*, 22 (23): 12827. doi:10.3390/ijms222312827.

Godoy, J.R., Funke, M., Ackermann, W., et al. (2011a) Redox atlas of the mouse. Immunohistochemical detection of glutaredoxin-, peroxiredoxin-, and thioredoxin-family proteins in various tissues of the laboratory mouse. *Biochim Biophys Acta*, 1810 (1): 2–92. doi:10.1016/j.bbagen.2010.05.006.

Godoy, J.R., Oesteritz, S., Hanschmann, E.-M., et al. (2011b) Segment-specific overexpression of redoxins after renal ischemia and reperfusion: protective roles of glutaredoxin 2, peroxiredoxin 3, and peroxiredoxin 6. *Free Radic Biol Med*, 51 (2): 552–561. doi:10.1016/j.freeradbiomed.2011.04.036.

Gorelenkova Miller, O., Behring, J.B., Siedlak, S.L., et al. (2016) Upregulation of Glutaredoxin-1 Activates Microglia and Promotes Neurodegeneration: Implications for Parkinson's Disease. *Antioxid Redox Signal*, 25 (18): 967–982. doi:10.1089/ars.2015.6598.

Grapov, D., Adams, S.H., Pedersen, T.L., et al. (2012) Type 2 diabetes associated changes in the plasma non-esterified fatty acids, oxylipins and endocannabinoids. *PloS One*, 7 (11): e48852. doi:10.1371/journal.pone.0048852.

Guo, B., Phillips, J.D., Yu, Y., et al. (1995) Iron regulates the intracellular degradation of iron regulatory protein 2 by the proteasome. *The Journal of Biological Chemistry*, 270 (37): 21645–21651. doi:10.1074/jbc.270.37.21645.

Guo, M., Huang, X., Zhang, J., et al. (2024) Palmitic acid induces β-cell ferroptosis by activating ceramide signaling pathway. *Experimental Cell Research*, 440 (2): 114134. doi:10.1016/j.yexcr.2024.114134.

Gupta, D., Jetton, T.L., LaRock, K., et al. (2017) Temporal characterization of β cell-adaptive and -maladaptive mechanisms during chronic high-fat feeding in C57BL/6NTac mice. *The Journal of Biological Chemistry*, 292 (30): 12449–12459. doi:10.1074/jbc.M117.781047.

Hansen, J.B., Tonnesen, M.F., Madsen, A.N., et al. (2012) Divalent metal transporter 1 regulates iron-mediated ROS and pancreatic β cell fate in response to cytokines. *Cell Metabolism*, 16 (4): 449–461. doi:10.1016/j.cmet.2012.09.001.

von Hanstein, A.-S., Tsikas, D., Lenzen, S., et al. (2023) Potentiation of Lipotoxicity in Human EndoC-βH1 β-Cells by Glucose is Dependent on the Structure of Free Fatty Acids. *Molecular Nutrition & Food Research*, 67 (5): e2200582. doi:10.1002/mnfr.202200582.

Haunhorst, P., Berndt, C., Eitner, S., et al. (2010) Characterization of the human monothiol glutaredoxin 3 (PICOT) as iron-sulfur protein. *Biochem Biophys Res Commun*, 394 (2): 372–376. doi:10.1016/j.bbrc.2010.03.016.

Haunhorst, P., Hanschmann, E.-M., Bräutigam, L., et al. (2013) Crucial function of vertebrate glutaredoxin 3 (PICOT) in iron homeostasis and hemoglobin maturation. *Mol Biol Cell*, 24 (12): 1895–1903. doi:10.1091/mbc.E12-09-0648.

Henquin, J.C. (2000) Triggering and amplifying pathways of regulation of insulin secretion by glucose. *Diabetes*, 49 (11): 1751–1760. doi:10.2337/diabetes.49.11.1751.

Hentze, M.W. and Kühn, L.C. (1996) Molecular control of vertebrate iron metabolism: mRNA-based regulatory circuits operated by iron, nitric oxide, and oxidative stress. *Proceedings of the National Academy of Sciences of the United States of America*, 93 (16): 8175–8182. doi:10.1073/pnas.93.16.8175.

Hentze, M.W., Muckenthaler, M.U., Galy, B., et al. (2010) Two to tango: regulation of Mammalian iron metabolism. *Cell*, 142 (1): 24–38. doi:10.1016/j.cell.2010.06.028.

Heydemann, A. (2016) An Overview of Murine High Fat Diet as a Model for Type 2 Diabetes Mellitus. *Journal of Diabetes Research*, 2016: 2902351. doi:10.1155/2016/2902351.

Hill, C.P., Dauter, Z., Dodson, E.J., et al. (1991) X-ray structure of an unusual Ca2+ site and the roles of Zn2+ and Ca2+ in the assembly, stability, and storage of the insulin hexamer. *Biochemistry*, 30 (4): 917–924. doi:10.1021/bi00218a006.

Hirasawa, A., Tsumaya, K., Awaji, T., et al. (2005) Free fatty acids regulate gut incretin glucagon-like peptide-1 secretion through GPR120. *Nature Medicine*, 11 (1): 90–94. doi:10.1038/nm1168.

Hirota, K., Matsui, M., Murata, M., et al. (2000) Nucleoredoxin, glutaredoxin, and thioredoxin differentially regulate NF-kappaB, AP-1, and CREB activation in HEK293 cells. *Biochem Biophys Res Commun*, 274 (1): 177–182. doi:10.1006/bbrc.2000.3106.

Hou, J.C., Min, L. and Pessin, J.E. (2009) Insulin granule biogenesis, trafficking and exocytosis. *Vitamins and Hormones*, 80: 473–506. doi:10.1016/S0083-6729(08)00616-X.

Hudemann, C., Lönn, M.E., Godoy, J.R., et al. (2009) Identification, expression pattern, and characterization of mouse glutaredoxin 2 isoforms. *Antioxid Redox Signal*, 11 (1): 1–14. doi:10.1089/ars.2008.2068.

Ighodaro, O.M. (2018) Molecular pathways associated with oxidative stress in diabetes mellitus. *Biomedicine & Pharmacotherapy = Biomedecine & Pharmacotherapie*, 108: 656–662. doi:10.1016/j.biopha.2018.09.058.

Isakov, N., Witte, S. and Altman, A. (2000) PICOT-HD: a highly conserved protein domain that is often associated with thioredoxin and glutaredoxin modules. *Trends In Biochemical Sciences*, 25 (11): 537–539. doi:10.1016/s0968-0004(00)01685-6.

Ishihara, H., Asano, T., Tsukuda, K., et al. (1993) Pancreatic beta cell line MIN6 exhibits characteristics of glucose metabolism and glucose-stimulated insulin secretion similar to those of normal islets. *Diabetologia*, 36 (11): 1139–1145. doi:10.1007/BF00401058.

Itoh, Y., Kawamata, Y., Harada, M., et al. (2003) Free fatty acids regulate insulin secretion from pancreatic beta cells through GPR40. *Nature*, 422 (6928): 173–176. doi:10.1038/nature01478.

Jain, C., Ansarullah, null, Bilekova, S., et al. (2022) Targeting pancreatic β cells for diabetes treatment. *Nature Metabolism*, 4 (9): 1097–1108. doi:10.1038/s42255-022-00618-5.

Jeong, D., Cha, H., Kim, E., et al. (2006) PICOT inhibits cardiac hypertrophy and enhances ventricular function and cardiomyocyte contractility. *Circ Res*, 99 (3): 307–314. doi:10.1161/01.RES.0000234780.06115.2c.

Jeong, D., Kim, J.M., Cha, H., et al. (2008) PICOT attenuates cardiac hypertrophy by disrupting calcineurin-NFAT signaling. *Circ Res*, 102 (6): 711–719. doi:10.1161/CIRCRESAHA.107.165985.

Jerram, S.T. and Leslie, R.D. (2017) The Genetic Architecture of Type 1 Diabetes. *Genes*, 8 (8): 209. doi:10.3390/genes8080209.

Jhurry, N.D., Chakrabarti, M., McCormick, S.P., et al. (2012) Biophysical investigation of the ironome of human jurkat cells and mitochondria. *Biochemistry*, 51 (26): 5276–5284. doi:10.1021/bi300382d.

Johansen, J.S., Harris, A.K., Rychly, D.J., et al. (2005) Oxidative stress and the use of antioxidants in diabetes: linking basic science to clinical practice. *Cardiovascular Diabetology*, 4: 5. doi:10.1186/1475-2840-4-5.

Johansson, C., Roos, A.K., Montano, S.J., et al. (2011) The crystal structure of human GLRX5: iron-sulfur cluster co-ordination, tetrameric assembly and monomer activity. *The Biochemical Journal*, 433 (2): 303–311. doi:10.1042/BJ20101286.

Jomova, K. and Valko, M. (2011) Importance of iron chelation in free radical-induced oxidative stress and human disease. *Current Pharmaceutical Design*, 17 (31): 3460–3473. doi:10.2174/138161211798072463.

Jouihan, H.A., Cobine, P.A., Cooksey, R.C., et al. (2008) Iron-mediated inhibition of mitochondrial manganese uptake mediates mitochondrial dysfunction in a mouse model of hemochromatosis. *Molecular Medicine (Cambridge, Mass.)*, 14 (3–4): 98–108. doi:10.2119/2007-00114.Jouihan.

Kanaan, G.N., Ichim, B., Gharibeh, L., et al. (2018) Glutaredoxin-2 controls cardiac mitochondrial dynamics and energetics in mice, and protects against human cardiac pathologies. *Redox Biol*, 14: 509–521. doi:10.1016/j.redox.2017.10.019.

Karunakaran, S., Saeed, U., Ramakrishnan, S., et al. (2007) Constitutive expression and functional characterization of mitochondrial glutaredoxin (Grx2) in mouse and human brain. *Brain Research*, 1185: 8–17. doi:10.1016/j.brainres.2007.09.019.

Kashyap, S., Belfort, R., Gastaldelli, A., et al. (2003) A sustained increase in plasma free fatty acids impairs insulin secretion in nondiabetic subjects genetically predisposed to develop type 2 diabetes. *Diabetes*, 52 (10): 2461–2474. doi:10.2337/diabetes.52.10.2461.

Khamseekaew, J., Kumfu, S., Wongjaikam, S., et al. (2017) Effects of iron overload, an iron chelator and a T-Type calcium channel blocker on cardiac mitochondrial biogenesis and mitochondrial dynamics in thalassemic mice. *European Journal of Pharmacology*, 799: 118–127. doi:10.1016/j.ejphar.2017.02.015.

Kharroubi, I., Ladrière, L., Cardozo, A.K., et al. (2004) Free fatty acids and cytokines induce pancreatic beta-cell apoptosis by different mechanisms: role of nuclear factor-kappaB and endoplasmic reticulum stress. *Endocrinology*, 145 (11): 5087–5096. doi:10.1210/en.2004-0478.

Kish-Trier, E., Schwarz, E.L., Pasquali, M., et al. (2016) Quantitation of total fatty acids in plasma and serum by GC-NCI-MS. *Clinical Mass Spectrometry*, 2: 11–17. doi:10.1016/j.clinms.2016.12.001.

Kleinfeld, A.M., Prothro, D., Brown, D.L., et al. (1996) Increases in serum unbound free fatty acid levels following coronary angioplasty. *The American Journal of Cardiology*, 78 (12): 1350–1354. doi:10.1016/s0002-9149(96)00651-0.

Kong, C.-C., Cheng, J.-D. and Wang, W. (2023) Neurotransmitters regulate β cells insulin secretion: A neglected factor. *World Journal of Clinical Cases*, 11 (28): 6670–6679. doi:10.12998/wjcc.v11.i28.6670.

Koshkin, V., Wang, X., Scherer, P.E., et al. (2003) Mitochondrial functional state in clonal pancreatic beta-cells exposed to free fatty acids. *The Journal of Biological Chemistry*, 278 (22): 19709–19715. doi:10.1074/jbc.M209709200.

Koulajian, K., Desai, T., Liu, G.C., et al. (2013) NADPH oxidase inhibition prevents beta cell dysfunction induced by prolonged elevation of oleate in rodents. *Diabetologia*, 56 (5): 1078–1087. doi:10.1007/s00125-013-2858-4.

Kowluru, A. (2020) Oxidative Stress in Cytokine-Induced Dysfunction of the Pancreatic Beta Cell: Known Knowns and Known Unknowns. *Metabolites*, 10 (12): 480. doi:10.3390/metabo10120480.

Kreienkamp, R.J., Voight, B.F., Gloyn, A.L., et al. (2023) “Genetics of Type 2 Diabetes.” In Lawrence, J.M., Casagrande, S.S., Herman, W.H., et al. (eds.) *Diabetes in America*. Bethesda (MD): National Institute of Diabetes and Digestive and Kidney Diseases (NIDDK). Available at: http://www.ncbi.nlm.nih.gov/books/NBK597726/ (Downloaded: 1 September 2024).

Kühn, L.C. (2015) Iron regulatory proteins and their role in controlling iron metabolism. *Metallomics: Integrated Biometal Science*, 7 (2): 232–243. doi:10.1039/c4mt00164h.

Kulkarni, R.N. (2004) The islet beta-cell. *The International Journal of Biochemistry & Cell Biology*, 36 (3): 365–371. doi:10.1016/j.biocel.2003.08.010.

Kumfu, S., Chattipakorn, S., Fucharoen, S., et al. (2012) Mitochondrial calcium uniporter blocker prevents cardiac mitochondrial dysfunction induced by iron overload in thalassemic mice. *Biometals: An International Journal on the Role of Metal Ions in Biology, Biochemistry, and Medicine*, 25 (6): 1167–1175. doi:10.1007/s10534-012-9579-x.

Ladrière, L., Igoillo-Esteve, M., Cunha, D.A., et al. (2010) Enhanced signaling downstream of ribonucleic Acid-activated protein kinase-like endoplasmic reticulum kinase potentiates lipotoxic endoplasmic reticulum stress in human islets. *The Journal of Clinical Endocrinology and Metabolism*, 95 (3): 1442–1449. doi:10.1210/jc.2009-2322.

Lai, E., Bikopoulos, G., Wheeler, M.B., et al. (2008) Differential activation of ER stress and apoptosis in response to chronically elevated free fatty acids in pancreatic beta-cells. *American Journal of Physiology. Endocrinology and Metabolism*, 294 (3): E540-550. doi:10.1152/ajpendo.00478.2007.

Lan, M.S., Lu, J., Goto, Y., et al. (1994) Molecular cloning and identification of a receptor-type protein tyrosine phosphatase, IA-2, from human insulinoma. *DNA and cell biology*, 13 (5): 505–514. doi:10.1089/dna.1994.13.505.

Lane, D.J.R., Merlot, A.M., Huang, M.L.-H., et al. (2015) Cellular iron uptake, trafficking and metabolism: Key molecules and mechanisms and their roles in disease. *Biochimica Et Biophysica Acta*, 1853 (5): 1130–1144. doi:10.1016/j.bbamcr.2015.01.021.

Langerhans, P. (1869) *Beitrage zur mikroscopischen anatomie der bauchspeichel druse*. Inaugural-dissertation.

Lawen, A. and Lane, D.J.R. (2013) Mammalian iron homeostasis in health and disease: uptake, storage, transport, and molecular mechanisms of action. *Antioxidants & Redox Signaling*, 18 (18): 2473–2507. doi:10.1089/ars.2011.4271.

Lawlor, N., Márquez, E.J., Orchard, P., et al. (2019) Multiomic Profiling Identifies cis-Regulatory Networks Underlying Human Pancreatic β Cell Identity and Function. *Cell Reports*, 26 (3): 788-801.e6. doi:10.1016/j.celrep.2018.12.083.

Lecomte, M.-J., Pechberty, S., Machado, C., et al. (2016) Aggregation of Engineered Human β-Cells Into Pseudoislets: Insulin Secretion and Gene Expression Profile in Normoxic and Hypoxic Milieu. *Cell Medicine*, 8 (3): 99–112. doi:10.3727/215517916X692843.

Lee, C.D., Folsom, A.R., Pankow, J.S., et al. (2004) Cardiovascular events in diabetic and nondiabetic adults with or without history of myocardial infarction. *Circulation*, 109 (7): 855–860. doi:10.1161/01.CIR.0000116389.61864.DE.

Lee, J., You, J.H., Shin, D., et al. (2020) Inhibition of Glutaredoxin 5 predisposes Cis-platin-resistant Head and Neck Cancer Cells to Ferroptosis. *Theranostics*, 10 (17): 7775–7786. doi:10.7150/thno.46903.

Lee, S.-H., Park, S.-Y. and Choi, C.S. (2022) Insulin Resistance: From Mechanisms to Therapeutic Strategies. *Diabetes & Metabolism Journal*, 46 (1): 15–37. doi:10.4093/dmj.2021.0280.

Lee, Y., Hirose, H., Ohneda, M., et al. (1994) Beta-cell lipotoxicity in the pathogenesis of non-insulin-dependent diabetes mellitus of obese rats: impairment in adipocyte-beta-cell relationships. *Proceedings of the National Academy of Sciences of the United States of America*, 91 (23): 10878–10882. doi:10.1073/pnas.91.23.10878.

Lee, Y.S., Li, P., Huh, J.Y., et al. (2011) Inflammation is necessary for long-term but not short-term high-fat diet-induced insulin resistance. *Diabetes*, 60 (10): 2474–2483. doi:10.2337/db11-0194.

Lekli, I., Mukherjee, S., Ray, D., et al. (2010) Functional recovery of diabetic mouse hearts by glutaredoxin-1 gene therapy: role of Akt-FoxO-signaling network. *Gene Ther*, 17 (4): 478–485. doi:10.1038/gt.2010.9.

Leloup, C., Tourrel-Cuzin, C., Magnan, C., et al. (2009) Mitochondrial reactive oxygen species are obligatory signals for glucose-induced insulin secretion. *Diabetes*, 58 (3): 673–681. doi:10.2337/db07-1056.

Lenzen, S., Drinkgern, J. and Tiedge, M. (1996) Low antioxidant enzyme gene expression in pancreatic islets compared with various other mouse tissues. *Free Radical Biology & Medicine*, 20 (3): 463–466. doi:10.1016/0891-5849(96)02051-5.

Li, D., Jiang, C., Mei, G., et al. (2020) Quercetin Alleviates Ferroptosis of Pancreatic β Cells in Type 2 Diabetes. *Nutrients*, 12 (10): 2954. doi:10.3390/nu12102954.

Li, S., Sun, Y., Qi, X., et al. (2014) Protective effect and mechanism of glutaredoxin 1 on coronary arteries endothelial cells damage induced by high glucose. *Biomed Mater Eng*, 24 (6): 3897–903. doi:10.3233/bme-141221.

Lill, R., Dutkiewicz, R., Freibert, S.A., et al. (2015) The role of mitochondria and the CIA machinery in the maturation of cytosolic and nuclear iron-sulfur proteins. *European Journal of Cell Biology*, 94 (7–9): 280–291. doi:10.1016/j.ejcb.2015.05.002.

Lill, R. and Freibert, S.-A. (2020) Mechanisms of Mitochondrial Iron-Sulfur Protein Biogenesis. *Annu Rev Biochem*, 89: 471–499. doi:10.1146/annurev-biochem-013118-111540.

Lill, R., Hoffmann, B., Molik, S., et al. (2012) The role of mitochondria in cellular iron-sulfur protein biogenesis and iron metabolism. *Biochim Biophys Acta*, 1823 (9): 1491–1508. doi:10.1016/j.bbamcr.2012.05.009.

Lillig, C.H., Berndt, C. and Holmgren, A. (2008) Glutaredoxin systems. *Biochim Biophys Acta*, 1780 (11): 1304–1317. doi:10.1016/j.bbagen.2008.06.003.

Lillig, C.H., Berndt, C., Vergnolle, O., et al. (2005) Characterization of human glutaredoxin 2 as iron-sulfur protein: a possible role as redox sensor. *Proc Natl Acad Sci U S A*, 102 (23): 8168–8173. doi:10.1073/pnas.0500735102.

Lillig, C.H., Lönn, M.E., Enoksson, M., et al. (2004) Short interfering RNA-mediated silencing of glutaredoxin 2 increases the sensitivity of HeLa cells toward doxorubicin and phenylarsine oxide. *Proc Natl Acad Sci U S A*, 101 (36): 13227–13232. doi:10.1073/pnas.0401896101.

Lima, A.L., Illing, T., Schliemann, S., et al. (2017) Cutaneous Manifestations of Diabetes Mellitus: A Review. *American Journal of Clinical Dermatology*, 18 (4): 541–553. doi:10.1007/s40257-017-0275-z.

Linares, G.R., Xing, W., Govoni, K.E., et al. (2009) Glutaredoxin 5 regulates osteoblast apoptosis by protecting against oxidative stress. *Bone*, 44 (5): 795–804. doi:10.1016/j.bone.2009.01.003.

Ling, S., Zaccardi, F., Issa, E., et al. (2023) Inequalities in cancer mortality trends in people with type 2 diabetes: 20 year population-based study in England. *Diabetologia*, 66 (4): 657–673. doi:10.1007/s00125-022-05854-8.

Liu, G., Guo, S., Anderson, G.J., et al. (2014) Heterozygous missense mutations in the GLRX5 gene cause sideroblastic anemia in a Chinese patient. *Blood*, 124 (17): 2750–2751. doi:10.1182/blood-2014-08-598508.

Liu, L., Li, Y., Guan, C., et al. (2010) Free fatty acid metabolic profile and biomarkers of isolated post-challenge diabetes and type 2 diabetes mellitus based on GC-MS and multivariate statistical analysis. *Journal of Chromatography. B, Analytical Technologies in the Biomedical and Life Sciences*, 878 (28): 2817–2825. doi:10.1016/j.jchromb.2010.08.035.

Liu, W., Zhu, M., Liu, J., et al. (2024) Comparison of the effects of monounsaturated fatty acids and polyunsaturated fatty acids on the lipotoxicity of islets. *Frontiers in Endocrinology*, 15: 1368853. doi:10.3389/fendo.2024.1368853.

Liu, X., Zeng, X., Chen, X., et al. (2019) Oleic acid protects insulin-secreting INS-1E cells against palmitic acid-induced lipotoxicity along with an amelioration of ER stress. *Endocrine*, 64 (3): 512–524. doi:10.1007/s12020-019-01867-3.

Lönn, M.E., Hudemann, C., Berndt, C., et al. (2008) Expression pattern of human glutaredoxin 2 isoforms: identification and characterization of two testis/cancer cell-specific isoforms. *Antioxid Redox Signal*, 10 (3): 547–557. doi:10.1089/ars.2007.1821.

Love, K.M., Jahn, L.A., Hartline, L.M., et al. (2024) Impact of Free Fatty Acids on Vascular Insulin Responses Across the Arterial Tree: A Randomized Crossover Study. *The Journal of Clinical Endocrinology and Metabolism*, 109 (4): 1041–1050. doi:10.1210/clinem/dgad656.

Lowell, B.B. and Shulman, G.I. (2005) Mitochondrial dysfunction and type 2 diabetes. *Science (New York, N.Y.)*, 307 (5708): 384–387. doi:10.1126/science.1104343.

Lu, Y., Wang, Y., Ong, C.-N., et al. (2016) Metabolic signatures and risk of type 2 diabetes in a Chinese population: an untargeted metabolomics study using both LC-MS and GC-MS. *Diabetologia*, 59 (11): 2349–2359. doi:10.1007/s00125-016-4069-2.

Luc, K., Schramm-Luc, A., Guzik, T.J., et al. (2019) Oxidative stress and inflammatory markers in prediabetes and diabetes. *Journal of Physiology and Pharmacology: An Official Journal of the Polish Physiological Society*, 70 (6). doi:10.26402/jpp.2019.6.01.

Lundberg, M., Fernandes, A.P., Kumar, S., et al. (2004) Cellular and plasma levels of human glutaredoxin 1 and 2 detected by sensitive ELISA systems. *Biochem Biophys Res Commun*, 319 (3): 801–809. doi:10.1016/j.bbrc.2004.04.199.

Lundberg, M., Johansson, C., Chandra, J., et al. (2001) Cloning and expression of a novel human glutaredoxin (Grx2) with mitochondrial and nuclear isoforms. *J Biol Chem*, 276 (28): 26269–26275. doi:10.1074/jbc.M011605200.

Ly, L.D., Xu, S., Choi, S.-K., et al. (2017) Oxidative stress and calcium dysregulation by palmitate in type 2 diabetes. *Experimental & Molecular Medicine*, 49 (2): e291. doi:10.1038/emm.2016.157.

Ma, T., Du, J., Zhang, Y., et al. (2022) GPX4-independent ferroptosis—a new strategy in disease's therapy. *Cell Death Discovery*, 8 (1): 1–8. doi:10.1038/s41420-022-01212-0.

Maedler, K., Oberholzer, J., Bucher, P., et al. (2003) Monounsaturated fatty acids prevent the deleterious effects of palmitate and high glucose on human pancreatic beta-cell turnover and function. *Diabetes*, 52 (3): 726–733. doi:10.2337/diabetes.52.3.726.

Magtanong, L., Ko, P.-J., To, M., et al. (2019) Exogenous Monounsaturated Fatty Acids Promote a Ferroptosis-Resistant Cell State. *Cell Chemical Biology*, 26 (3): 420-432.e9. doi:10.1016/j.chembiol.2018.11.016.

Malmberg, K., Yusuf, S., Gerstein, H.C., et al. (2000) Impact of diabetes on long-term prognosis in patients with unstable angina and non-Q-wave myocardial infarction: results of the OASIS (Organization to Assess Strategies for Ischemic Syndromes) Registry. *Circulation*, 102 (9): 1014–1019. doi:10.1161/01.cir.102.9.1014.

Marku, A., Galli, A., Marciani, P., et al. (2021) Iron Metabolism in Pancreatic Beta-Cell Function and Dysfunction. *Cells*, 10 (11): 2841. doi:10.3390/cells10112841.

Martin, J.L. (1995) Thioredoxin--a fold for all reasons. *Structure*, 3 (3): 245–250. doi:10.1016/s0969-2126(01)00154-x.

Martín-Timón, I., Sevillano-Collantes, C., Segura-Galindo, A., et al. (2014) Type 2 diabetes and cardiovascular disease: Have all risk factors the same strength? *World Journal of Diabetes*, 5 (4): 444–470. doi:10.4239/wjd.v5.i4.444.

McAdams, B.H. and Rizvi, A.A. (2016) An Overview of Insulin Pumps and Glucose Sensors for the Generalist. *Journal of Clinical Medicine*, 5 (1): 5. doi:10.3390/jcm5010005.

McElduff, A. (2017) Iron: how much is too much? *Diabetologia*, 60 (2): 237–239. doi:10.1007/s00125-016-4176-0.

Mensah, G.A., Wei, G.S., Sorlie, P.D., et al. (2017) Decline in Cardiovascular Mortality: Possible Causes and Implications. *Circulation Research*, 120 (2): 366–380. doi:10.1161/CIRCRESAHA.116.309115.

Meurs, M., Roest, A.M., Wolffenbuttel, B.H.R., et al. (2016) Association of Depressive and Anxiety Disorders With Diagnosed Versus Undiagnosed Diabetes: An Epidemiological Study of 90,686 Participants. *Psychosomatic Medicine*, 78 (2): 233–241. doi:10.1097/PSY.0000000000000255.

Miotto, G., Rossetto, M., Di Paolo, M.L., et al. (2020) Insight into the mechanism of ferroptosis inhibition by ferrostatin-1. *Redox Biology*, 28: 101328. doi:10.1016/j.redox.2019.101328.

Mirhashemi, S.M. (2011) To determine the possible roles of two essential trace elements and ascorbic acid concerning amyloidal beta-sheet formation in diabetes mellitus. *Scientific Research and Essays*, 6. doi:10.5897/SRE11.718.

Miyazaki, J.-I., ARAKI, K., YAMATO, E., et al. (1990) Establishment of a Pancreatic β Cell Line That Retains Glucose-Inducible Insulin Secretion: Special Reference to Expression of Glucose Transporter Isoforms*. *Endocrinology*, 127 (1): 126–132. doi:10.1210/endo-127-1-126.

Moon, J.S. and Won, K.C. (2015) Pancreatic α-Cell Dysfunction in Type 2 Diabetes: Old Kids on the Block. *Diabetes & Metabolism Journal*, 39 (1): 1–9. doi:10.4093/dmj.2015.39.1.1.

Morgan, D., Oliveira-Emilio, H.R., Keane, D., et al. (2007) Glucose, palmitate and pro-inflammatory cytokines modulate production and activity of a phagocyte-like NADPH oxidase in rat pancreatic islets and a clonal beta cell line. *Diabetologia*, 50 (2): 359–369. doi:10.1007/s00125-006-0462-6.

Morgan, N.G. and Dhayal, S. (2009) G-protein coupled receptors mediating long chain fatty acid signalling in the pancreatic beta-cell. *Biochemical Pharmacology*, 78 (12): 1419–1427. doi:10.1016/j.bcp.2009.07.020.

Mosmann, T. (1983) Rapid colorimetric assay for cellular growth and survival: application to proliferation and cytotoxicity assays. *Journal of Immunological Methods*, 65 (1–2): 55–63. doi:10.1016/0022-1759(83)90303-4.

Mrugacz, M., Pony-Uram, M., Bryl, A., et al. (2023) Current Approach to the Pathogenesis of Diabetic Cataracts. *International Journal of Molecular Sciences*, 24 (7): 6317. doi:10.3390/ijms24076317.

Muckenthaler, M.U., Galy, B. and Hentze, M.W. (2008) Systemic iron homeostasis and the iron-responsive element/iron-regulatory protein (IRE/IRP) regulatory network. *Annual Review of Nutrition*, 28: 197–213. doi:10.1146/annurev.nutr.28.061807.155521.

Mühlenhoff, U., Braymer, J.J., Christ, S., et al. (2020) Glutaredoxins and iron-sulfur protein biogenesis at the interface of redox biology and iron metabolism. *Biol Chem*, 401 (12): 1407–1428. doi:10.1515/hsz-2020-0237.

Mukherjee, S. and Dey, S.G. (2013) Heme bound amylin: spectroscopic characterization, reactivity, and relevance to type 2 diabetes. *Inorganic Chemistry*, 52 (9): 5226–5235. doi:10.1021/ic4001413.

Murata, H., Ihara, Y., Nakamura, H., et al. (2003) Glutaredoxin exerts an antiapoptotic effect by regulating the redox state of Akt. *J Biol Chem*, 278 (50): 50226–50233. doi:10.1074/jbc.M310171200.

Mustafa Rizvi, S.H., Shao, D., Tsukahara, Y., et al. (2021) Oxidized GAPDH transfers S-glutathionylation to a nuclear protein Sirtuin-1 leading to apoptosis. *Free Radical Biology & Medicine*, 174: 73–83. doi:10.1016/j.freeradbiomed.2021.07.037.

Nasta, V., Giachetti, A., Ciofi-Baffoni, S., et al. (2017) Structural insights into the molecular function of human [2Fe-2S] BOLA1-GRX5 and [2Fe-2S] BOLA3-GRX5 complexes. *Biochim Biophys Acta Gen Subj*, 1861 (8): 2119–2131. doi:10.1016/j.bbagen.2017.05.005.

Navina, S., Acharya, C., DeLany, J.P., et al. (2011) Lipotoxicity causes multisystem organ failure and exacerbates acute pancreatitis in obesity. *Science Translational Medicine*, 3 (107): 107ra110. doi:10.1126/scitranslmed.3002573.

Nemecz, M., Constantin, A., Dumitrescu, M., et al. (2018) The Distinct Effects of Palmitic and Oleic Acid on Pancreatic Beta Cell Function: The Elucidation of Associated

Mechanisms and Effector Molecules. *Frontiers in Pharmacology*, 9: 1554. doi:10.3389/fphar.2018.01554.

Nichols, G.A., Reinier, K. and Chugh, S.S. (2009) Independent contribution of diabetes to increased prevalence and incidence of atrial fibrillation. *Diabetes Care*, 32 (10): 1851–1856. doi:10.2337/dc09-0939.

Ogata, F.T., Branco, V., Vale, F.F., et al. (2021) Glutaredoxin: Discovery, redox defense and much more. *Redox Biology*, 43: 101975. doi:10.1016/j.redox.2021.101975.

Oguntibeju, O.O. (2019) Type 2 diabetes mellitus, oxidative stress and inflammation: examining the links. *International Journal of Physiology, Pathophysiology and Pharmacology*, 11 (3): 45–63.

Oh, Y.S., Bae, G.D., Baek, D.J., et al. (2018) Fatty Acid-Induced Lipotoxicity in Pancreatic Beta-Cells During Development of Type 2 Diabetes. *Frontiers in Endocrinology*, 9: 384. doi:10.3389/fendo.2018.00384.

Ohayon, A., Babichev, Y., Pasvolsky, R., et al. (2010) Hodgkin's lymphoma cells exhibit high expression levels of the PICOT protein. *Journal of Immunotoxicology*, 7 (1): 8–14. doi:10.3109/15476910903427654.

de Oliveira, C., Khatua, B., Noel, P., et al. (2020) Pancreatic triglyceride lipase mediates lipotoxic systemic inflammation. *The Journal of Clinical Investigation*, 130 (4): 1931–1947. doi:10.1172/JCI132767.

Orci, L., Halban, P., Amherdt, M., et al. (1984) Nonconverted, amino acid analog-modified proinsulin stays in a Golgi-derived clathrin-coated membrane compartment. *The Journal of Cell Biology*, 99 (6): 2187–2192. doi:10.1083/jcb.99.6.2187.

Orci, L., Ravazzola, M., Amherdt, M., et al. (1986) Conversion of proinsulin to insulin occurs coordinately with acidification of maturing secretory vesicles. *The Journal of Cell Biology*, 103 (6 Pt 1): 2273–2281. doi:10.1083/jcb.103.6.2273.

Oshima, M., Pechberty, S., Bellini, L., et al. (2020) Stearoyl CoA desaturase is a gatekeeper that protects human beta cells against lipotoxicity and maintains their identity. *Diabetologia*, 63 (2): 395–409. doi:10.1007/s00125-019-05046-x.

Padgett, L.E., Broniowska, K.A., Hansen, P.A., et al. (2013) The role of reactive oxygen species and proinflammatory cytokines in type 1 diabetes pathogenesis. *Annals of the New York Academy of Sciences*, 1281 (1): 16–35. doi:10.1111/j.1749-6632.2012.06826.x.

Padhi, S., Nayak, A.K. and Behera, A. (2020) Type II diabetes mellitus: a review on recent drug based therapeutics. *Biomedicine & Pharmacotherapy = Biomedecine & Pharmacotherapie*, 131: 110708. doi:10.1016/j.biopha.2020.110708.

Pai, H.V., Starke, D.W., Lesnefsky, E.J., et al. (2007) What is the functional significance of the unique location of glutaredoxin 1 (GRx1) in the intermembrane space of mitochondria? *Antioxid Redox Signal*, 9 (11): 2027–2033. doi:10.1089/ars.2007.1642.

Palmer, J.P., Asplin, C.M., Clemons, P., et al. (1983) Insulin antibodies in insulin-dependent diabetics before insulin treatment. *Science (New York, N.Y.)*, 222 (4630): 1337–1339. doi:10.1126/science.6362005.

Pandol, S.J. (2010) *The Exocrine Pancreas*. Colloquium Series on Integrated Systems Physiology: From Molecule to Function to Disease. San Rafael (CA): Morgan & Claypool Life Sciences. Available at: http://www.ncbi.nlm.nih.gov/books/NBK54128/ (Downloaded: 16 July 2024).

Pandya, P., Braiman, A. and Isakov, N. (2019) PICOT (GLRX3) is a positive regulator of stress-induced DNA-damage response. *Cell Signal*, 62: 109340. doi:10.1016/j.cellsig.2019.06.005.

Paolisso, G., Gambardella, A., Amato, L., et al. (1995) Opposite effects of short- and long-term fatty acid infusion on insulin secretion in healthy subjects. *Diabetologia*, 38 (11): 1295–1299. doi:10.1007/BF00401761.

Papa, F.R. (2012) Endoplasmic reticulum stress, pancreatic β-cell degeneration, and diabetes. *Cold Spring Harbor Perspectives in Medicine*, 2 (9): a007666. doi:10.1101/cshperspect.a007666.

Pasquel, F.J. and Umpierrez, G.E. (2014) Hyperosmolar hyperglycemic state: a historic review of the clinical presentation, diagnosis, and treatment. *Diabetes Care*, 37 (11): 3124–3131. doi:10.2337/dc14-0984.

Paul, B.T., Manz, D.H., Torti, F.M., et al. (2017) Mitochondria and Iron: Current Questions. *Expert review of hematology*, 10 (1): 65–79. doi:10.1080/17474086.2016.1268047.

Pepino, M.Y., Kuda, O., Samovski, D., et al. (2014) Structure-function of CD36 and importance of fatty acid signal transduction in fat metabolism. *Annual Review of Nutrition*, 34: 281–303. doi:10.1146/annurev-nutr-071812-161220.

Petry, S.F., Römer, A., Rawat, D., et al. (2022) Loss and Recovery of Glutaredoxin 5 Is Inducible by Diet in a Murine Model of Diabesity and Mediated by Free Fatty Acids In Vitro. *Antioxidants (Basel, Switzerland)*, 11 (4): 788. doi:10.3390/antiox11040788.

Petry, S.F., Sharifpanah, F., Sauer, H., et al. (2017) Differential expression of islet glutaredoxin 1 and 5 with high reactive oxygen species production in a mouse model of diabesity. *PLoS One*, 12 (5): e0176267. doi:10.1371/journal.pone.0176267.

Petry, S.F., Sun, L.M., Knapp, A., et al. (2018) Distinct Shift in Beta-Cell Glutaredoxin 5 Expression Is Mediated by Hypoxia and Lipotoxicity Both In Vivo and In Vitro. *Front Endocrinol (Lausanne)*, 9: 84. doi:10.3389/fendo.2018.00084.

Pham, K., Pal, R., Qu, Y., et al. (2015) Nuclear glutaredoxin 3 is critical for protection against oxidative stress-induced cell death. *Free Radic Biol Med*, 85: 197–206. doi:10.1016/j.freeradbiomed.2015.05.003.

Pietropaolo, M., Becker, D.J., LaPorte, R.E., et al. (2002) Progression to insulin-requiring diabetes in seronegative prediabetic subjects: the role of two HLA-DQ high-risk haplotypes. *Diabetologia*, 45 (1): 66–76. doi:10.1007/s125-002-8246-5.

Plötz, T., von Hanstein, A.S., Krümmel, B., et al. (2019) Structure-toxicity relationships of saturated and unsaturated free fatty acids for elucidating the lipotoxic effects in human EndoC-βH1 beta-cells. *Biochimica Et Biophysica Acta. Molecular Basis of Disease*, 1865 (11): 165525. doi:10.1016/j.bbadis.2019.08.001.

Plötz, T., Krümmel, B., Laporte, A., et al. (2017) The monounsaturated fatty acid oleate is the major physiological toxic free fatty acid for human beta cells. *Nutrition & Diabetes*, 7 (12): 305. doi:10.1038/s41387-017-0005-x.

Plötz, T. and Lenzen, S. (2024) Mechanisms of lipotoxicity-induced dysfunction and death of human pancreatic beta cells under obesity and type 2 diabetes conditions. *Obesity Reviews: An Official Journal of the International Association for the Study of Obesity*, 25 (5): e13703. doi:10.1111/obr.13703.

Poitout, V. and Robertson, R.P. (2002) Minireview: Secondary beta-cell failure in type 2 diabetes--a convergence of glucotoxicity and lipotoxicity. *Endocrinology*, 143 (2): 339–342. doi:10.1210/endo.143.2.8623.

Ponka, P. (1997) Tissue-specific regulation of iron metabolism and heme synthesis: distinct control mechanisms in erythroid cells. *Blood*, 89 (1): 1–25.

PrayGod, G., Filteau, S., Range, N., et al. (2021) β-cell dysfunction and insulin resistance in relation to pre-diabetes and diabetes among adults in north-western Tanzania: a cross-sectional study. *Tropical medicine & international health: TM & IH*, 26 (4): 435–443. doi:10.1111/tmi.13545.

Prentki, M. and Corkey, B.E. (1996) Are the beta-cell signaling molecules malonyl-CoA and cystolic long-chain acyl-CoA implicated in multiple tissue defects of obesity and NIDDM? *Diabetes*, 45 (3): 273–283. doi:10.2337/diab.45.3.273.

Prentki, M., Joly, E., El-Assaad, W., et al. (2002) Malonyl-CoA signaling, lipid partitioning, and glucolipotoxicity: role in beta-cell adaptation and failure in the etiology of diabetes. *Diabetes*, 51 Suppl 3: S405-413. doi:10.2337/diabetes.51.2007.s405.

Pugliese, L.A., De Lorenzi, V., Bernardi, M., et al. (2023) Unveiling nanoscale optical signatures of cytokine-induced β-cell dysfunction. *Scientific Reports*, 13 (1): 13342. doi:10.1038/s41598-023-40272-9.

Qi, X., Xu, A., Gao, Y., et al. (2016) Cardiac damage and dysfunction in diabetic cardiomyopathy are ameliorated by Grx1. *Genet Mol Res*, 15 (3). doi:10.4238/gmr.15039000.

Qu, Y., Wang, J., Ray, P.S., et al. (2011) Thioredoxin-like 2 regulates human cancer cell growth and metastasis via redox homeostasis and NF-κB signaling. *The Journal of Clinical Investigation*, 121 (1): 212–225. doi:10.1172/JCI43144.

Quehenberger, O., Armando, A.M., Brown, A.H., et al. (2010) Lipidomics reveals a remarkable diversity of lipids in human plasma. *Journal of Lipid Research*, 51 (11): 3299–3305. doi:10.1194/jlr.M009449.

Rajpathak, S.N., Crandall, J.P., Wylie-Rosett, J., et al. (2009) The role of iron in type 2 diabetes in humans. *Biochimica Et Biophysica Acta*, 1790 (7): 671–681. doi:10.1016/j.bbagen.2008.04.005.

Ramlo-Halsted, B.A. and Edelman, S.V. (1999) The natural history of type 2 diabetes. Implications for clinical practice. *Primary Care*, 26 (4): 771–789. doi:10.1016/s0095-4543(05)70130-5.

Rauen, U., Springer, A., Weisheit, D., et al. (2007) Assessment of chelatable mitochondrial iron by using mitochondrion-selective fluorescent iron indicators with different iron-binding affinities. *Chembiochem: A European Journal of Chemical Biology*, 8 (3): 341–352. doi:10.1002/cbic.200600311.

Ravassard, P., Hazhouz, Y., Pechberty, S., et al. (2011) A genetically engineered human pancreatic β cell line exhibiting glucose-inducible insulin secretion. *The Journal of Clinical Investigation*, 121 (9): 3589–3597. doi:10.1172/JCI58447.

Rawal, S., Hinkle, S.N., Bao, W., et al. (2017) A longitudinal study of iron status during pregnancy and the risk of gestational diabetes: findings from a prospective, multiracial cohort. *Diabetologia*, 60 (2): 249–257. doi:10.1007/s00125-016-4149-3.

Redondo, M.J., Yu, L., Hawa, M., et al. (2001) Heterogeneity of type I diabetes: analysis of monozygotic twins in Great Britain and the United States. *Diabetologia*, 44 (3): 354–362. doi:10.1007/s001250051626.

Rewers, M. and Ludvigsson, J. (2016) Environmental risk factors for type 1 diabetes. *Lancet (London, England)*, 387 (10035): 2340–2348. doi:10.1016/S0140-6736(16)30507-4.

Reynaert, N.L., van der Vliet, A., Guala, A.S., et al. (2006) Dynamic redox control of NF-kappaB through glutaredoxin-regulated S-glutathionylation of inhibitory kappaB kinase beta. *Proc Natl Acad Sci U S A*, 103 (35): 13086–13091. doi:10.1073/pnas.0603290103.

Rhodes, C.J. and Halban, P.A. (1987) Newly synthesized proinsulin/insulin and stored insulin are released from pancreatic B cells predominantly via a regulated, rather than

a constitutive, pathway. *The Journal of Cell Biology*, 105 (1): 145–153. doi:10.1083/jcb.105.1.145.

Riancho, J.A., Vázquez, L., García-Pérez, M.A., et al. (2011) Association of ACACB polymorphisms with obesity and diabetes. *Molecular Genetics and Metabolism*, 104 (4): 670–676. doi:10.1016/j.ymgme.2011.08.013.

Ricordi, C. and Strom, T.B. (2004) Clinical islet transplantation: advances and immunological challenges. *Nature Reviews. Immunology*, 4 (4): 259–268. doi:10.1038/nri1332.

Riegman, M., Sagie, L., Galed, C., et al. (2020) Ferroptosis occurs through an osmotic mechanism and propagates independently of cell rupture. *Nature Cell Biology*, 22 (9): 1042–1048. doi:10.1038/s41556-020-0565-1.

Robertson, R.P., Harmon, J., Tran, P.O., et al. (2003) Glucose toxicity in beta-cells: type 2 diabetes, good radicals gone bad, and the glutathione connection. *Diabetes*, 52 (3): 581–587. doi:10.2337/diabetes.52.3.581.

Rodríguez-Manzaneque, M.T., Ros, J., Cabiscol, E., et al. (1999) Grx5 glutaredoxin plays a central role in protection against protein oxidative damage in Saccharomyces cerevisiae. *Molecular and Cellular Biology*, 19 (12): 8180–8190. doi:10.1128/MCB.19.12.8180.

Rodríguez-Manzaneque, M.T., Tamarit, J., Bellí, G., et al. (2002) Grx5 is a mitochondrial glutaredoxin required for the activity of iron/sulfur enzymes. *Molecular Biology of the Cell*, 13 (4): 1109–1121. doi:10.1091/mbc.01-10-0517.

Roma, L.P. and Jonas, J.-C. (2020) Nutrient Metabolism, Subcellular Redox State, and Oxidative Stress in Pancreatic Islets and β-Cells. *Journal of Molecular Biology*, 432 (5): 1461–1493. doi:10.1016/j.jmb.2019.10.012.

Römer, A., Linn, T. and Petry, S.F. (2021) Lipotoxic Impairment of Mitochondrial Function in β-Cells: A Review. *Antioxidants (Basel, Switzerland)*, 10 (2): 293. doi:10.3390/antiox10020293.

Römer, A., Rawat, D., Linn, T., et al. (2022) Preparation of fatty acid solutions exerts significant impact on experimental outcomes in cell culture models of lipotoxicity. *Biology Methods & Protocols*, 7 (1): bpab023. doi:10.1093/biomethods/bpab023.

Rouault, T.A. (2006) The role of iron regulatory proteins in mammalian iron homeostasis and disease. *Nature Chemical Biology*, 2 (8): 406–414. doi:10.1038/nchembio807.

Rouault, T.A. (2012) Biogenesis of iron-sulfur clusters in mammalian cells: new insights and relevance to human disease. *Disease Models & Mechanisms*, 5 (2): 155–164. doi:10.1242/dmm.009019.

Rutter, G.A. (2001) Nutrient-secretion coupling in the pancreatic islet beta-cell: recent advances. *Molecular Aspects of Medicine*, 22 (6): 247–284. doi:10.1016/s0098-2997(01)00013-9.

Sankaran, B.P., Gupta, S., Tchan, M., et al. (2021) GLRX5-associated [Fe-S] cluster biogenesis disorder: further characterisation of the neurological phenotype and long-term outcome. *Orphanet J Rare Dis*, 16 (1): 465. doi:10.1186/s13023-021-02073-z.

Santos, M.C.F.D., Anderson, C.P., Neschen, S., et al. (2020) Irp2 regulates insulin production through iron-mediated Cdkal1-catalyzed tRNA modification. *Nat Commun*, 11 (1): 296. doi:10.1038/s41467-019-14004-5.

Sargsyan, E. and Bergsten, P. (2011) Lipotoxicity is glucose-dependent in INS-1E cells but not in human islets and MIN6 cells. *Lipids in Health and Disease*, 10: 115. doi:10.1186/1476-511X-10-115.

Scalcon, V., Folda, A., Lupo, M.G., et al. (2022) Mitochondrial depletion of glutaredoxin 2 induces metabolic dysfunction-associated fatty liver disease in mice. *Redox Biol*, 51: 102277. doi:10.1016/j.redox.2022.102277.

Scharfmann, R., Pechberty, S., Hazhouz, Y., et al. (2014) Development of a conditionally immortalized human pancreatic β cell line. *The Journal of Clinical Investigation*, 124 (5): 2087–2098. doi:10.1172/JCI72674.

Schaur, R.J., Siems, W., Bresgen, N., et al. (2015) 4-Hydroxy-nonenal-A Bioactive Lipid Peroxidation Product. *Biomolecules*, 5 (4): 2247–2337. doi:10.3390/biom5042247.

Schönfeld, P. and Wojtczak, L. (2007) Fatty acids decrease mitochondrial generation of reactive oxygen species at the reverse electron transport but increase it at the forward transport. *Biochimica Et Biophysica Acta*, 1767 (8): 1032–1040. doi:10.1016/j.bbabio.2007.04.005.

Seal, M., Mukherjee, S. and Dey, S.G. (2016) Fe-oxy adducts of heme-Aβ and heme-hIAPP complexes: intermediates in ROS generation. *Metallomics: Integrated Biometal Science*, 8 (12): 1266–1272. doi:10.1039/c6mt00214e.

Sehgal, P., Szalai, P., Olesen, C., et al. (2017) Inhibition of the sarco/endoplasmic reticulum (ER) Ca2+-ATPase by thapsigargin analogs induces cell death via ER Ca2+ depletion and the unfolded protein response. *The Journal of Biological Chemistry*, 292 (48): 19656–19673. doi:10.1074/jbc.M117.796920.

Sen, S., Rao, B., Wachnowsky, C., et al. (2018) Cluster exchange reactivity of [2Fe-2S] cluster-bridged complexes of BOLA3 with monothiol glutaredoxins. *Metallomics : Integrated Biometal Science*, 10 (9): 1282–1290. doi:10.1039/c8mt00128f.

Sergeant, S., Ruczinski, I., Ivester, P., et al. (2016) Impact of methods used to express levels of circulating fatty acids on the degree and direction of associations with blood

lipids in humans. *The British Journal of Nutrition*, 115 (2): 251–261. doi:10.1017/S0007114515004341.

Shabalala, S.C., Johnson, R., Basson, A.K., et al. (2022) Detrimental Effects of Lipid Peroxidation in Type 2 Diabetes: Exploring the Neutralizing Influence of Antioxidants. *Antioxidants (Basel, Switzerland)*, 11 (10): 2071. doi:10.3390/antiox11102071.

Sharma, R.B. and Alonso, L.C. (2014) Lipotoxicity in the Pancreatic Beta Cell: Not Just Survival and Function, but Proliferation as Well? *Current diabetes reports*, 14 (6): 492. doi:10.1007/s11892-014-0492-2.

Sheftel, A.D., Zhang, A.-S., Brown, C., et al. (2007) Direct interorganellar transfer of iron from endosome to mitochondrion. *Blood*, 110 (1): 125–132. doi:10.1182/blood-2007-01-068148.

Shirasuga, N., Hayashi, K. and Awai, M. (1989) Pancreatic islets after repeated injection of Fe3+-NTA. An ultrastructural study of diabetic rats. *Acta Pathologica Japonica*, 39 (3): 159–168. doi:10.1111/j.1440-1827.1989.tb01495.x.

Shiri, H., Fallah, H., Abolhassani, M., et al. (2024) Relationship between types and levels of free fatty acids, peripheral insulin resistance, and oxidative stress in T2DM: A case-control study. *PloS One*, 19 (8): e0306977. doi:10.1371/journal.pone.0306977.

Sies, H. (1985) "Oxidative Stress: Introductory Remarks." In Sies, H. (ed.) *Oxidative Stress*. London: Academic Press. pp. 1–8. doi:10.1016/B978-0-12-642760-8.50005-3.

Sies, H. (2015) Oxidative stress: a concept in redox biology and medicine. *Redox Biol*, 4: 180–183. doi:10.1016/j.redox.2015.01.002.

Sies, H., Berndt, C. and Jones, D.P. (2017) Oxidative Stress. *Annual Review of Biochemistry*, 86: 715–748. doi:10.1146/annurev-biochem-061516-045037.

Sies, H. and Jones, D.P. (2020) Reactive oxygen species (ROS) as pleiotropic physiological signalling agents. *Nature Reviews. Molecular Cell Biology*, 21 (7): 363–383. doi:10.1038/s41580-020-0230-3.

Singh, G. and Chawla, S. (2006) Amputation in Diabetic Patients. *Medical Journal, Armed Forces India*, 62 (1): 36–39. doi:10.1016/S0377-1237(06)80151-6.

Song, M. (2021) Cancer overtakes vascular disease as leading cause of excess death associated with diabetes. *The Lancet. Diabetes & Endocrinology*, 9 (3): 131–133. doi:10.1016/S2213-8587(21)00016-4.

Stancic, A., Saksida, T., Markelic, M., et al. (2022) Ferroptosis as a Novel Determinant of β-Cell Death in Diabetic Conditions. *Oxidative Medicine and Cellular Longevity*, 2022: 3873420. doi:10.1155/2022/3873420.

Stehling, O. and Lill, R. (2013) The role of mitochondria in cellular iron-sulfur protein biogenesis: mechanisms, connected processes, and diseases. *Cold Spring Harbor Perspectives in Biology*, 5 (8): a011312. doi:10.1101/cshperspect.a011312.

Steiner, D.J., Kim, A., Miller, K., et al. (2010) Pancreatic islet plasticity: interspecies comparison of islet architecture and composition. *Islets*, 2 (3): 135–145. doi:10.4161/isl.2.3.11815.

Storgaard, H., Jensen, C.B., Vaag, A.A., et al. (2003) Insulin secretion after short- and long-term low-grade free fatty acid infusion in men with increased risk of developing type 2 diabetes. *Metabolism: Clinical and Experimental*, 52 (7): 885–894. doi:10.1016/s0026-0495(03)00102-1.

Straub, S.G. and Sharp, G.W.G. (2002) Glucose-stimulated signaling pathways in biphasic insulin secretion. *Diabetes/Metabolism Research and Reviews*, 18 (6): 451–463. doi:10.1002/dmrr.329.

Stumvoll, M., Goldstein, B.J. and van Haeften, T.W. (2005) Type 2 diabetes: principles of pathogenesis and therapy. *Lancet (London, England)*, 365 (9467): 1333–1346. doi:10.1016/S0140-6736(05)61032-X.

Sun, C., Wu, Q.-J., Gao, S.-Y., et al. (2020) Association between the ferritin level and risk of gestational diabetes mellitus: A meta-analysis of observational studies. *Journal of Diabetes Investigation*, 11 (3): 707–718. doi:10.1111/jdi.13170.

Sun, H., Saeedi, P., Karuranga, S., et al. (2022) IDF Diabetes Atlas: Global, regional and country-level diabetes prevalence estimates for 2021 and projections for 2045. *Diabetes Res Clin Pract*, 183: 109119. doi:10.1016/j.diabres.2021.109119.

Sun, J., Cui, J., He, Q., et al. (2015) Proinsulin misfolding and endoplasmic reticulum stress during the development and progression of diabetes. *Molecular Aspects of Medicine*, 42: 105–118. doi:10.1016/j.mam.2015.01.001.

Sun, W., Wu, Y., Gao, M., et al. (2019) C-reactive protein promotes inflammation through TLR4/NF-κB/TGF-β pathway in HL-1 cells. *Bioscience Reports*, 39 (8): BSR20190888. doi:10.1042/BSR20190888.

Tanaka, Y., Tran, P.O.T., Harmon, J., et al. (2002) A role for glutathione peroxidase in protecting pancreatic beta cells against oxidative stress in a model of glucose toxicity. *Proceedings of the National Academy of Sciences of the United States of America*, 99 (19): 12363–12368. doi:10.1073/pnas.192445199.

Tang, Y., Shi, Y. and Fan, Z. (2023) The mechanism and therapeutic strategies for neovascular glaucoma secondary to diabetic retinopathy. *Frontiers in Endocrinology*, 14: 1102361. doi:10.3389/fendo.2023.1102361.

Thorens, B. (1992) Molecular and cellular physiology of GLUT-2, a high-Km facilitated diffusion glucose transporter. *International Review of Cytology*, 137: 209–238. doi:10.1016/s0074-7696(08)62677-7.

Thörn, K., Hovsepyan, M. and Bergsten, P. (2010) Reduced levels of SCD1 accentuate palmitate-induced stress in insulin-producing β-cells. *Lipids in Health and Disease*, 9: 108. doi:10.1186/1476-511X-9-108.

Trnka, D., Engelke, A.D., Gellert, M., et al. (2020) Molecular basis for the distinct functions of redox-active and FeS-transfering glutaredoxins. *Nature Communications*, 11 (1): 3445. doi:10.1038/s41467-020-17323-0.

Tsonkova, V.G., Sand, F.W., Wolf, X.A., et al. (2018) The EndoC-βH1 cell line is a valid model of human beta cells and applicable for screenings to identify novel drug target candidates. *Molecular Metabolism*, 8: 144–157. doi:10.1016/j.molmet.2017.12.007.

Tuei, V.C., Ha, J.-S. and Ha, C.-E. (2011) Effects of human serum albumin complexed with free fatty acids on cell viability and insulin secretion in the hamster pancreatic β-cell line HIT-T15. *Life Sciences*, 88 (17–18): 810–818. doi:10.1016/j.lfs.2011.02.022.

Turk, H.M., Sevinc, A., Camci, C., et al. (2002) Plasma lipid peroxidation products and antioxidant enzyme activities in patients with type 2 diabetes mellitus. *Acta Diabetologica*, 39 (3): 117–122. doi:10.1007/s005920200029.

Umpierrez, G. and Korytkowski, M. (2016) Diabetic emergencies - ketoacidosis, hyperglycaemic hyperosmolar state and hypoglycaemia. *Nature Reviews. Endocrinology*, 12 (4): 222–232. doi:10.1038/nrendo.2016.15.

Undlien, D.E., Lie, B.A. and Thorsby, E. (2001) HLA complex genes in type 1 diabetes and other autoimmune diseases. Which genes are involved? *Trends in genetics: TIG*, 17 (2): 93–100. doi:10.1016/s0168-9525(00)02180-6.

Verge, C.F., Gianani, R., Yu, L., et al. (1995) Late progression to diabetes and evidence for chronic beta-cell autoimmunity in identical twins of patients with type I diabetes. *Diabetes*, 44 (10): 1176–1179. doi:10.2337/diab.44.10.1176.

Vijan, S. (2010) In the clinic. Type 2 diabetes. *Annals of Internal Medicine*, 152 (5): ITC31-15; quiz ITC316. doi:10.7326/0003-4819-152-5-201003020-01003.

Vinik, A.I., Maser, R.E., Mitchell, B.D., et al. (2003) Diabetic autonomic neuropathy. *Diabetes Care*, 26 (5): 1553–1579. doi:10.2337/diacare.26.5.1553.

Volmer-Thole, M. and Lobmann, R. (2016) Neuropathy and Diabetic Foot Syndrome. *International Journal of Molecular Sciences*, 17 (6): 917. doi:10.3390/ijms17060917.

Wagner, B.K. (2022) Small-molecule discovery in the pancreatic beta cell. *Current opinion in chemical biology*, 68: 102150. doi:10.1016/j.cbpa.2022.102150.

Walter, P. and Ron, D. (2011) The unfolded protein response: from stress pathway to homeostatic regulation. *Science (New York, N.Y.)*, 334 (6059): 1081–1086. doi:10.1126/science.1209038.

Wang, H., Zhang, H., Chen, Y., et al. (2022) Targeting Wnt/β-Catenin Signaling Exacerbates Ferroptosis and Increases the Efficacy of Melanoma Immunotherapy via the Regulation of MITF. *Cells*, 11 (22): 3580. doi:10.3390/cells11223580.

Wang, Y., Liu, S., Ying, L., et al. (2024) Nicotinamide Mononucleotide (NMN) Ameliorates Free Fatty Acid-Induced Pancreatic β-Cell Dysfunction via the NAD+/AMPK/SIRT1/HIF-1α Pathway. *International Journal of Molecular Sciences*, 25 (19): 10534. doi:10.3390/ijms251910534.

Wei, F.-Y., Suzuki, T., Watanabe, S., et al. (2011) Deficit of tRNA(Lys) modification by Cdkal1 causes the development of type 2 diabetes in mice. *The Journal of Clinical Investigation*, 121 (9): 3598–3608. doi:10.1172/JCI58056.

Weir, G.C. and Bonner-Weir, S. (2011) Finally! A human pancreatic β cell line. *The Journal of Clinical Investigation*, 121 (9): 3395–3397. doi:10.1172/JCI58899.

Welters, H.J., Diakogiannaki, E., Mordue, J.M., et al. (2006) Differential protective effects of palmitoleic acid and cAMP on caspase activation and cell viability in pancreatic beta-cells exposed to palmitate. *Apoptosis: An International Journal on Programmed Cell Death*, 11 (7): 1231–1238. doi:10.1007/s10495-006-7450-7.

Welters, H.J., Tadayyon, M., Scarpello, J.H.B., et al. (2004) Mono-unsaturated fatty acids protect against beta-cell apoptosis induced by saturated fatty acids, serum withdrawal or cytokine exposure. *FEBS letters*, 560 (1–3): 103–108. doi:10.1016/S0014-5793(04)00079-1.

Wenzlau, J.M., Juhl, K., Yu, L., et al. (2007) The cation efflux transporter ZnT8 (Slc30A8) is a major autoantigen in human type 1 diabetes. *Proceedings of the National Academy of Sciences of the United States of America*, 104 (43): 17040–17045. doi:10.1073/pnas.0705894104.

Whiting, D.R., Guariguata, L., Weil, C., et al. (2011) IDF diabetes atlas: global estimates of the prevalence of diabetes for 2011 and 2030. *Diabetes Research and Clinical Practice*, 94 (3): 311–321. doi:10.1016/j.diabres.2011.10.029.

Wingert, R.A., Galloway, J.L., Barut, B., et al. (2005) Deficiency of glutaredoxin 5 reveals Fe-S clusters are required for vertebrate haem synthesis. *Nature*, 436 (7053): 1035–1039. doi:10.1038/nature03887.

Witte, S., Villalba, M., Bi, K., et al. (2000) Inhibition of the c-Jun N-terminal kinase/AP-1 and NF-kappaB pathways by PICOT, a novel protein kinase C-interacting protein with a thioredoxin homology domain. *J Biol Chem*, 275 (3): 1902–1909. doi:10.1074/jbc.275.3.1902.

Wohua, Z. and Weiming, X. (2019) Glutaredoxin 2 (GRX2) deficiency exacerbates high fat diet (HFD)-induced insulin resistance, inflammation and mitochondrial dysfunction in brain injury: A mechanism involving GSK-3β. *Biomed Pharmacother*, 118: 108940. doi:10.1016/j.biopha.2019.108940.

Wong-Ekkabut, J., Xu, Z., Triampo, W., et al. (2007) Effect of lipid peroxidation on the properties of lipid bilayers: a molecular dynamics study. *Biophysical Journal*, 93 (12): 4225–4236. doi:10.1529/biophysj.107.112565.

World Health Organization (2019) *Classification of diabetes mellitus*. Geneva: World Health Organization. Available at: https://iris.who.int/handle/10665/325182 (Downloaded: 23 August 2024).

Wu, H., Yu, Y., David, L., et al. (2014) Glutaredoxin 2 (Grx2) gene deletion induces early onset of age-dependent cataracts in mice. *J Biol Chem*, 289 (52): 36125–36139. doi:10.1074/jbc.M114.620047.

Wu, Y., Wu, T., Wu, J., et al. (2013) Chronic inflammation exacerbates glucose metabolism disorders in C57BL/6J mice fed with high-fat diet. *The Journal of Endocrinology*, 219 (3): 195–204. doi:10.1530/JOE-13-0160.

Yang, W.S., Kim, K.J., Gaschler, M.M., et al. (2016) Peroxidation of polyunsaturated fatty acids by lipoxygenases drives ferroptosis. *Proceedings of the National Academy of Sciences of the United States of America*, 113 (34): E4966-4975. doi:10.1073/pnas.1603244113.

Yang, W.S., SriRamaratnam, R., Welsch, M.E., et al. (2014) Regulation of ferroptotic cancer cell death by GPX4. *Cell*, 156 (1–2): 317–331. doi:10.1016/j.cell.2013.12.010.

Yang, W.S. and Stockwell, B.R. (2008) Synthetic lethal screening identifies compounds activating iron-dependent, nonapoptotic cell death in oncogenic-RAS-harboring cancer cells. *Chemistry & Biology*, 15 (3): 234–245. doi:10.1016/j.chembiol.2008.02.010.

Yaribeygi, H., Sathyapalan, T., Atkin, S.L., et al. (2020) Molecular Mechanisms Linking Oxidative Stress and Diabetes Mellitus. *Oxidative Medicine and Cellular Longevity*, 2020: 8609213. doi:10.1155/2020/8609213.

Ye, H., Jeong, S.Y., Ghosh, M.C., et al. (2010) Glutaredoxin 5 deficiency causes sideroblastic anemia by specifically impairing heme biosynthesis and depleting cytosolic iron in human erythroblasts. *The Journal of Clinical Investigation*, 120 (5): 1749–1761. doi:10.1172/JCI40372.

Yi, L., He, J., Liang, Y., et al. (2007) Simultaneously quantitative measurement of comprehensive profiles of esterified and non-esterified fatty acid in plasma of type 2 diabetic patients. *Chemistry and Physics of Lipids*, 150 (2): 204–216. doi:10.1016/j.chemphyslip.2007.08.002.

Yi, X., Cai, X., Wang, S., et al. (2020) Mechanisms of impaired pancreatic β-cell function in high-fat diet-induced obese mice: The role of endoplasmic reticulum stress. *Molecular Medicine Reports*, 21 (5): 2041–2050. doi:10.3892/mmr.2020.11013.

Yin, H., Xu, L. and Porter, N.A. (2011) Free radical lipid peroxidation: mechanisms and analysis. *Chemical Reviews*, 111 (10): 5944–5972. doi:10.1021/cr200084z.

Zhang, L., Shen, Z.-Y., Wang, K., et al. (2019) C-reactive protein exacerbates epithelial-mesenchymal transition through Wnt/β-catenin and ERK signaling in streptozocin-induced diabetic nephropathy. *FASEB journal: official publication of the Federation of American Societies for Experimental Biology*, 33 (5): 6551–6563. doi:10.1096/fj.201801865RR.

Zhou, H., Zhang, X. and Lu, J. (2014) Progress on diabetic cerebrovascular diseases. *Bosnian Journal of Basic Medical Sciences*, 14 (4): 185–190. doi:10.17305/bjbms.2014.4.203.

Zhou, M., Hanschmann, E.-M., Römer, A., et al. (2024a) The significance of glutaredoxins for diabetes mellitus and its complications. *Redox Biology*, 71: 103043. doi:10.1016/j.redox.2024.103043.

Zhou, M., Linn, T. and Petry, S.F. (2024b) EndoC-βH3 pseudoislets are suitable for intraportal transplantation in diabetic mice. *Islets*, 16 (1): 2406041. doi:10.1080/19382014.2024.2406041.

Zhou, Y.P. and Grill, V.E. (1994) Long-term exposure of rat pancreatic islets to fatty acids inhibits glucose-induced insulin secretion and biosynthesis through a glucose fatty acid cycle. *The Journal of Clinical Investigation*, 93 (2): 870–876. doi:10.1172/JCI117042.

Zilliox, L.A., Chadrasekaran, K., Kwan, J.Y., et al. (2016) Diabetes and Cognitive Impairment. *Current Diabetes Reports*, 16 (9): 87. doi:10.1007/s11892-016-0775-x.

8 Publications

Zhou M, Linn T, Petry SF. EndoC-βH3 pseudoislets are suitable for intraportal transplantation in diabetic mice. Islets. 2024 Dec 31;16(1):2406041.

Zhou M, Hanschmann EM, Römer A, Linn T, Petry SF. The significance of glutaredoxins for diabetes mellitus and its complications. Redox Biol. 2024 May; 71:103043.

Petry SF, Römer A, Rawat D, Brunner L, Lerch N, **Zhou M**, Grewal R, Sharifpanah F, Sauer H, Eckert GP, Linn T. Loss and Recovery of Glutaredoxin 5 Is Inducible by Diet in a Murine Model of Diabesity and Mediated by Free Fatty Acids In Vitro. Antioxidants (Basel). 2022 Apr 15;11(4):788.

9 Acknowledgements

First and foremost, I would like to express my deepest gratitude to my supervisor, Prof. Dr. med. Thomas Linn, whose profound knowledge, integrity, and optimism have been invaluable in helping me overcome many challenges throughout my doctoral journey. I consider myself incredibly fortunate to have such a supportive and insightful supervisor. He is one of the best professors I have ever had, and I will always be grateful for his guidance, encouragement, and belief in me.

I am also grateful to my co-supervisor, Prof. Dr. Sybille Mazurek, for her valuable guidance and kind support. Her insightful feedback during our regular discussions greatly enriched this work. I particularly appreciate her guidance and encouragement during the *Fachgruppentagung Physiologie und Biochemie 2022*, which was instrumental in building my confidence as an early-career researcher.

My sincere thanks go to Dr. Sebastian Petry. His guidance in experimental design, data interpretation, troubleshooting, and manuscript revisions was essential at every stage of this project. I am truly grateful for his patience and the countless hours he devoted to helping me accomplish this work.

Special thanks go to our skilled laboratory technicians, Ms. Doris Erb, Ms. Gundula Hertl, and Ms. Birte Hußmann. They patiently trained me in essential laboratory techniques, offered solutions to every technical challenge, and made the practical execution of this dissertation possible. I am also grateful to my colleagues, Dr. Divya Rawat and Axel Roemer, for their helpful suggestions and scientific discussions.

I would like to thank Prof. Dr. Gunter Eckert for giving me the opportunity to work in his lab and culture the EndoC-βH3 cells. I gratefully acknowledge the Reinhard-und-Barbara-Bretzel-Stiftung for funding my research. I would also like to thank the

International Giessen Graduate School for the Life Sciences (GGL) for arranging practical courses.

Finally, I would like to thank my grandmother, my mom and dad, and my sister and brother for their unconditional support, love, and encouragement. My special thanks go to my wonderful husband, Fufei Yang. His support, patience, and love have supported me in ways words cannot fully express.

10 Curriculum vitae

The curriculum vitae was removed in the published version of the thesis.